NUREG/CR-1240, Vol. IV
HEDL-TME 80-3
R5

LWR PRESSURE VESSEL IRRADIATION SUPVEILLANCE DOSIMETRY

QUARTERLY PROGRESS REPORT
OCTOBER - DECEMBER 1979

Hanford Engineering Development Laboratory

Operated by Westinghouse Hanford Company
P.O. Box 1970 Richland, WA 99352
A Subsidiary of Westinghouse Electric Corporation

Preparation coordinated by
G.L. Guthrie
W.N. McElroy

Manuscript Completed: August 1980
Date Published: December 1980

Prepared for Division of Reactor Safety Research
Office of Nuclear Regulatory Research
U.S. Nuclear Regulatory Commission
Washington, DC 20555
NRC FIN No. B5988-7

NUREG/CR-1240, Vol. IV
HEDL-TME 79-41
R5

LWR PRESSURE VESSEL IRRADIATION SURVEILLANCE DOSIMETRY

QUARTERLY PROGRESS REPORT

January, February, March 1979

Preparation Coordinated by G. L. Guthrie, and W. N. McElroy

Hanford Engineering Development Laboratory

ABSTRACT

This report was compiled at the Hanford Engineering Development Laboratory operated by Westinghouse Hanford Company, a subsidiary of Westinghouse Electric Corporation, for the United States Department of Energy and the Nuclear Regulatory Commission, under DOE contract number DE-AC14-76FF02170 and NRC service request number TV-0176. It describes progress made in the Light Water Reactor Pressure Vessel Irradiation Surveillance Dosimetry Program during the reporting period.

ACKNOWLEDGMENTS

The following organizations are presently participating in the Light Water Reactor Pressure Vessel Irradiation Surveillance Dosimetry Program and will periodically contribute to this report.

Atomic Energy Research Establishment, Harwell, England (AERE-H)

California State University Northridge (CSU-N)

Centre d'Etude de l'Energie Nucleaire - Studiecentrum Voor Kern Energie (CEN/SCK), Mol, Belgium

Electric Power Research Institute (EPRI)

Fracture Control Corporation (FCC)

General Electric Vallecitos Nuclear Center (GE-VNC)

Hanford Engineering Development Laboratory (HEDL)

IRT Corporation (IRT)

Kernforschungsanlage Julich Gmbh, Germany (KFA)

Macalester College (MC)

National Bureau of Standards (NBS)

Oak Ridge National Laboratory (ORNL)

Pacific Northwest Laboratories (PNL)

Radiation Research Associates (RRA)

Rockwell International Energy Systems Group (RIES)

Rolls-Royce and Associates Limited, Derby, England (RRAL)

Science Applications Incorporated (SAI)

University of California, Santa Barbara (UCSB)

University of Tennessee (UT)

Westinghouse Electric Corporation - PWR Systems Division (WEC-PWR-SD)

Westinghouse Electric Corporation - Research Division (WEC-RD)

FOREWORD

The light water reactor pressure vessel (LWR-PV) surveillance dosimetry program has been established by NRC in recognition of the importance of improving, maintaining, and standardizing neutron dosimetry, damage correlation, and the associated reactor analysis procedures used for predicting the integrated effect of neutron exposure to LWR pressure vessels. A vigorous research effort attacking the same measurement and analysis problems goes forward worldwide, and strong cooperative links between the NRC supported activities at HEDL, ORNL, and NBS and those supported by CEN/SCK (Mol, Belgium), EPRI (Palo Alto, USA), KFA (Jülich, Germany) and several U. K. laboratories have been established. The major benefit of this program will be a significant improvement in the accuracy of the assessment of the remaining safe operating lifetime of light water reactor pressure vessels.

The primary objective of the multilaboratory program is to prepare an updated and improved set of dosimetry, damage correlation, and associated reactor analysis ASTM Standards for LWR-PV irradiation surveillance programs. Supporting this objective are a series of analytical and experimental validation and calibration studies in "Standard, Reference, and Controlled Environment Benchmark Fields," reactor "Test Regions," and operating power reactor "Surveillance Positions."

These studies will establish and certify the precision and accuracy of the measurement and predictive methods which are recommended for use in the ASTM Standards. Consistent and accurate measurement and data analysis techniques and methods, therefore, will have been developed and validated along with guidelines for required neutron field calculations that are used to correlate changes in material properties with the characteristics of the neutron radiation field. It is expected that the application of the established ASTM Standards will permit the reporting of measured materials property changes and neutron exposures to an accuracy and precision within bounds of 10 to 30%, depending on the measured metallurgical variable and neutron environment.

The assessment of the radiation-induced degradation of material properties in a power reactor pressure vessel requires accurate definition of the neutron field from the outer region of the reactor core to the outer boundaries of the pressure vessel. Problems with measuring neutron flux and spectrum are associated with two distinct components of LWR-PV irradiation surveillance procedures: (1) proper application of calculational estimates of the neutron fluence delivered to in-vessel surveillance positions, various locations in the vessel wall, and ex-vessel support structures and surveillance positions, and (2) understanding the relationship between material property changes in reactor vessels, in vessel support structures, and in metallurgical test specimens in test reactors and at accelerated neutron flux positions in operating power reactors.

The first component requires validation and calibration experiments in a variety of neutron irradiation test facilities including LWR-PV mock-ups, power reactor surveillance positions, and related benchmark neutron fields. The benchmarks serve as a permanent measurement reference for neutron flux and fluence detection techniques, which are continually under development and widely applied by laboratories with different levels of capability. The second component requires a serious extrapolation of an observed neutron-induced mechanical property change from test reactor "test regions" and operating power reactor "surveillance positions" to locations inside the body of the pressure vessel wall and ex-vessel support structures. The neutron flux at the vessel inner wall is up to one order of magnitude lower than at surveillance specimen positions and up to two orders of magnitude lower than for test reactor positions. At the vessel outer wall, the neutron flux is one order of magnitude or more lower than at the vessel inner wall. Further, the neutron spectrum at, within, and leaving the vessel is substantially altered.

In order to meet the reactor pressure vessel radiation monitoring requirements, a variety of neutron flux and fluence detectors are employed, most of which are passive. Each detector must be validated for application to the higher flux and harder neutron spectrum of the test reactor "test region"

and to the lower flux and degraded neutron spectrum at "surveillance positions". Required detectors must respond to neutrons of various energies so that multigroup spectra can be determined with accuracy sufficient for adequate damage response estimates. Proposed detectors for the program include radiometric detectors, helium accumulation fluence monitors, solid state track recorders, and damage monitors.

The necessity for pressure vessel mock-up facilities for dosimetry investigations and for irradiation of metallurgical specimens was recognized early in the formation of the NRC program. Experimental studies associated with high and low flux versions of a PWR pressure vessel mock-up are in progress. The low flux version is known as the Poolside Critical Assembly (PCA) and the high flux version is known as the Pool Side Facility (PSF). Both are located at ORNL. As specialized benchmarks, these facilities will provide well-characterized neutron environments where active and passive neutron dosimetry, various types of LWR-PV neutron field calculations, and temperature-controlled metallurgical damage exposures are brought together.

The results of the measurement and calculational strategies outlined here will be made available for use by the nuclear industry as ASTM Standards. Federal Regulation 10CFR50 already calls for adherence to several ASTM Standards which require establishment of a surveillance program for each power reactor and incorporation of flux monitors and post-irradiation neutron field evaluation. Revised and new standards in preparation will be carefully structured to be up-to-date, flexible, and, above all, consistent.

CONTENTS

CONTENTS (Cont'd)

FIGURES

FIGURES (Cont'd) Page

TABLES

SUMMARY

HANFORD ENGINEERING DEVELOPMENT LABORATORY

(HEDL)

A description is given of the gamma ray spectrometry used at the Pool Critical Assembly (PCA). Graphical results are given for the measurements at the quarter-thickness position in the simulated pressure vessel wall. The current status of Compton Recoil Gamma Ray Spectrometry is summarized.

E. G. & G., Idaho, Inc.

(EGG)

A description is given of the Proton-Recoil Proportional Counter Neutron Spectrometry performed at the Pool Critical Assembly (PCA). Measurements were made at the front surface, quarter-thickness, and half-thickness positions of the simulated pressure vessel wall and also in the void box. The neutron energy range covered extends from 60 KeV to 2 MeV. A general softening of the spectrum was observed with increasing radial distance from the core. Changes in the detailed structure of the neutron spectral shape were also observed.

OAK RIDGE NATIONAL LABORATORY

(ORNL)

Funds to continue the transport calculations have been delayed to FY-81. Assembly of the Simulated Surveillance Capsule (SSC) nears completion. The assembly of the Simulated Pressure Vessel Capsule (SPVC), except for the containment box which is being reworked, was completed, and the review of heat tranasfer analysis for the capsules was completed.

Work in dosimetry was performed in three categories: 1) Evaluation and uncertainty analysis of the dosimetry in the PCA 8/7 and 12/13 configuration for comparison with calculated values from the PCA "Blind Test". 2) Evaluation of dosimetry in the ORR-OSF startup program for the determination of optimal irradiation ties in the PSF-PV metallurgical experiment. 3) Review of the procedures used at NBS for the determination of fast fluxes in the cavity of the Arkansas power reactor. This is done in the framework of a more general review of unfolding and uncertainty analysis in commercial power reactor for the ASTM E10.05.01 Task Group on Uncertainty Analysis.

NATIONAL BUREAU OF STANDARDS

(NBS)

An analysis is given of fast neutron flux measurements accomplished in the ex-vessel cavity of an operating U.S. power rector. This analysis is particularly significant in that it represents one of the first serious attempts at defining the uncertainties in ex-vessel neutron dosimetry. The report of analysis addresses two other important issues:

(1) The advantages to be gained in reducing uncertainties in fast neutron dosimetry by benchmark referencing the measurements against a known, standard, neutron field;

(2) Methods for computing the variances of the benchmark-referenced measurements. In particular, the methods provide physical insight about the sources of uncertainties by newly derived error propagation equations which explicitly consider the energy regions of significant response for the various reaction rates. The report does not address the issue of covariance error propagation or treatment of uncertainty correlations in formation of selected averages, ratios or other colletive uses of the individual measurements.

HANFORD ENGINEERING DEVEOPMENT LABORATORY

(HEDL)

A. STATUS OF IN-SITU REACTOR GAMMA RAY SPECTROMETRY

Raymond Gold
Bruce J. Kaiser

Objective

The objective is to determine absolute gamma ray spectra and dose rates in Light Water Reactor-Pressure Vessel (LWR-PV) environments. Absolute gamma ray data are needed in the LWR Pressure Vessel Irradiation Surveillance Dosimetry Program to:

(1) Provide gamma ray heating estimates for designing high power LWR metallurgical irradiation tests.

(2) Provide for correction of fission neutron dosimetry due to photofission background.

At present, gamma radiation comprises the most uncertain element of the LWR-PV radiation field.

Summary

The current status of Compton Recoil Gamma Ray Spectrometry is summarized. Special attention is given to advances in experimental technique for measurements in reactor environments. In-situ gamma ray spectrometry efforts at HEDL in the U.S. Light Water Reactor (LWR) and Breeder Reactor (BR) programs are described.

Accomplishments and Status

1. Introduction

In reactor environments, the radiation field is comprised of two principal components, neutrons and gamma rays. The history of reactor development reveals an initial overriding concern for the neutron component of the radiation field. Such initial emphasis is completely understandable, since fission reactors are neutron chain multiplying assemblies. Significant effects due to the gamma ray component in reactor design, shielding, and safety were recognized only after a considerable amount of time. Recognition of these effects provided the impetus for improved characterization of reactor gamma ray deposition and spectra. These general motivations have been reviewed in depth[1,2] and were also summarized in the 11th Interlaboratory Reaction Rate Program (ILRR) progress report.[3]

In contrast to these general motivations, more specialized needs often arise for reactor gamma ray spectral data. For example, specific needs exist for radiation damage specialists using high power radiation test facilities to test, develop, and improve reactor fuels and materials. For these specialists, the temperature of a given radiation damage experiment is a crucial variable. Such radiation damage experiments can neither be properly designed nor analyzed without an adequate knowledge of the irradiation temperature history. The temperature history can ultimately depend upon the reactor gamma ray component, since the source of reactor heat generation can principally arise through gamma ray interactions.

The most fundamental quantity underlying the description of the reactor gamma ray component is the absolute gamma ray energy spectrum. Radiation effects arising from the gamma-component are induced by the interaction of the absolute gamma ray energy spectrum in the reactor environment. Consequently, accurate definition of this absolute spectrum is the goal of both theory and experiment. An urgent and pragmatic need now exists for reactor benchmark gamma ray spectrometry in the U.S. LWR and BR programs.

In reactor environments, gamma ray spectra are continuous, so the absolute magnitude, as well as the general shape of the gamma continuum, is of paramount importance. Conventional methods of gamma ray detection are, thus, not suitable for in-core gamma ray spectrometry. To meet such specific needs, a method of continuous gamma ray spectrometry, namely Compton Recoil Gamma Ray Spectrometry, was developed for in-situ observations in reactor environments.[4-6] In addition to applications in reactor science, [7-10] it has been used to measure gamma continua which arise in such applied disciplines as shielding, dosimetry,[11] health physics,[12] radiobiology and environmental science.[13,14] A brief summary of earlier efforts can be found in references 1 and 2.

The current status of the method is described in the next two sections, which deal with gamma ray spectrometry probe design and response characteristics, respectively. In the last two sections, emphasis is given to gamma ray spectrometry work in U.S. LWR and BR programs. Gamma ray spectometry in BR environments is outlined by focusing on startup plans for the Fast Test Reactor (FTR),[15] and gamma ray spectrometry results are presented for an LWR pressure vessel mockup in the Poolside Critical Assembly (PCA) at Oak Ridge National Laboratory (ORNL).[16]

2. Spectrometer Design

The basic principles underlying Compton Recoil Gamma Ray Spectrometry are adequately descried in the literature [4-6]. The basic elements that comprise the current gamma probe are displayed in Figure HEDL 1. Different lithium-drifted silicon solid-state detectors (Si(Li)) can be housed in the same vacuum chamber with little or no change in mounting hardware. Two configurations have been used to date: a 1-cm^3 planar detector and a 2-cm^3 planar detector.

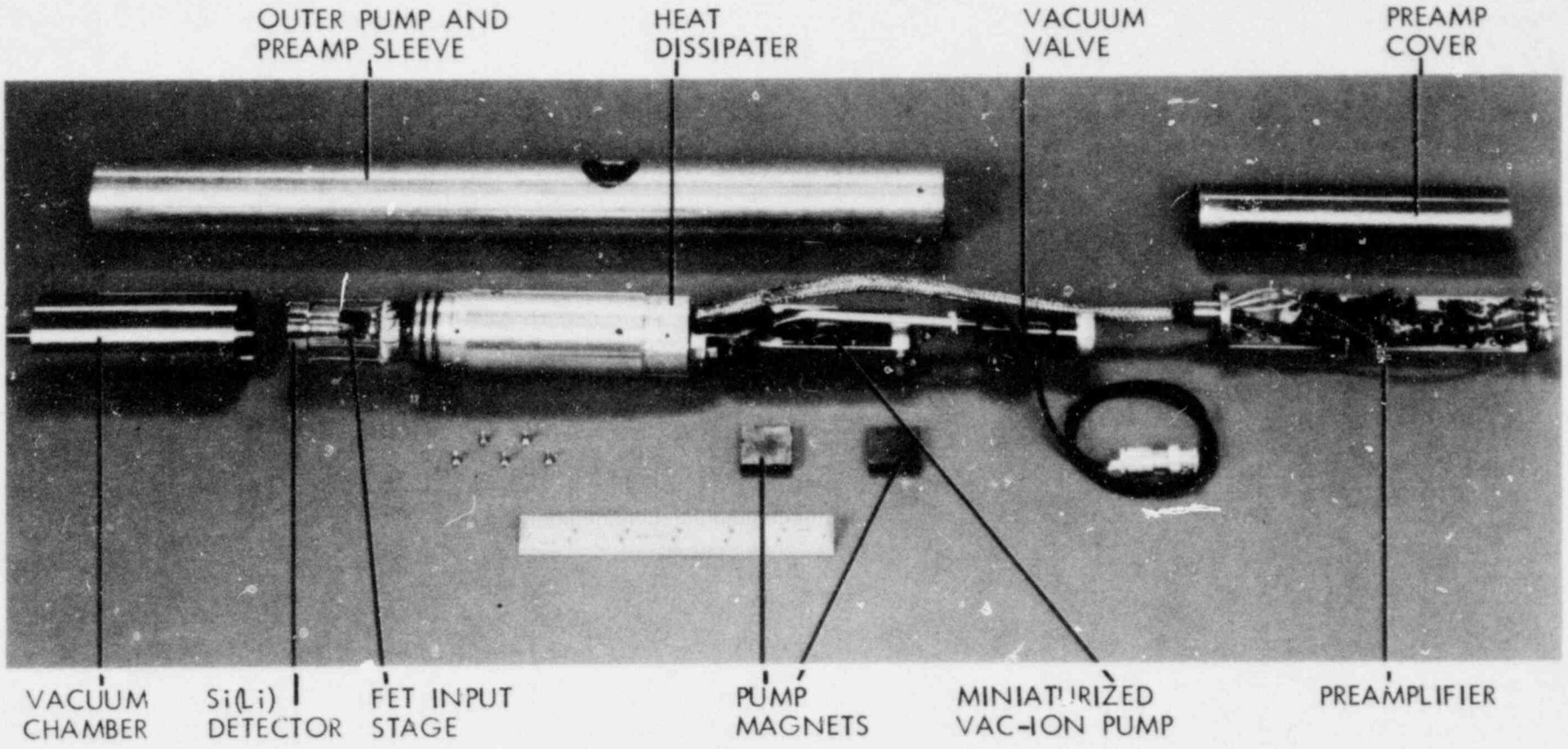

FIGURE HEDL 1. Detector Probe for Continuous Compton Recoil Gamma-Ray Spectrometry.

a. Summary Status of the Current Spectrometer Design

Vac-Ion Pump -- The inclusion of a miniaturized vac-ion pump (0.1 ℓ/s), capable of maintaining a probe pressure of 10^{-6} Torr at 43°C ambient, offers three improvements:

- Increased thermal insulation due to reduction factor of 10^3 or more in vacuum chamber pressure
- Reduced overall probe size
- Extended probe flexibility

Thermolectric Cooler -- A smaller, more efficient, Peltier junction thermoelectric cooler (TEC) is used, which increases cooling capacity, reduces the heat load, and is capable of cooling the sensor and Field Effect Transistor (FET) first input stage to 50°C below the aluminum dissipator temperature.

Aluminum Radiator -- A slotted aluminum radiator, which acts as a heat dissipator, can maintain the hot side of the TEC at -20°C in small reactor access ports of up to 40°C ambient. If necessary, this slotted aluminum radiator can be cooled by forced gas flow.

The net result of the vac-ion pump, TEC, and Aluminum Radiator acting together is to improve probe temperature stability, thus eliminating temperature dependent effects for most in-core gamma ray spectometry.

Preamplifier -- The preamplifier, a slightly modified and extensively reconfigured version of the ORTEC 142A design, possesses near-ideal characteristics for Compton Recoil Gamma-Ray Spectrometry with a rise time adjusted to 50 nsec and a combined preamp plus cooled sensor noise level of ∿50 μV (RMS). As a consequence, electron energy resolution of ∿5 keV (FWHM) at 0.661 MeV (^{137}Cs photo-peak energy) has been achieved.

Pulse Processing -- Overall pulse processing instrumentation has evolved significantly over earlier electronic circuitry (see Figure HEDL-2).

The net result of the preamplifier and improved pulse processing instrumentation acting together produces:

- Excellent rise time resolution (see Figure HEDL-3)
- Rise time observations that are essentially independent of pulse height (energy) aside from noise broadening
- The capability of accurately measuring Si(Li) detector sensitive volume (see Section 3)
- Accurate characterization of overall energy-angular response.

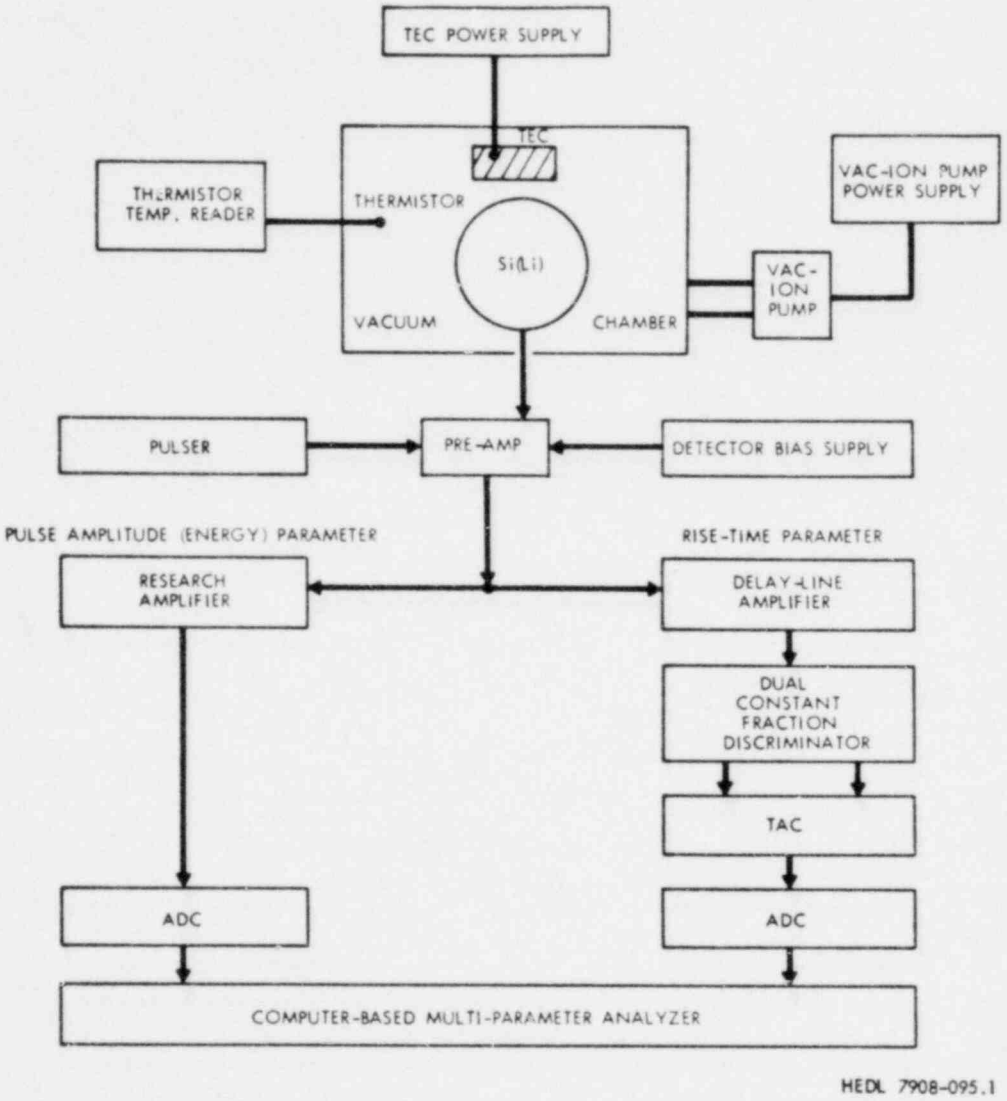

FIGURE HEDL 2. Instrumentation Block Diagram for Compton Recoil Gamma Ray Spectrometry.

3. Response Characteristics

For absolute measurements, the extent of the sensitive region of the Si(Li) detectors used in Compton Recoil Gamma Ray Spectrometry is of critical importance.[11] Current spectrometry system capabilities now permit quantitative measurement of this sensitive region by resolving differences in pulse rise time between the sensitive region and semi-sensitive regions. To date the planar 1- and 2-cm^3 Si(Li) detectors have been investigated by stepping a 0.1524 cm diameter beam of ^{54}Mn gamma rays across appropriate orthogonal surfaces.

Typical response rise time spectra (RTS) for a 2-cm^3 detector are displayed in Figure HEDL-3. Note the shift from predominantly slow to fast rise time events as one steps the source and down the side of the detector away from the detector face. The c-type spectrum is observed as the traverse continues until the last two 0.127 cm steps, where the b- then a-type spectra are repeated. Traverses across the face and back of the detector follow the same general pattern. Thus, the two important regions of the detector are dimensionally defined; the semi-sensitive outer shell with its slower rising pulses (due to trapping and E-field reduction resulting from under or over compensation of lattice impurities), and the sensitive volume with its faster rising pulses.

Of, perhaps, greater significance is the sensitivity of these RTS observations that enables measurement of the finite-size retention probability of recoil electrons in these Si(Li) detectors. The retention probability, P, of electrons in the finite sensitive volume of a detector depends on a number of variables. In general, P depends upon the gamma ray energy ε_0, the recoil electron energy, E, and the angle of incidence of the gamma ray θ. Hence, the retention probability is generally denoted by $P(\varepsilon_0, E, \theta)$.

RTS measurements of such sensitivity were not possible before, so certain simplifying assumptions were made in the unfolding analysis of observed

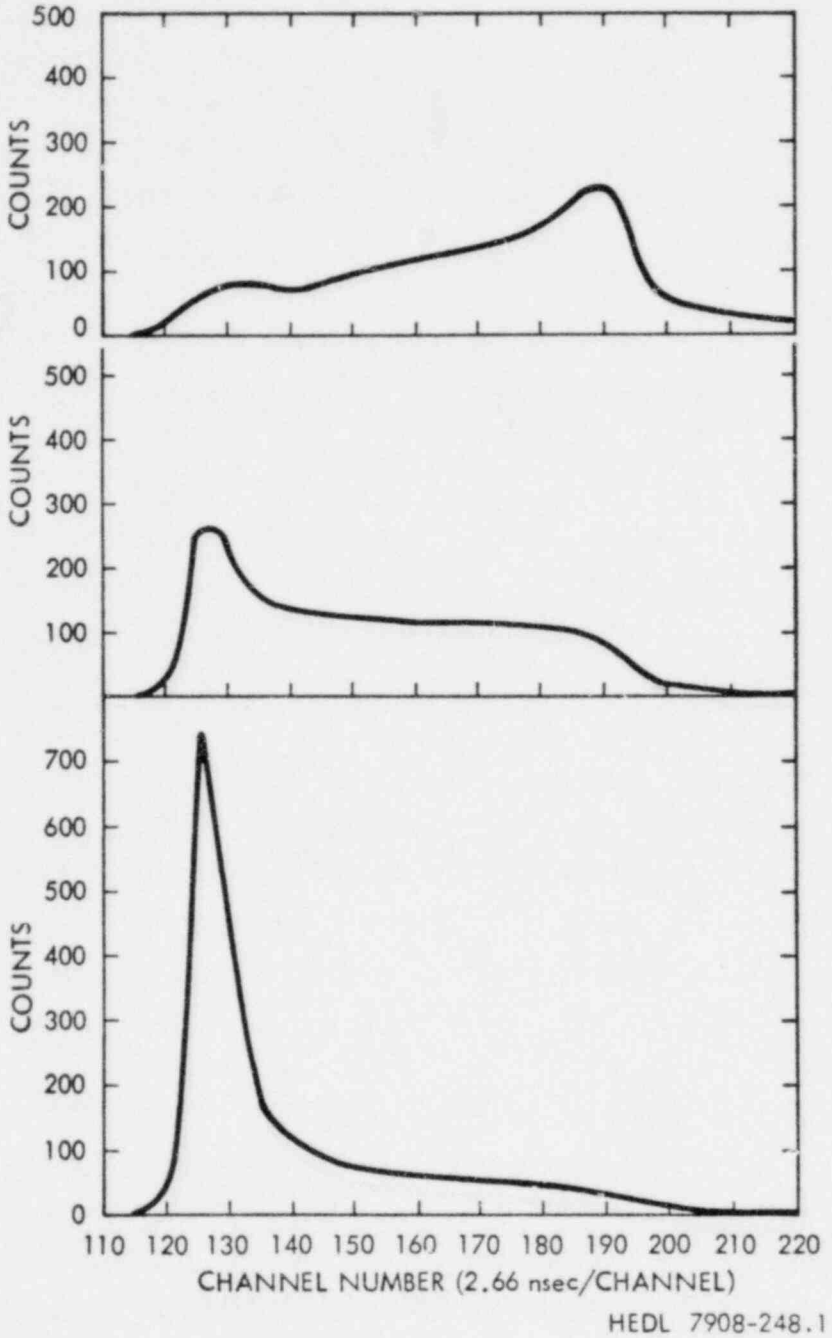

FIGURE HEDL-3. Typical Rise Time Spectra Used for Defining the Sensitive Volume of a 2-cm^3 Planar Si(Li) Detector. The electron energy window chosen for the collimated beam of ^{54}Mn gamma rays was 0.64 to 0.32 MeV. (a), (b), and (c) are the 0.00, 0.127 cm and 0.254 cm side traverse spectra, respectively. The 0.00 cm position corresponds to the edge of the detector. The total integrated counts for each step was 20,000.

electron spectra.[4-6] In particular, P was assumed independent of both ε_o and θ. With the present capabilities of observing RTS, one no longer need rely on such assumptions, so more accurate data analysis can be performed. On the other hand, these very capabilities permit investigation of the validity of these earlier assumptions.

Response measurements are made with a point source of gamma rays rotated about the detector from the face (0^o incidence) to the back (180^o incidence) in 45^o steps. Rise time and energy data are accumulated at each position in a two-parameter, 64 x 64 channel mode. Figure HEDL-3 displays typical response RTS. The retention probability, $P(\varepsilon_o, E, \theta)$, is obtained by first fitting the faster rise time peak with a Gaussian distribution, then the area under this Gaussian distribution is divided by the total number of counts in the RTS to obtain $P(\varepsilon_o, E, \theta)$. Calculations are performed for all electron energy bins, E_i, at each angle of incidence.

4. Gamma Ray Spectrometry Plans for the FTR

A reactor characterization program (RCP), which consists of Very Low Power (VLP), Low Power (LP), and High Power (HP) irradiations[15], has been planned and scheduled for the Fast Test Reactor (FTR) at startup. In-core gamma ray spectrometry will be carried out at VLP in a specially designed FTR insert called the In-Reactor Thimble (IRT). The IRT insert replaces a centrally located fuel assembly (No. 2201) in the FTR core for VLP measurements and provides an adequate environment for the operation of the in-core fission chamber, ionization chamhers, and spectrometry probes.

In-core continuous gamma ray spectrometry is planned as the first experiment in the IRT. As such, it will be conducted concurrently with fuel loading in the third trisector of the FTR. Axial locations at mid-plane and in the lower axial reflector, about 80 cm below mid-plane, have been assigned for these measurements.

Two Si(Li) detectors, planar 1-cm^3 and 2-cm^3, will be used in the IRT. Background rates for these experiments are expected to be very high.

Estimated background rates at mid-plane with all rods in ($k_{eff} \cong 0.90$) are roughly 5×10^3 and 10^4 count/s for the smaller and larger detector, respectively. These high background count rates stem from the sponataneous fission rate of FTR core 1 fuel, which is 22 wt % plutonium.

Total VLP gamma ray count rates, with rods adjusted for $k_{eff} = 0.95$ to 0.98, will be roughly 2 to 5 times higher. Even for these very high rates, it may still be possible to collect data in a two-parameter mode for the smaller 1-cm^3 planar detector. However, data collection for the larger 2-cm^3 detector will probably be restricted to the one-parameter mode. In this manner, spectral sensitivity will be extended up to roughly 4 MeV and perhaps higher.

5. Gamma Spectrometry in LWR Environments

Gamma continua were observed in the low pressure vessel (PV) mockup at the PCA. This mockup represents a controlled irradiation field set up at ORNL to study and quantify the complex radiation field that arises in the LWR-PV Irradiation Surveillance Dosimetry Program. There is a need for improved gamma heating data to aid in the design of high power LWR-PV irradiation experiments. In addition, the response of fission threshold dosimeters used in LWR-PV environs can possess non-negligible contributions induced by photofission. Consequently, these photofission contributions must be more accurately assessed.[17,18,19]

Gamma measurements were restricted to the interior of the PV block in this work. Observations were carried out at midplane in the T/4, T/2, and 3T/4 locations* using a 12/13 configuration (i.e., water gaps of 12 cm and 13 cm for the distance between the core face and thermal shield and between the thermal shield and PV face, respectively). At each location, foreground data were collected with the reactor at a power level of a few watts, and

*The T/4, T/2, and 3T/4 designations represent distances from the front face of a PV block whose total thickness is T.

background data were collected with the reactor shutdown. As a representative case, the background and foreground electron spectra observed at the T/4 location with a 2-cm^3 planar Si(Li) detector are presented in Figure HEDL-4 and HEDL-5. The corresponding unfolded gamma spectra are displayed in Figure HEDL-6 and HEDL-7. These results can only be regarded as preliminary because analyses for both finite-size effects and experimental error have not yet been performed.

Expected Achievements

Analysis of finite-size effects for in-situ gamma probes will be completed. Experimental error estimates will be generated for reactor gamma spectrometry. These analyses will be incorporated in computer codes to produce spectral measurements which account for systematic effects and experimental error. Startup gamma spectrometry measurements will be carried out in the FTR.

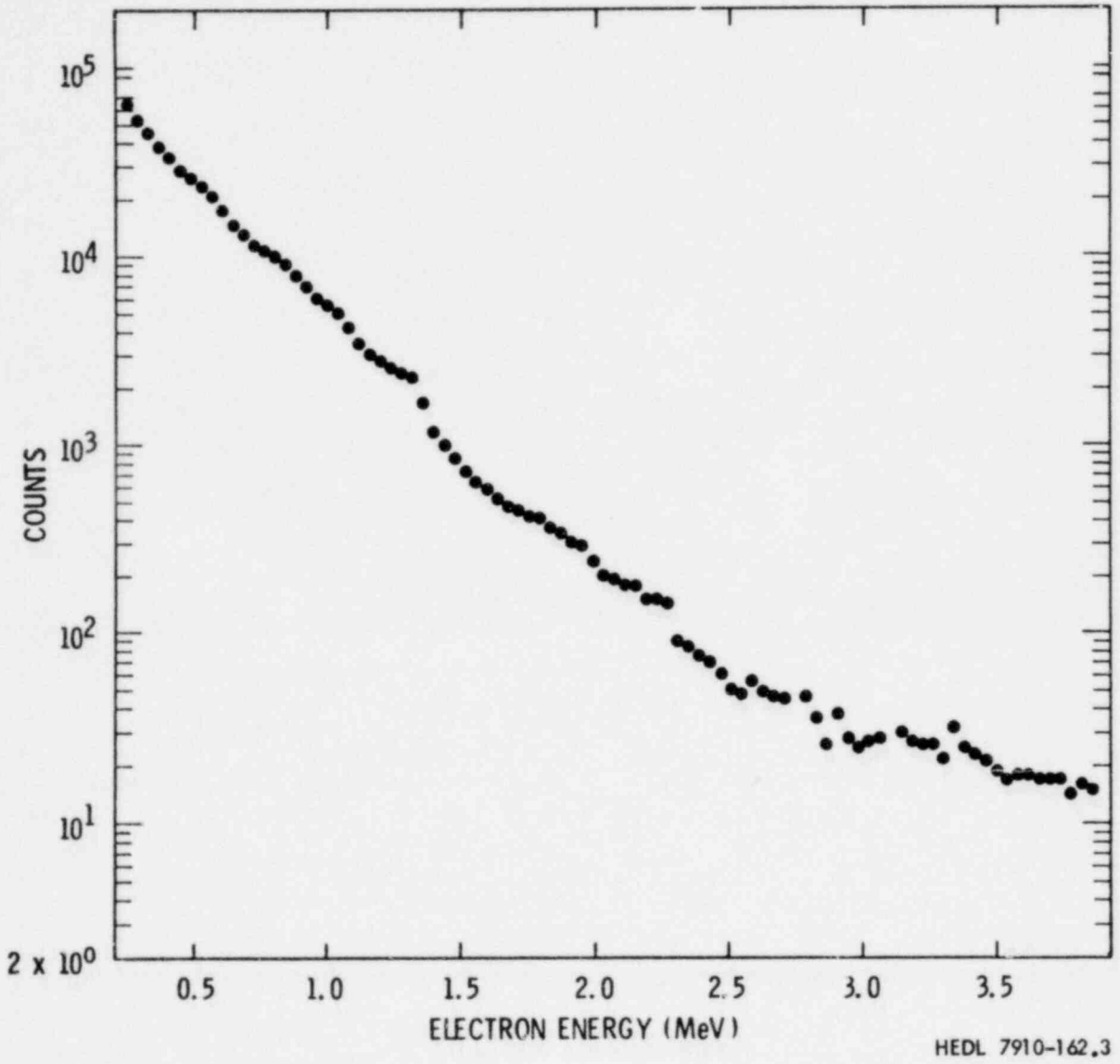

FIGURE HEDL 4. Background Spectrum.

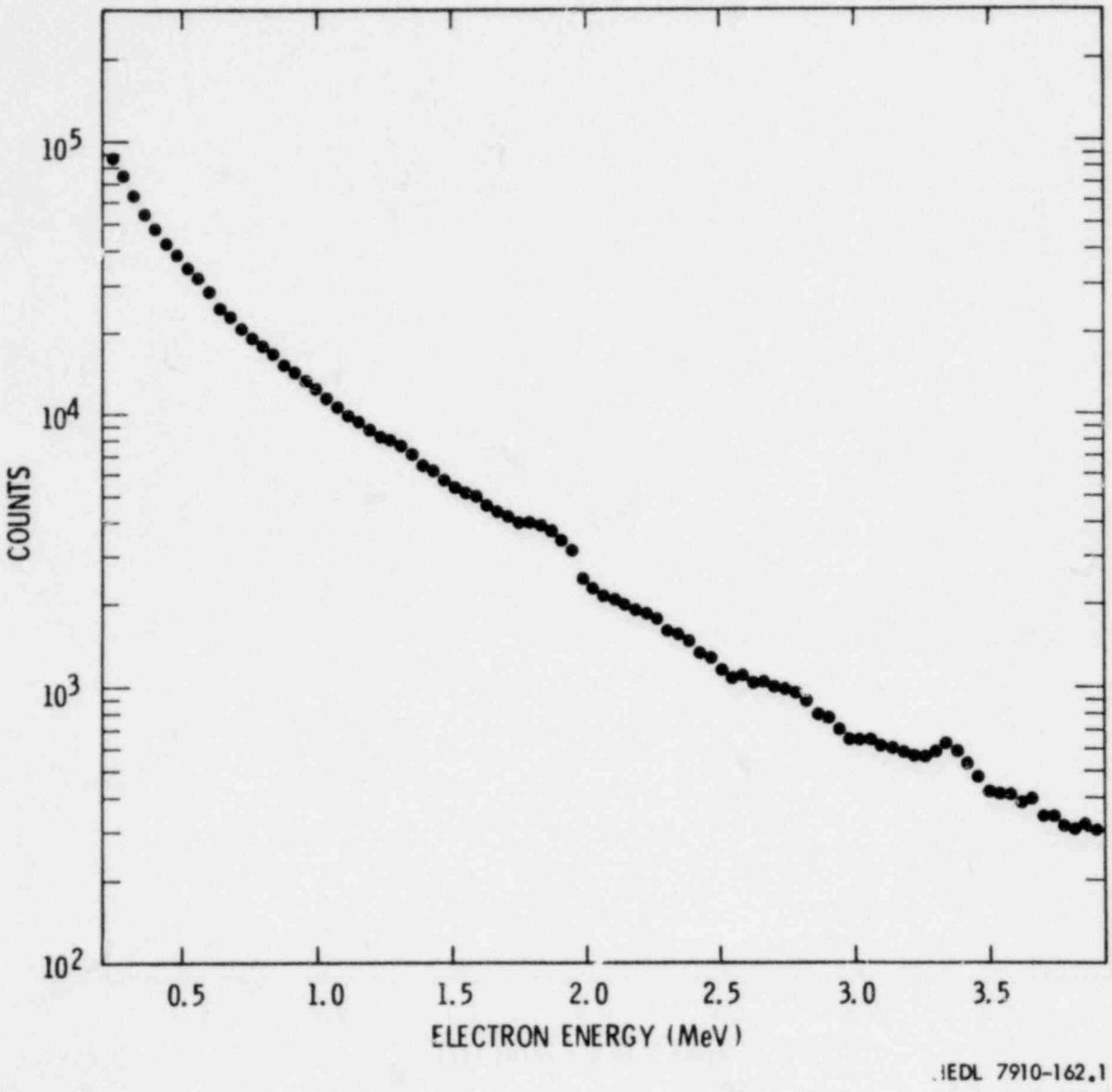

FIGURE HEDL 5. Foreground Electron Spectrum

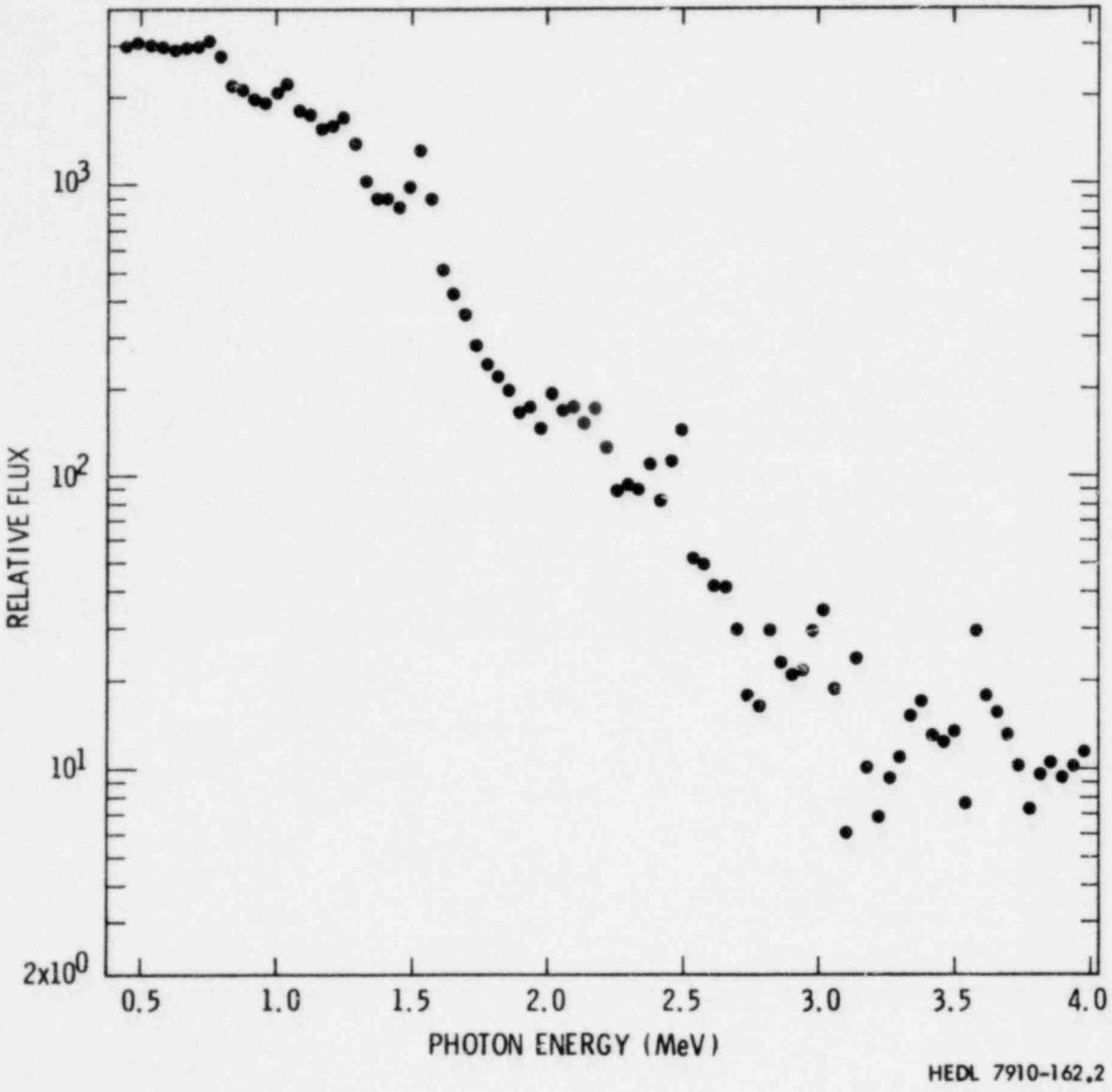

FIGURE HEDL 6. Background Gamma Ray Spectrum.

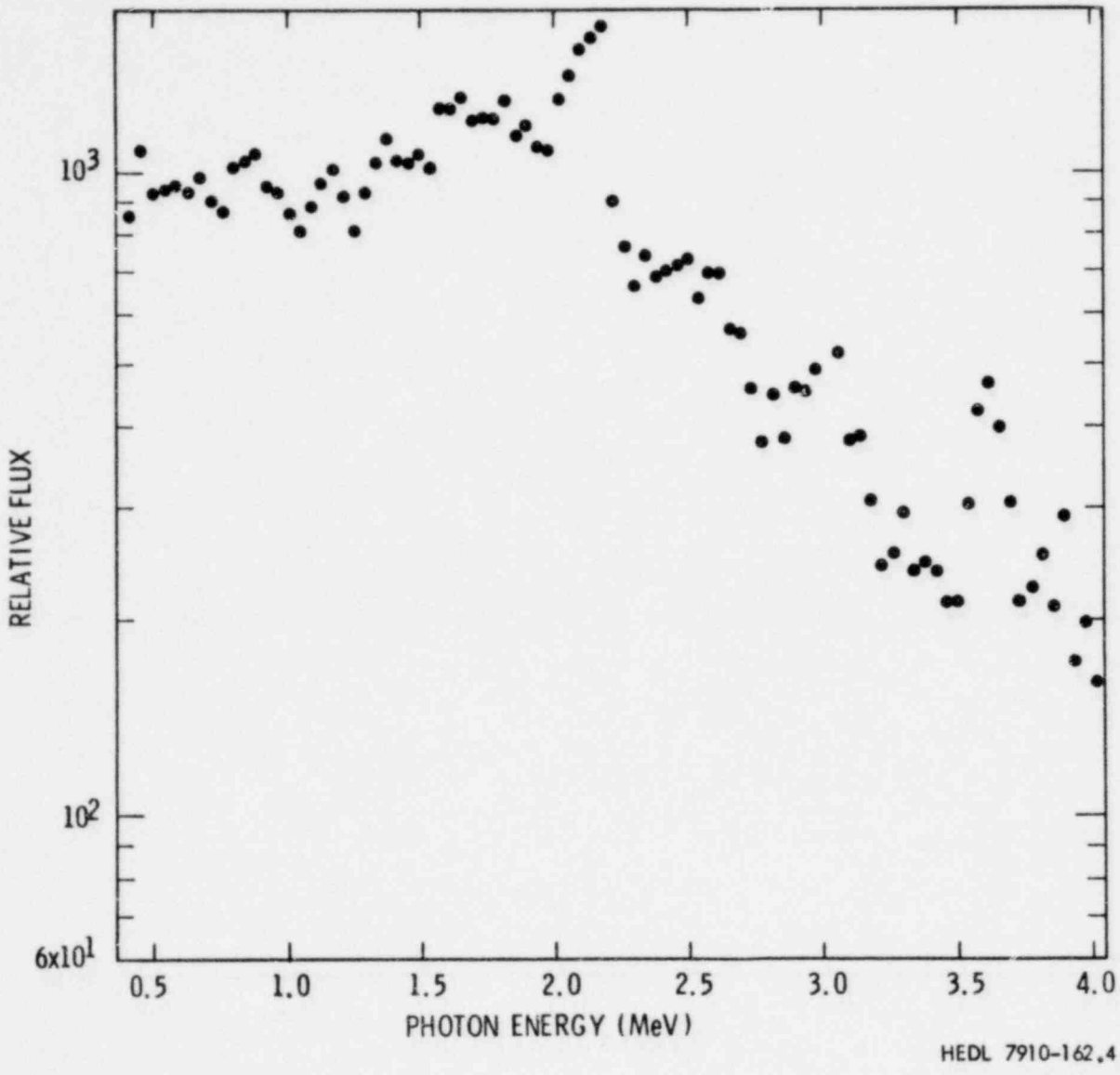

FIGURE HEDL 7. Foreground Gamma Ray Spectrum.

REFERENCES

1. R. Gold, Status of Gammay-Ray Heating Characterization in LMFBR, HEDL-TME 75-126, Hanford Engineering Development Laboratory, Richland, WA, 1975.

2. R. Gold, "Overview of Gamma Ray Energy Deposition and Spectra in Fast Reactor Environments," Proceedings of the Second ASTM-Euratom Symposium on Reactor Dosimetry, 1, p. 101, Palo Alto, CA, 1977.

3. R. Gold, "Gamma Ray Heating in Breeder Reactors." Interlaboratory Reaction Rate Program 11th Progress Report November 1975-October 1976, HEDL-TME 77-34, Hanford Engineering Development Laboratory, Richland, WA, 1978.

4. R. Gold, "Compton Continum Measurements for Continuous Gamma Ray Spectroscopy," Bull. Am. Phys. Soc. 13, p. 1405, 1968.

5. M. G. Silk, Iterative Unfolding of Compton Spectra, AERE-R5653, U.K. Atomic Energy Research Establishment, 1968.

6. R. Gold, "Compton Recoil Gamma Ray Spectroscopy," Nucl, Instr. Methods 84, p. 173, 1970.

7. M. G. Silk, "Energy Spectrum of the Gamma Radiation in the DAPHINE Core," J. Nuclear Energy, 23, p. 308, 1969.

8. R. Gold, "Compton Recoil Measurements of Continuous Gamma Ray Spectra," Trans. Am. Nucl. Soc., 13, p. 421, 1970.

9. H. E. Korn, Measurement of the Energy Distribution of the Gamma Field in a Fast Reactor, KFK 2211, Karlsruhe Nuclear Research Center, 1975.

10. S. H. Jiang and H. Werle, "Fission Neutron-Induced Gamma Fields in Iron," Nucl. Sci, Engng., 66, p. 354, 1978.

11. A. N. Strash and R. Gold, "Absolute Gamma Ray Dosimetry by Recoil Electron Spectroscopy," Nature, 234, p. 260, 1971.

12. R. Gold, "Gamma-Continuum at the Air-Land Interface," Health Physics, 21, p. 79, 1971.

13. R. Gold, A. M. Strash, F. J. Congel and J. H. Roberts, "Continuous Gamma Ray Spectroscopy in the Natural Environment," IEEE Trans. NS-20, 48, 1973.

14. R. Gold, B. G. Oltman, K. F. Eckerman, and A. M. Strash, "Environmental Radiation at the EBR-II Site," IEEE Trans. NS-21, p. 596, 1974.

REFERENCES (Cont'd)

15. J. W. Daughtry, R. A. Bennett, W. L. Bunch, W. N. McElroy and T. L. King, "FFTF Reactor Characterization Program," Proceedings of the Second ASTM-Euratom Symposium on Reactor Dosimetry, 1, 69, Palo Alto, CA, 1977.

16. F. B. K. Kam and Z. H. Swanks, "Pool Critical Facility," LWR Pressure Vessel Irradiation Surveillance Dosimetry Quarterly Progress Report, July-September 1977, NUREG/CR-0038 HEDL-TME 78-4, 1978.*

17. C. D. Bowman, C. M. Eisenhauer, and D. M. Gilliam, "Photofission Effects in Reactor Pressure Vessel Dosimetry, "Proc. of the second ASTM-Euratom Symposium on Reactor Dosimetry, 2, p. 575, Palo Alto, CA, 1977

18. G. L. Simmons, V. V. Verbinski, W. K. Hagan and C. G. Cassapakis, Measurement and Analysis of Gamma-Ray Induced Contamination of Neutron Dosimetry Procedures Used for Reactor Pressure Vessel Applications, EPRI NP-1056, 1979.

19. R. Gold, "Estimates of High Energy Gamma and Neutron Flux from Continuous Gamma Ray Spectrometry," LWR Pressure Vessel Irradiation Surveillance Dosimetry Quarterly Progress Report, July-September 1978, NUREG/CR-0551 HEDL-TME 78-8, 1979.**

*Available for purchase from the National Technical Information Service, Springfield, VA 22161

**Available for purchase from the NRC/GPO Sales Program, U.S. Nuclear Regulatory Commission, Washington, D.C. 20555, and the National Technical Information Service, Springfield, VA 22161

E. G. & G., Idaho, Inc.

(EGG)

PROTON-RECOIL NEUTRON SPECTROMETRY AT THE POOL CRITICAL ASSEMBLY

J. W. Rogers
E. G. & G., Idaho, Inc.

Objective

To obtain neutron spectral scoping measurements in the Poolside Critical Assembly (PCA) at Oak Ridge National Laboratory (ORNL).

Summary

Fast neutron spectrum measurements have been made in the Pool Critical Assembly (PCA) associated Light Water Reactor (LWR) Dosimetry Pressure Vessel Benchmark (PVB) fields. These measurements cover the neutron energy range between approximately 60 keV and approximately 2 MeV. Hydrogen and methane filled proton-recoil detectors were used to obtain the proton-recoil spectra from which the neutron spectra were derived. Measurements were taken at the midplane elevation on the surface, at 1/4 thickness of the steel, at 1/2 thickness of the steel and in the void box positions of the PVB. The neutron spectra showed considerable variation at the various positions with the energy distribution shifting toward lower energy between the face and void box of the PVB. In a similar manner considerable spectral structure developed in the spectra. These measurements were performed to provide neutron spectral definition which is required to appropriately perform and interpret neutron dosimetry measurements related to fast neutron damage in light-water pressure vessel steels. These measurements also provide data for comparison with calculated spectra.

Accomplishments and Status

I. INTRODUCTION

The U. S. Nuclear Regulatory Commission (NRC) has established a light water reactor pressure vessel (LWR-PV) surveillance dosimetry program to improve,

maintain and standardize neutron dosimetry and damage analysis procedures used to assess the damage in the steel of LWR-PV. Part of this program involves validation and calibration experiments in neutron fields relevant to LWR-PV. The Pool Critical Assembly (PCA) associated LWR Pressure Vessel Benchmark (PVB) neutron field has been established to simulate the neutron fields to which LWR-PV are exposed. This is a low neutron flux density field where measurements can be made to study dosimetry and damage analysis techniques and to guide neutron field calculations.

The accurate assessment of radiation induced damage requires a good knowledge of the neutron energy spectrum of the neutron field involved since damage is neutron energy dependent. The well established proton-recoil proportional counter technique (1,2) is one of the more accurate methods for obtaining high resolution neutron energy spectrum measurements. This method has been used to measure the neutron energy spectra found in the PCA-PVB fields covering the energy range between approximately 60 keV and approximately 2 MeV. Hydrogen and methane filled detectors were used to obtain the proton-recoil spectra from which the neutron spectra were derived. SMeasurements were taken at the midplane elevation on the surface, at 1/4 thickness and 1/2 thickness of steel and in the void box positions ofthe pressure vesselsimulator (PVS). The neutron spectra showed considerable variation at the various positions with the energy distribution shifting toward lower energy between the face and void box of the PVB. In a similar manner considerable spectral structure developed in the spectra.

II. EXPERIMENTAL DESCRIPTION

The PCA-PVB has been established at Oak Ridge National Laboratory (ORNL). This facility provides experimental access to locations in the Pressure Vessel Simulator (PVS) so measurements related to dosimetry and damage can be made in conditions similar to those existing in a LWR-PV. A conceptual drawing of the PCA-PVB is shown in Figure EGG-1. The PCA core is a light water moderated, enriched uranium fueled, Material Test Reactor (MTR) plate

type elements critical assembly which provides the source of leakage neutrons for the PVB. The facility is located in a large pool of water maintained at approximately 100°F.

The PVB consists of the reactor core plus variable slab configurations of simulated thermal shields, pressure vessel containment and void region. Experimental access tubes allow for measurements to be made in and around these components. The PVB can be positioned at the desired distance from the face of the core. Measurements were made at the midplane elevation on the surface of the PVS, at 1/4 thickness of the PVS, at 1/2 thickness of the PVS and in the void box of the PVS. The PVB was in the "8/7" designated configuration which refers to the geometrical arrangement of the thermal shield (stainless steel) and PVS where the "8" refers to the distance (cm) between the face of the PCA core and the thermal shield, and "7" refers to the distance (cm) between the thermal shield and the PVS.

Proton-recoil detectors of cylindrical geometry were used for these measurements and are described in Table EGG-1. Five detectors, three predominantly hydrogen filled and two methane filled, were used where gas pressure was used as the parameter to discriminate against gamma events and to cover neutron energy ranges with energy overlap between detectors of different pressures. The detectors were positioned so that the sensitive region of the detector was centered at midplane of the PVB. The space surrounding the detectors was filled with plastic (to simulate water) for the measurements at the surface of the PVS and with steel for the measurements in the PVS. No fillers wre used in the void box. During the fast neutron measurements the detectors were shrouded with cadmium to inhibit the $^{14}N(n,p)^{14}C$ reaction in the filling gas.

The preamplifier and associated filler pieces were placed in close proximity with the detectors. Cables were routed out through the access tubes to the analog electronics, power supply and data acquisition system which recorded the data. Because of the very high humidity in the access tubes, it was necessary to continuously purge the preamplifier-detector region with dry nitrogen to prevent high voltage breakdown.

III. EXPERIMENTAL RESULTS

Measurements were made to assess the gamma-ray counting rates and their influence on the proton-recoil distributions. The gamma-ray counting rate is greatest at the face of the PVS and decreases going through the PVS. Total counting rates of up to a few thousand counts per second were observed with approximately 25% of the counts due to proton recoils above the maximum energy of the gammas in each detector. Proton-recoil distribution distortion due to the gamma-ray counts was assessed by comparing the shape of the $^{14}N(n,P)^{14}C$ peak obtained in a very low gamma-ray and neutron field with that obtained in the PCA-PVB field. No changes in the shape of the $^{14}N(n,p)^{14}C$ peak were observed.

Energy calibration was obtained with the $^{14}N(n,p)^{14}C$ reaction from thermal energy neutrons which produces monoenergetic neutrons of approximately 600 keV. This could be done at all of the PVB locations by shrouding the detector with plastic. It was found that moving the detector preamp assembly from one position to another did not cause detectable shifts in the calibration thus reducing the number of calibration runs required in a series of measurements. The energy of the $^{14}N(n,p)^{14}C$ peak was taken to be 600 ± 15 keV which places an error of approximately ± 3% (1σ) on the energy scale for these measurements.

Proton-recoil spectra were obtained with each of the detectors at the center midplane elevation in the experimental access tubes at the surface of the PVS, in the 1/4 and 1/2 thickness of the PVS, and in the void box of the PVS. The experimental access tube at the surface of the PVS was removed during all other measurements. An 0.05 cm thick cadmium shroud was placed around each detector during the measurements to inhibit the thermal neutron induced $^{14}N(n,p)^{14}C$ reaction. Measurements with and without the cadmium at the surface of the PVS showed that the cadmium removed the peak from the $^{14}N(n,p)^{14}C$ reaction. Each detector was also exposed to only ^{60}Co gamma rays of approximately the same intensity as the gamma rays of the PVS environment to determine the minimum energy to which the data could be analyzed for neutron spectra.

In order to keep the total counting rates at acceptable levels the power level of the PCA was adjusted on a measurement-to-measurement basis. Total counting rates of up to 8000 c/s were necessary for the measurements at the face of the PVS and up to 5000 c/s at the other locations. It was not possible to take data with the PCA operating under servomechanism control because of the noise generated by the system. The PCA was operated under manual control at power levels between 0.2 and 4.0 watts (thermal) during the measurements, and no data were collected while the manual adjustments were being made to stabilize the power level or to change the power level. Measurement times of 20 to 60 minutes were adequate to provide counting statistics equal to or less than 2% (1σ) in all channels of data used for spectral analyses.

The nominal energy ranges covered by each detector are found in Table EGG-1. The minimum energy to which the data could be analyzed depended upon the gamma to neutron ratio at each specific location.

The data were analyzed using the unfolding techniques and routines of Bennett, Gold and Olson (1). The neutron spectra obtained from these measurements are presented graphically in Figures EGG-2 through EGG-5 and are tabulated in Table EGG-2. Each spectrum has been arbitrarily scaled to a magnitude of unity at 0.1 MeV corresponding to the energy where neutron damage becomes significant. The corrected spectra have been corrected for response function effects as described in Reference (1). The uncorrected spectra were derived from the uncorrected proton-recoil distributions (see Reference 3). The relative fluxes in Table EGG-2 are estimated to have uncertainties of approximately ± 10% (1σ) between 0.1 and 1.0 MeV where there is very little difference between the neutron spectra derived from the uncorrected and corrected proton-recoil distributions. These measurements were made in neutron fields with significant flux gradients and perhaps with considerable energy anisotropy. Some of these spectra are considerably different in shape than those for which the unfolding techniques were developed, therefore, some caution should be taken in any conclusions drawn from these measurements. The spectra at the void box and 1/2 thickness

are very similar in shape to those for which the unfolding techniques were developed and should be very realistic results, but the PVS face and 1/4 thickness are considerably "harder" and may need some cautious interpretation or further study.

IV. CONCLUSIONS

These measurements have demonstrated that it is possible to obtain proton-recoil spectra in the PCA-PVS neutron fields over an energy range of approximately 60 keV to approximately 2 MeV without serious interference from gamma radiation at the existing conditions. These measurements show spectral changes in the PVS which are qualitatively expected. There is a general shift toward lower energy in the spectra between the face of the PVS and the void box. This information is significant in the interpretation of dosimetry measurements related to fast neutron damage because it provides the neutron energy distribution in the energy range where the onset of damage occurs.

Expected Achievements

As follow-on studies to these successful scoping measurements, more detailed proportional counter neutron spectrometry is scheduled for the LWR-PVB at the PCA.

REFERENCES

1. E. F. Benentt, R. Gold, I. K. Olson, "Analysis and Reduction of Proton-Recoil Data," ANL-7394, January 1968.

2. P. W. Benjamin, C. D. Kemshall, J. Radfearn, "The Use of Gas-Filled Spherical Proportional Counters for Neutron Spectrum Measurements," AWRE NR 2/64, July 1964.

3. E. F. Bennett, T. J. Yule, "Techniques and Analyses of Fast-Reactor Neutron Spectroscopy with Proton-Recoil Proportional Counters," ANL-7763, August 1971.

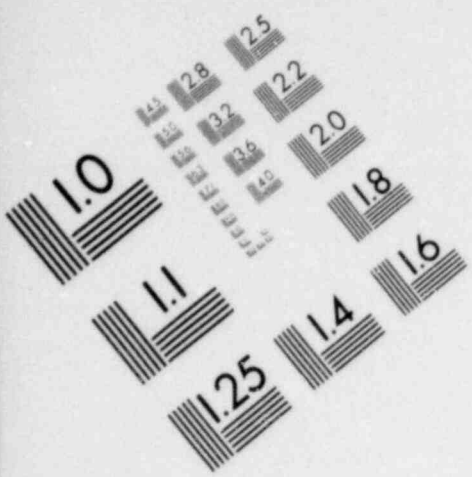

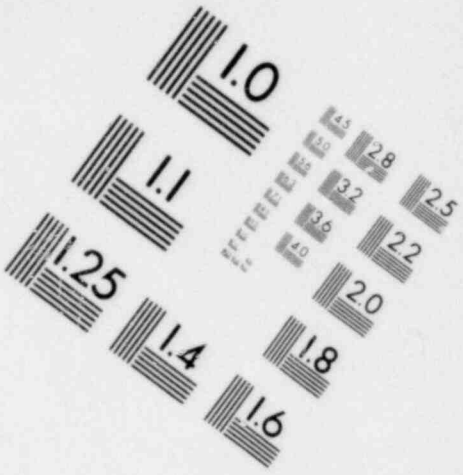

IMAGE EVALUATION
TEST TARGET (MT-3)

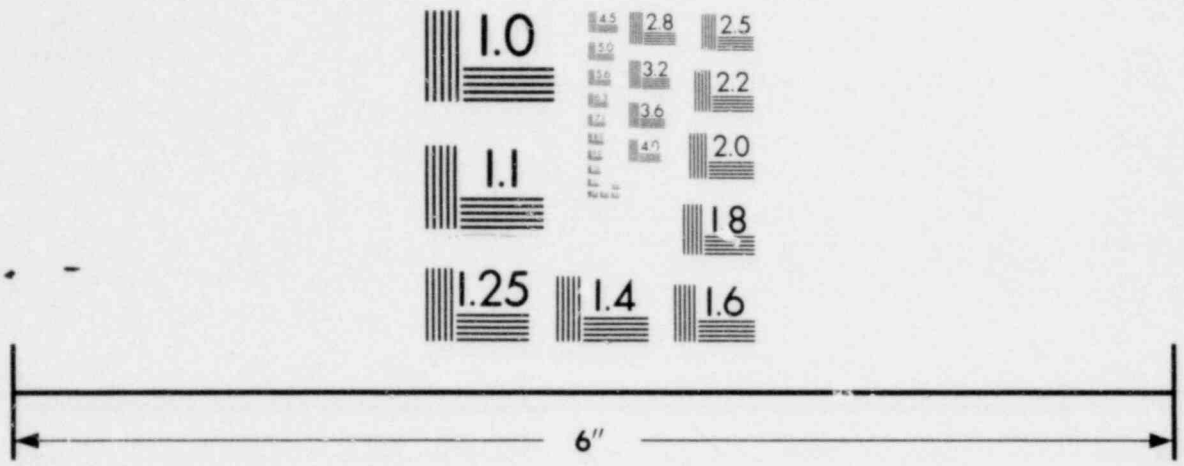

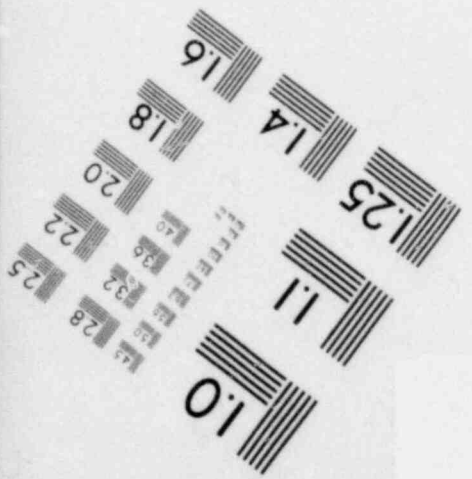

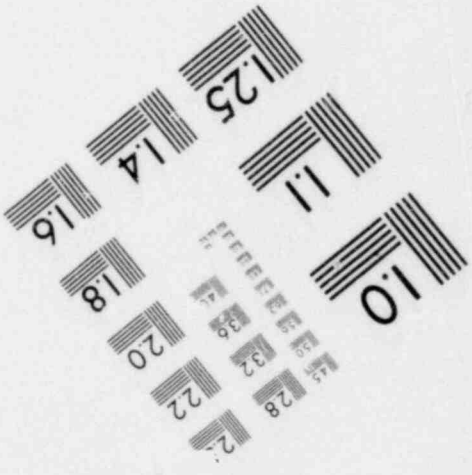

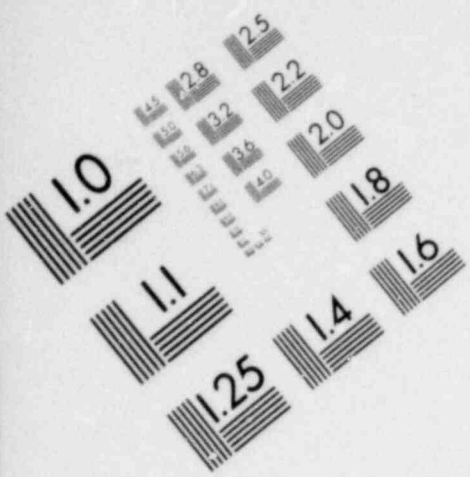

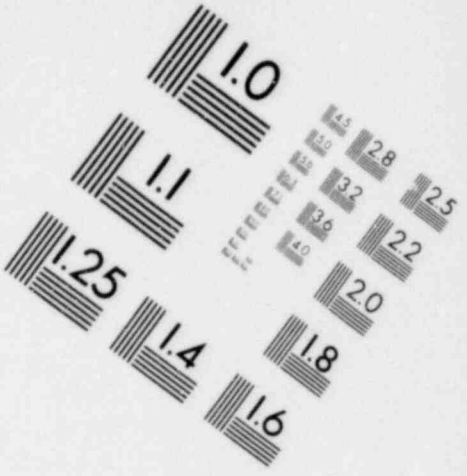

IMAGE EVALUATION TEST TARGET (MT-3)

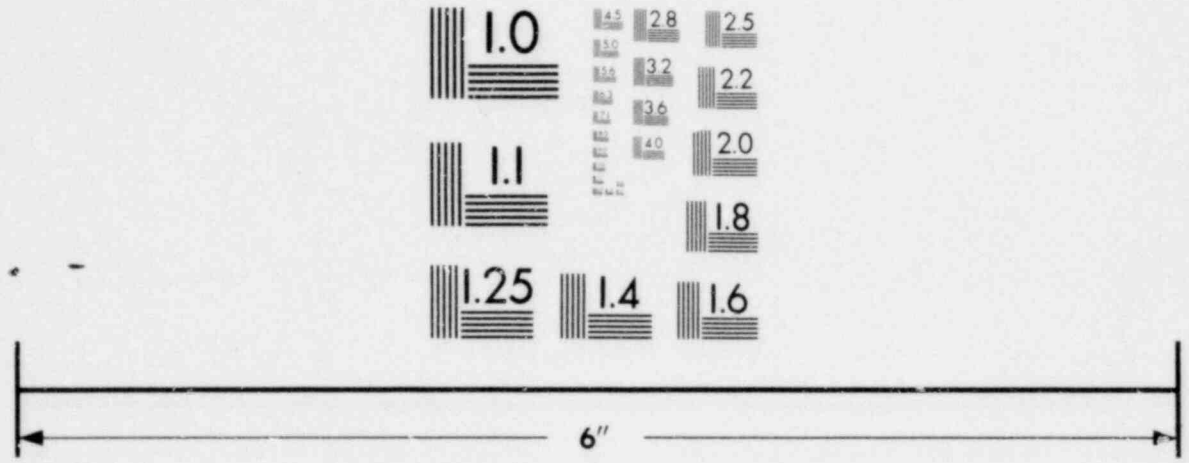

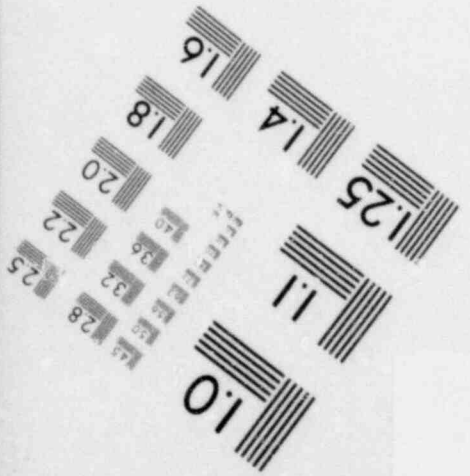

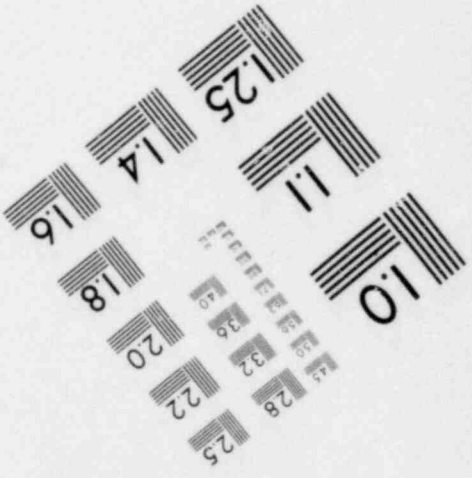

TABLE EGG-1

DESCRIPTION OF CYLINDRICAL PROPORTIONAL COUNTER DETECTORS

	1 atm H_2	2.63 atm H_2	5 atm H_2	2.63 atm CH_4	5 atm CH_4
Inside Diameter	2.46 cm	2.23 cm	2.46 cm	2.46 cm	2.23 cm
Body Length	12.7 cm	11.43 cm	12.7 cm	12.7 cm	11.43 cm
Center Wire Diameter	25.4 μm	25.4 μm	25.4 μm	25.4 μm	25.4 μm
Sensitive Length	7.62 cm	7.62 cm	7.62 cm	7.62 cm	7.62 cm
Field Tube Diameter	127.0 μm	127.0 μm	127.0 μm	127.0 μm	127.0 μm
Field Tube Lengths	2.38 cm	1.9 cm	2.38 cm	2.38 cm	1.9 cm
Sensitive Volume	36.7 cm^3	29.73 cm^3	36.7 cm^3	36.7 cm^3	29.73 cm^3
H_2 Pressure	76 cm Hg	200 cm Hg	380 cm Hg		
CH_4 Pressure	4 cm Hg	20 cm Hg	19 cm Hg	200 cm Hg	380 cm Hg
N_2 Pressure	4 cm Hg	10 cm Hg	19 cm Hg	10 cm Hg	19 cm Hg
Stainless Steel Body	40.6 μm thick	76.2 μm thick	40.6 μm thick	40.6 μm thick	76.2 μm thick
Resolution†	5% FWHM	5% FWHM	6 % FWHM	6% FWHM	8% FWHM
Minimum Energy	60 keV	120 keV	180 keV	280 keV	440 keV
Maximum Energy	350 keV	450 keV	620 keV	970 keV	2000 keV

† Full width at half maximum resulting from $^{14}N(n,p)^{14}C$ reaction at 600 keV.

TABLE EGG-2

COMPARISON OF RELATIVE FLUXES MEASURED IN PCA-PVS

Energy (MeV)	Measurement Positions			
	FACE	1/4 Thickness	1/2 Thickness	Void Box
0.10	1.00	1.00	1.00	1.00
0.12	1.18	1.25	1.52	1.85
0.14	1.21	1.47	1.89	2.12
0.16	1.36	1.53	1.82	1.84
0.18	1.48	1.78	1.95	2.09
0.20	1.59	1.69	1.82	1.90
0.23	1.73	1.95	2.22	2.40
0.26	1.90	2.20	2.70	3.25
0.30	2.18	2.78	3.20	3.35
0.35	2.40	2.95	3.30	3.35
0.40	2.31	2.80	2.80	2.45
0.45	2.50	2.85	3.13	2.60
0.50	2.80	3.09	3.35	3.03
0.55	2.83	3.30	3.75	3.55
0.60	3.30	4.00	4.57	4.04
0.65	3.82	4.30	4.50	3.70
0.70	3.53	3.83	3.55	2.75
0.75	3.41	3.17	2.80	2.00
0.80	3.52	2.88	2.73	1.85
0.85	3.60	2.82	2.70	2.03
0.90	3.55	2.87	2.51	2.01
0.95	3.35	2.86	2.35	1.85
1.00	3.20	2.75	2.29	1.67

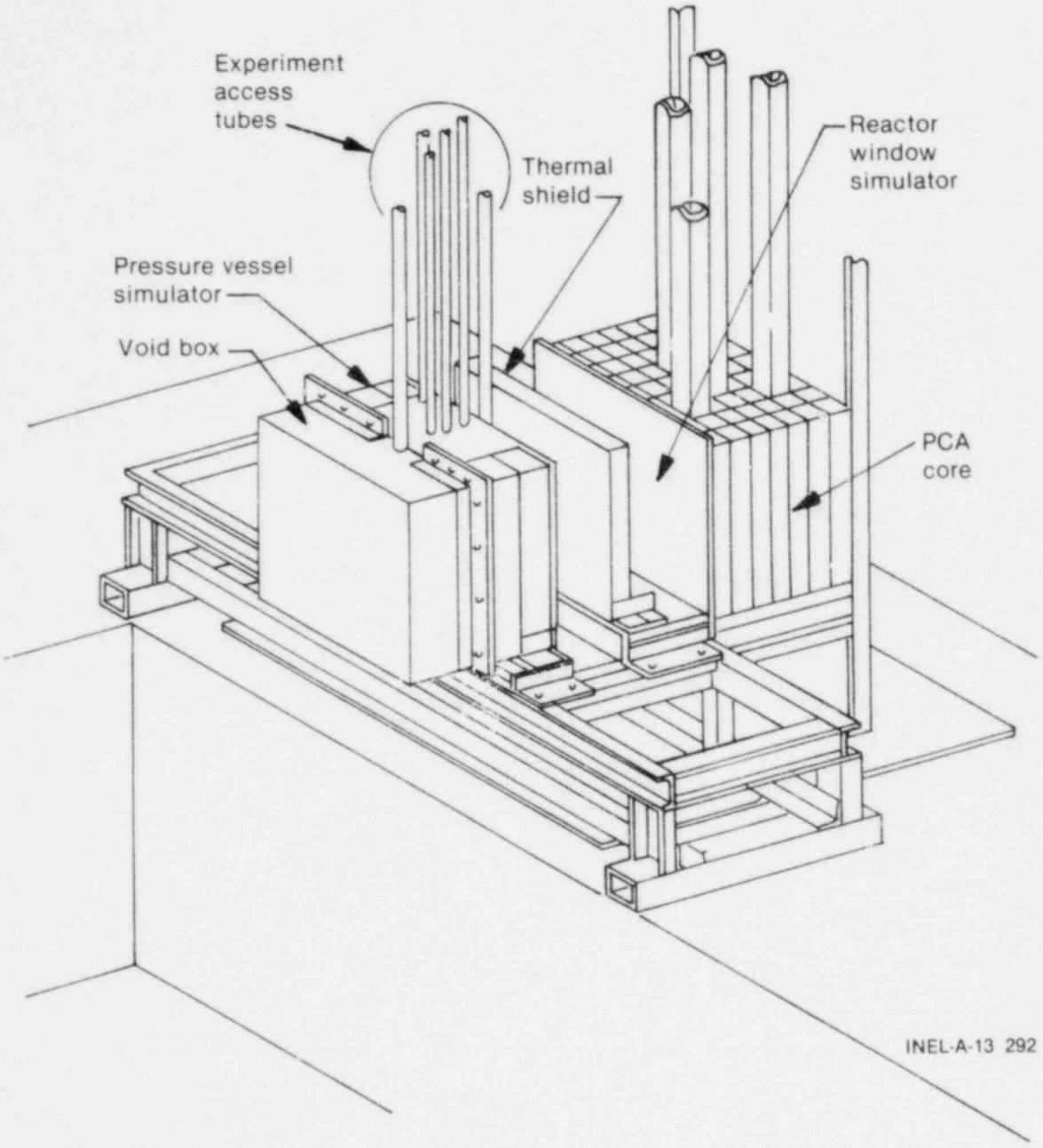

Figure EGG-1. Conceptual drawing of the PCA-PVS benchmark facility showing components and experimental access tubes.

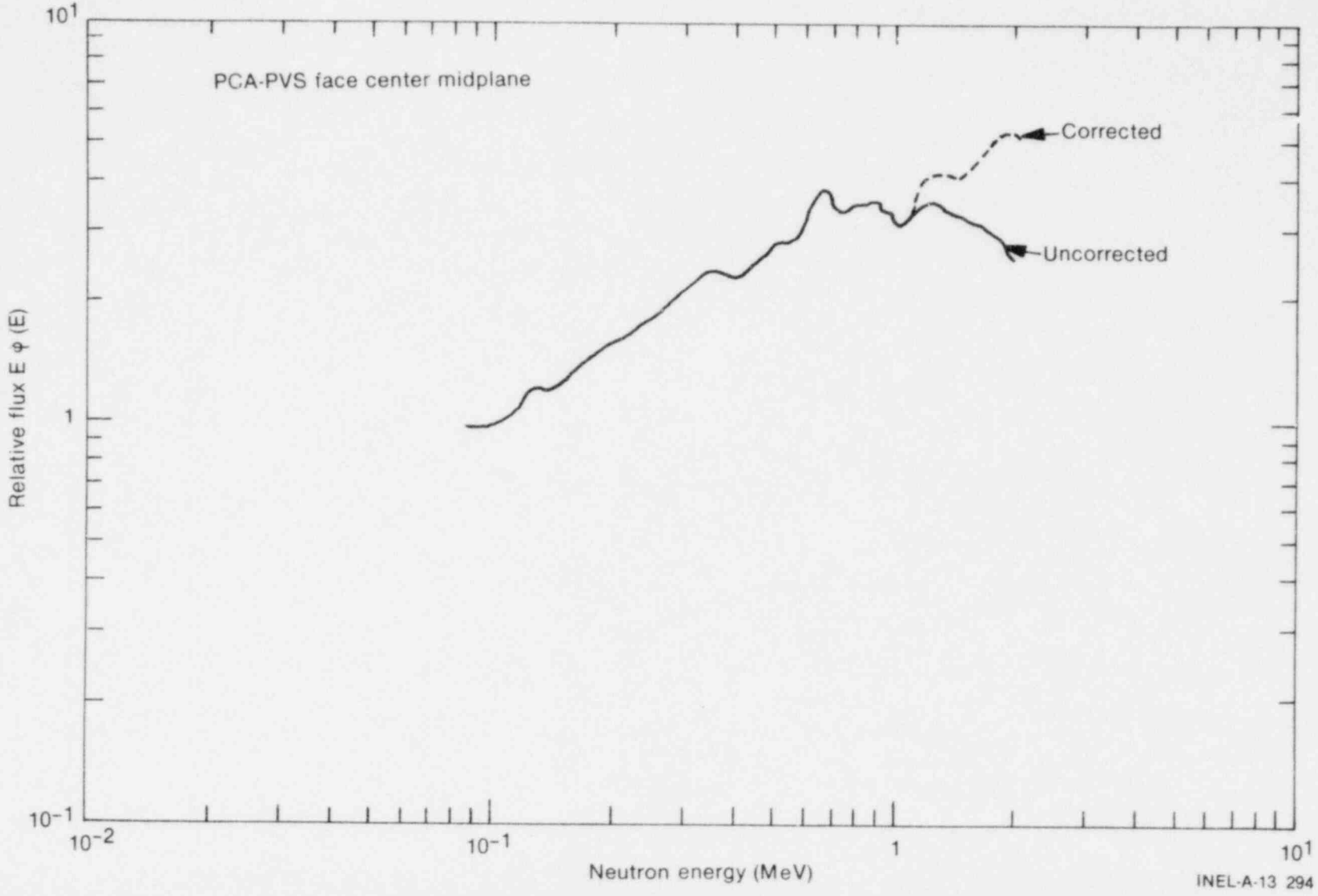

EGG-13

Figure EGG-2. Neutron energy spectrum obtained from proton-recoil measurements in the access tube at the face of the PCA-PVS.

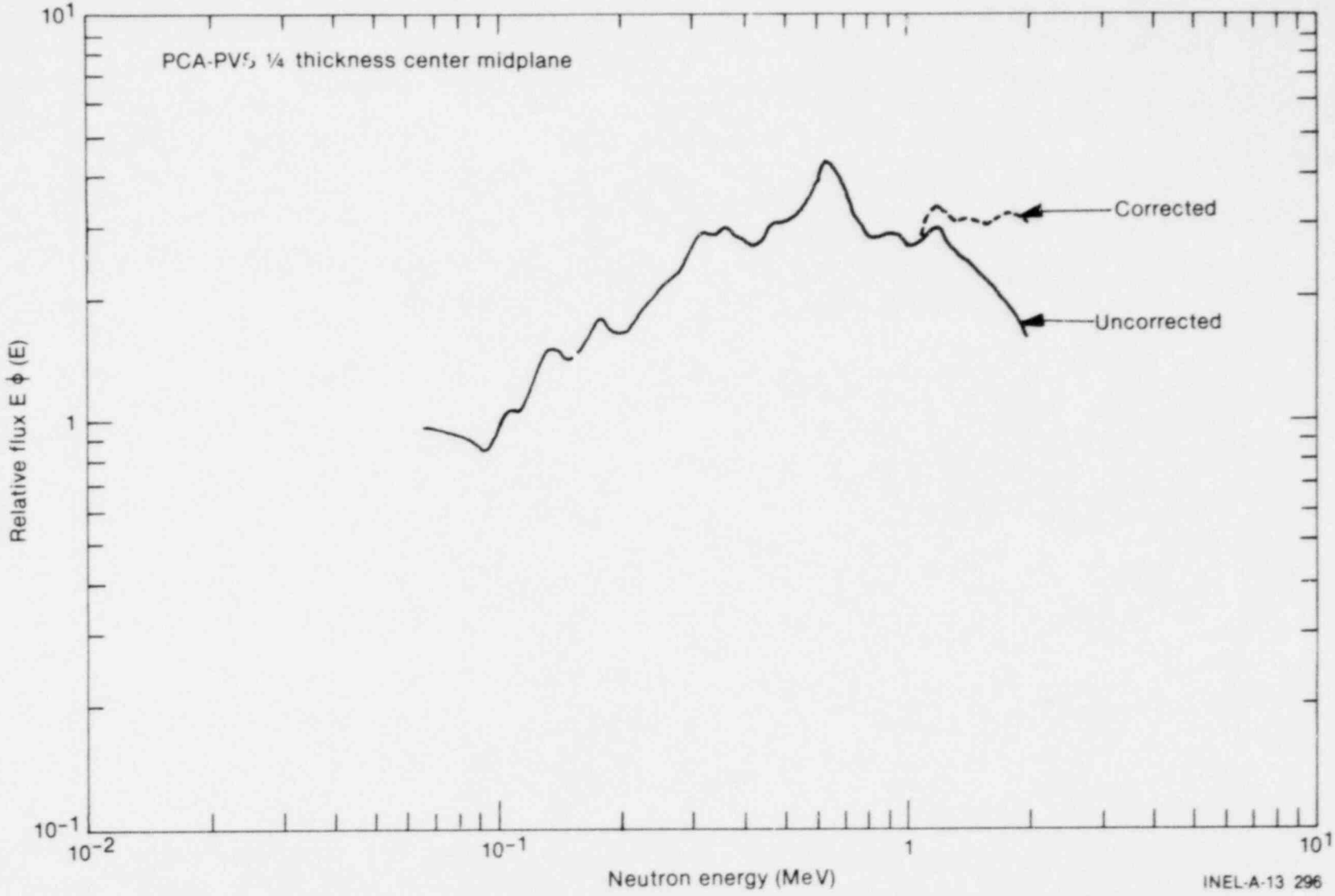

Figure EGG-3. Neutron energy spectrum obtained from proton-recoil measurements in the 1/4 thickness access tube of the PCA-PVS.

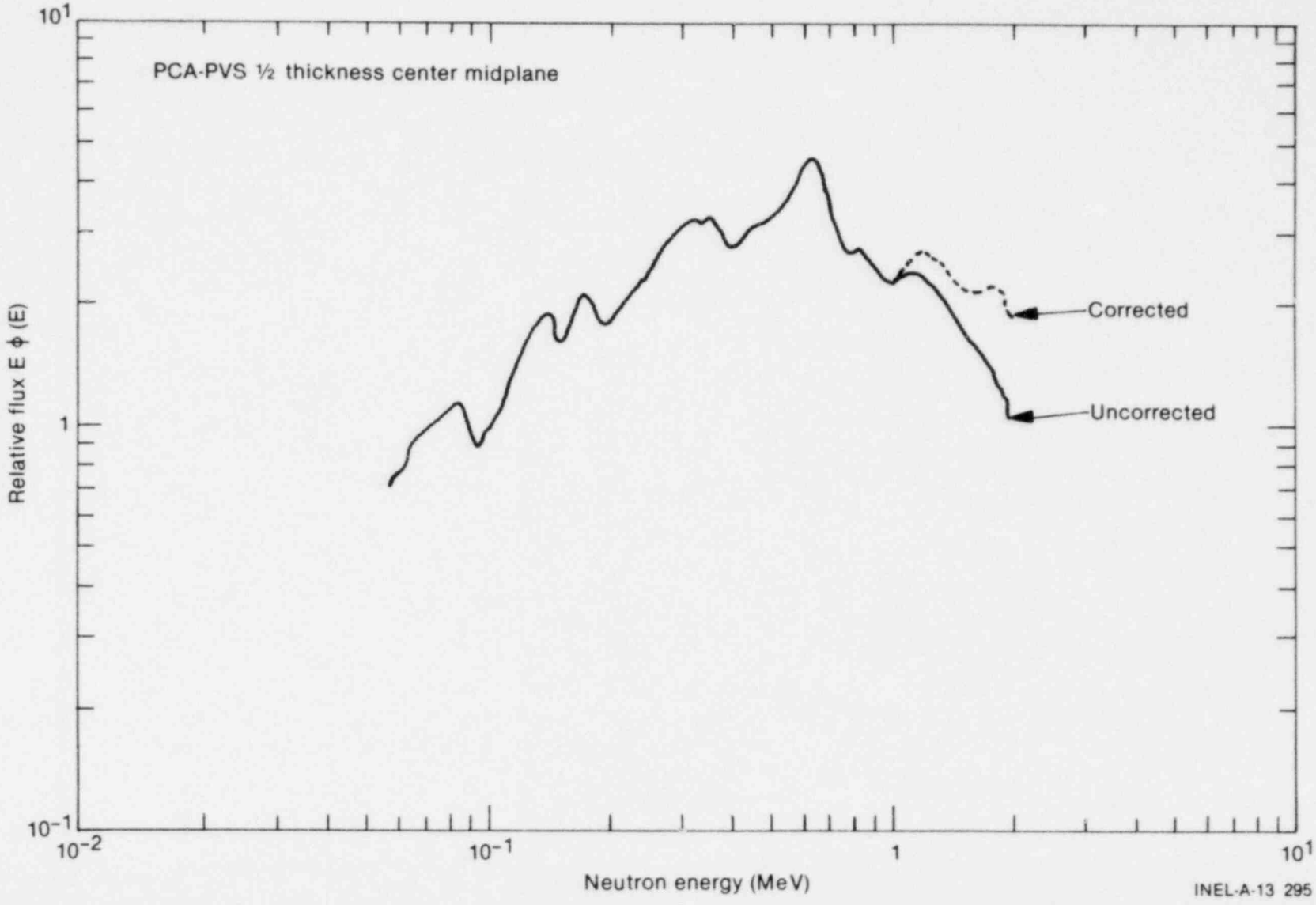

Figure EGG-4. Neutron energy spectrum obtained from proton-recoil measurements in the 1/2 thickness access tube of the PCA-PVS.

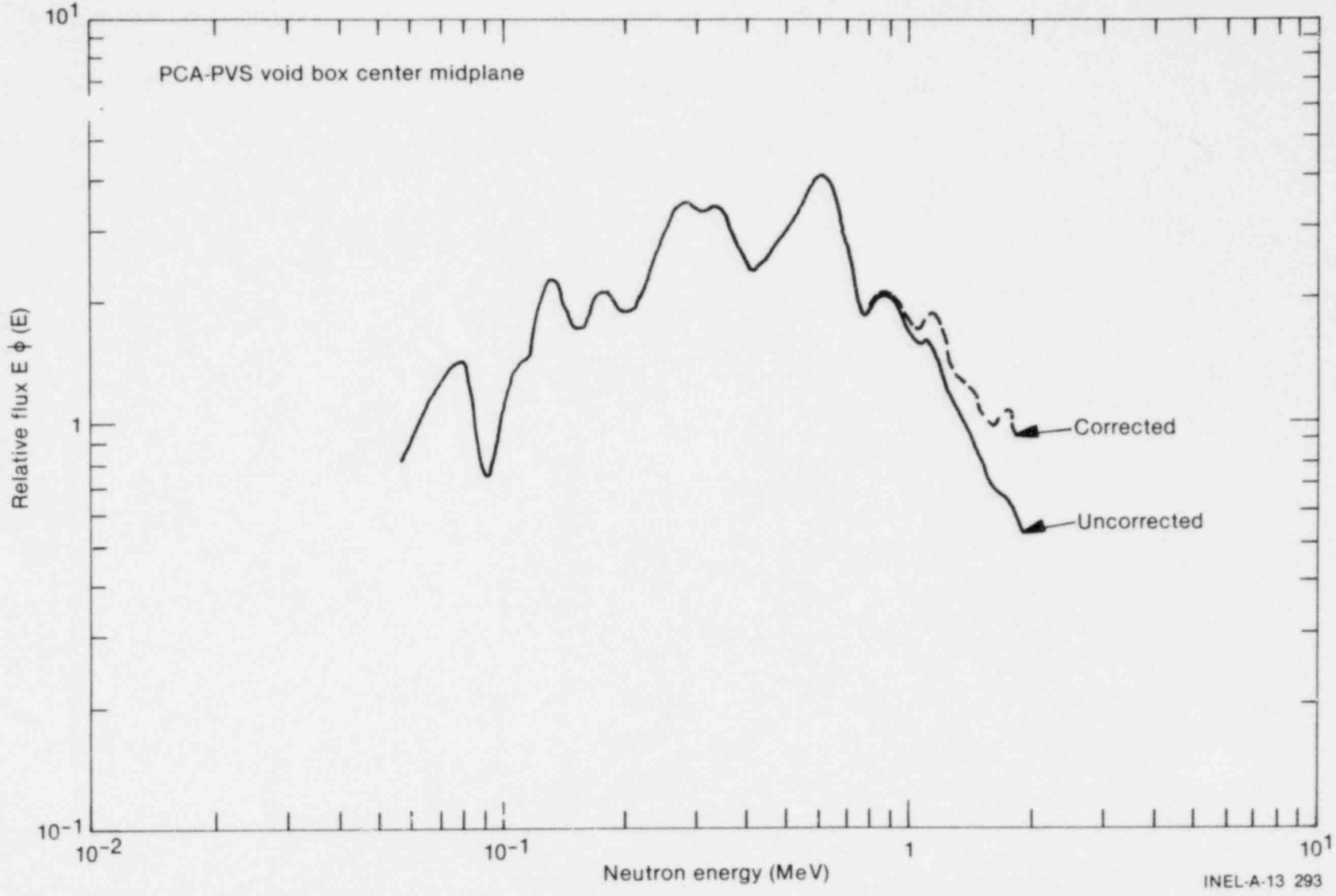

Figure EGG-5. Neutron energy spectrum obtained from proton-recoil measurements in the access tube of the PCA-PVS void box.

OAK RIDGE NATIONAL LABORATORY
(ORNL)

A. NEUTRON FIELD CHARACTERIZATION-TRANSPORT CALCULATIONS

L. F. Miller
C. A. Baldwin
R. E. Maerker
G. Minsart (CEN/SCK)
J. J. Wagschal

All transport theory calculations have been postponed to FY-81 due to lack of funding.

B. BENCHMARK FIELDS

J. A. Conlin
I. I Siman-Tov
T. M. Sims

Objectives

The objectives of this task are: 1) to validate and guide neutron transport calculations for the LWR-PV program, 2) to establish well-characterized neutron environments for the validation of dosimetry and damage correlation techniques, and 3) to demonstrate the applicability of the results in reactor pressure vessel configurations. The results of this task will have a direct impact in the preparation of ASTM Standards for Surveillance of Nuclear Reactor Pressure Vessels.

Summary

All scheduled reaction rate measurements for the PCA "Blind Test" were completed.

The structural components of the ORR poolside facility (PSF), which will simulate power reactor steel-water configurations have been completed. The dosimetry capsules for the PSF startup experiments and the PSF start-up dosimetry experiments were completed.

The two instrumented irradiation capsules (IIC), the simulated surveillance capsule (SSC) and the simulated pressure vessel capsule (SPVC) are in various stages of completion. The expected data of completion is April 1, 1980. A review of the heat transfer analysis for the capsule are complete and documentation of the heat transfer analysis is underway.

Accomplishments and Status

At the PCA, radiometric and fission chamber measurements were performed in the "Blind Test", 8/7 and 12/13 configurations. Also during the latter part of November, fission chamber checks of the core power level and fission chamber traverses in water for the PCA "Blind Test" in the 12/13 configuration were made. Further fission chamber traverses were run in the 8/7 configuration for all positions from the thermal shield front to the void box for the $^{235}U(n,f)$ reaction (cadmium covered) and checks of the reactor instrumentation linearity were made. The data from this work is being analyzed as indicated in Section C, Dosimetry and Damage Correlation Analysis, of this Quarterly Report. All scheduled experiments have now been completed at the PCA.

At the ORR-PSF, the fabrication, assembly, out-of-pool checkout, installation, and in-pool checkout of the structural support and dosimetry capsules for the simulated surveillance capsule (SSC) and the simulated pressure vessel (PV) capsule were completed. All engineering drawings were revised to reflect the as-built facility.

The questionnaire, required by ORNL's Reactor Experimental Review Committee, is essentially complete.

The results of the nuclear heating rates in iron in the 4/12 configuration are presented in Table ORNL-MOL-1. A three-dimensional heat transfer model of the nucelar heating test performed in the Oak Ridge Research Reactor Pool Side Facility (ORR-PSF) was used to compute temperatures at the thermocouple locations shown on Fig. ORNL-MOL-1. A comparison was made between the computed temperatures based on the computed heating rates and the experimental temperatures (for the 30 MW reactor power level). This comparison is presented in Fig. ORNL-MOL-1. Figs. ORNL-MOL-3 and 4 show the poster presented at the ANS 1979 Winter Meeting based on this work.

C. DOSIMETRY AND DAMAGE CORRELATION ANALYSIS

F. W. Stallmann (ORNL), A. Fabry (CEN/SCK)
J. F. Eastham

Objective

The objective of this portion of the program is to obtain reliable information from dosimetry measurements and neutron transport calculations and to correlate the spectral parameters with structural changes in reactor components. The information will be directly applicable to the preparation of several ASTM Practices for the PWR-PV Irradiation Surveillance Program.

Summary

Work performed during the reporting period in connection with this portion of the program falls into three major categories:

1. Evaluation and uncertainty analysis of the dosimetry in the PCA 8/7 and 12/13 configurations for comparison with calculated values from the PCA "Blind Test".
2. Evaluation of dosimetry in the ORR-PSF startup program for the determination of optimal irradiation times in the PSF-PV metallurgical experiment.
3. Review of the procedures used at NBS for the determination of fast fluxes in the cavity of the Arkansas power reactor. This is done in the framework of a more general review of unfolding and uncertainty analysis in commercial power reactors for the ASTM E10.05.01 Task Group on Uncertainty Analysis.

Accomplishments and Status

Raw counting data from fission chamber measurements in PCA performed by A. Fabry (CEN/SCK) and E. D. McGarry (NBS) have been transferred to DEC-10 files. These are being analyzed and summarized using computer programs which were developed earlier. The procedures are similar to those used in determination of the core power distribution (see Quarterly Report, Jan.-Mar., 1979). Raw counting data from radiometric measurements performed by A. Fabry were also transferred to the DEC-10 and processed. A first summary of the radiometric and fission chamber dosimetry which is suitable for comparison between calculated and measured data in the "Blind Test" is near completion. A more refined uncertainty analysis intercomparison with radiometric measurements from other installations will be performed later in order to reduce the uncertainty bounds.

The same procedures are being used to analyze the radiometric dosimetry in the PSF startup program. Preliminary data have been obtained, a more thorough analysis will be performed later. The data will be used to predict, in connection with the results obtained in the PCA, the flux spectra in the metallurgical capsules of the PSF metallurgical experiment. Optimal irradiation times for this experiment will be determined from these data to arrive at the correct neutron exposures for the metallurgical specimens.

In July 1979, J. A. Grundl et al, distributed a memorandum concerning the estimation of fast fluxes (>1 MeV) in the cavity of the Arkansas power reactor. The results of this paper were based on radiometric measurements and flux transfer from benchmark fission fields. In reviewing this paper, F. W. Stallmann suggested some simplifications of the procedures used and some improvements of the uncertainty analysis. A copy of this review appears in Appendix B.

Based on the ideas of the NBS paper and its review, a very general adjustment (unfolding) procedure can be constructed which operates on the logarithm of input data. In such a procedure, ratios like spectral indices and benchmark referenced reaction rates, can be handled directly. All uncertainties appear as relative accuracies as it is customary in these applications. Also the adjusted values can never become negative, as may happen with STAYSL or other linear adjustment procedures. A first version of the new adjustment code has been tested successfully. The bulk of the work on this new code will be performed in FY-81 if funds are available.

A more general paper concerning the use and impact of covariances in reactor dosimetry has been prepared by F. W. Stallmann for presentation at the meeting of the ASTM E10.05.01 Task Group on Uncertainty Analysis in New Orleans, Jan. 16, 1980. This paper addresses specifically the question about the role of the Task Group in providing guidance to researchers and practitioners in reactor dosimetry. The correct application of covariances can be important for the determination of spectral parameters and their uncertainties by means of adjustment codes. A copy of this paper is included in Appendix C.

Expected Accomplishments in the Next Report Period

The results from the PCA "Blind Test" will be evaluated and summarized. Deviations between calculated and measured reaction rates will be determined and, if possible, related to specific sources of errors (e.g. cross section library, source fission spectrum, modeling errors). Results will be ready for presentation at a meeting at NBS, May 23, 1980.

Evaluation of the PSF startup dosimetry will continue.

The PSF startup dosimetry program was completed in 18 days. The program consisted of low-, intermediate-, and full-power dosimetry runs. A. Alberman of Saclay was at ORNL three days to complete his damage monitor experiments using graphite and tungsten sensors. Mr. Alberman agreed to send the results of the damage monitor experiments by the second quarter of FY-81. A. Fabry (CEN/SCK) with the help of E. D. McGarry and ORNL staff performed the radiometric experiments. The dosimeters were removed in ORNL's hot cells and shipped to several participants (national and international) who agreed to count and report the results to A. Fabry. Some of these results are currently be analyzed by F. W. Stallmann, A. Fabry, and J. F. Eastham (see Section C).

Assembly of the SSC continued. Some minor modifications in the junction box were made to accommodate connectors in order to minimize the possibility of heater failure. A photograph of the SSC is presented in Fig. ORNL-MOL-2.

Assembly of the IIC components (heaters, coolers specimens, and filler blocks) is complete but the containment box for the SPVC is being reworked. A different fabrication procedure has been worked out which should solve the warping problem that was experienced during assembly of first unit.

Heat Transfer Analysis

The review of the heat transfer analysis for the IIC is attached as Appendix A. It was decided to enlarge the gas gap surrounding the coolant channels in the back cooler by 20% to reduce the back-heater power level.

Work has begun on a complete report describing the heat transfer analysis including associated experiments and tests.

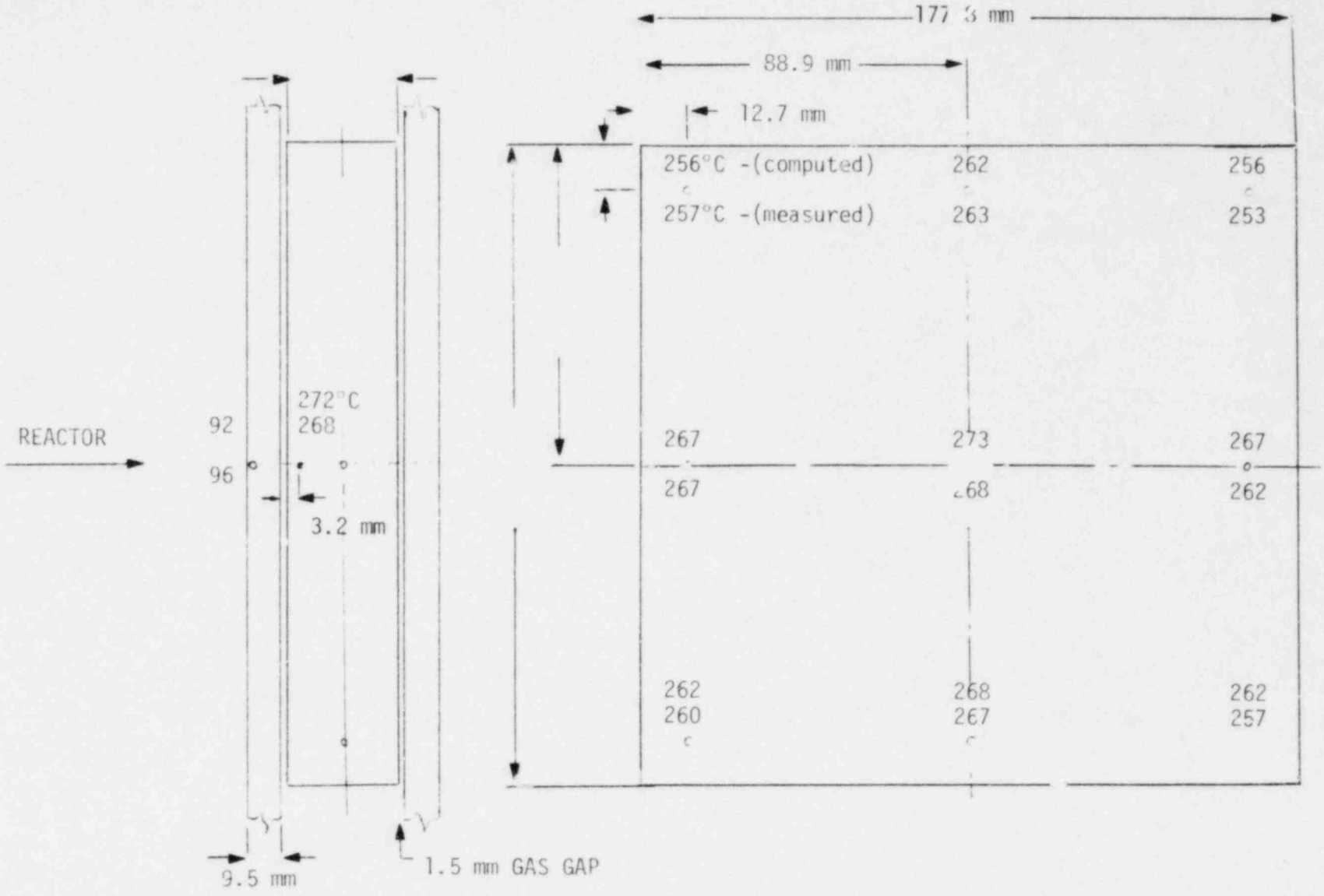

Fig. ORNL-MOL-1. Computed and Measured Temperature Distributions in the Surveillance Specimen Capsule Simulator Nuclear Heating Test.

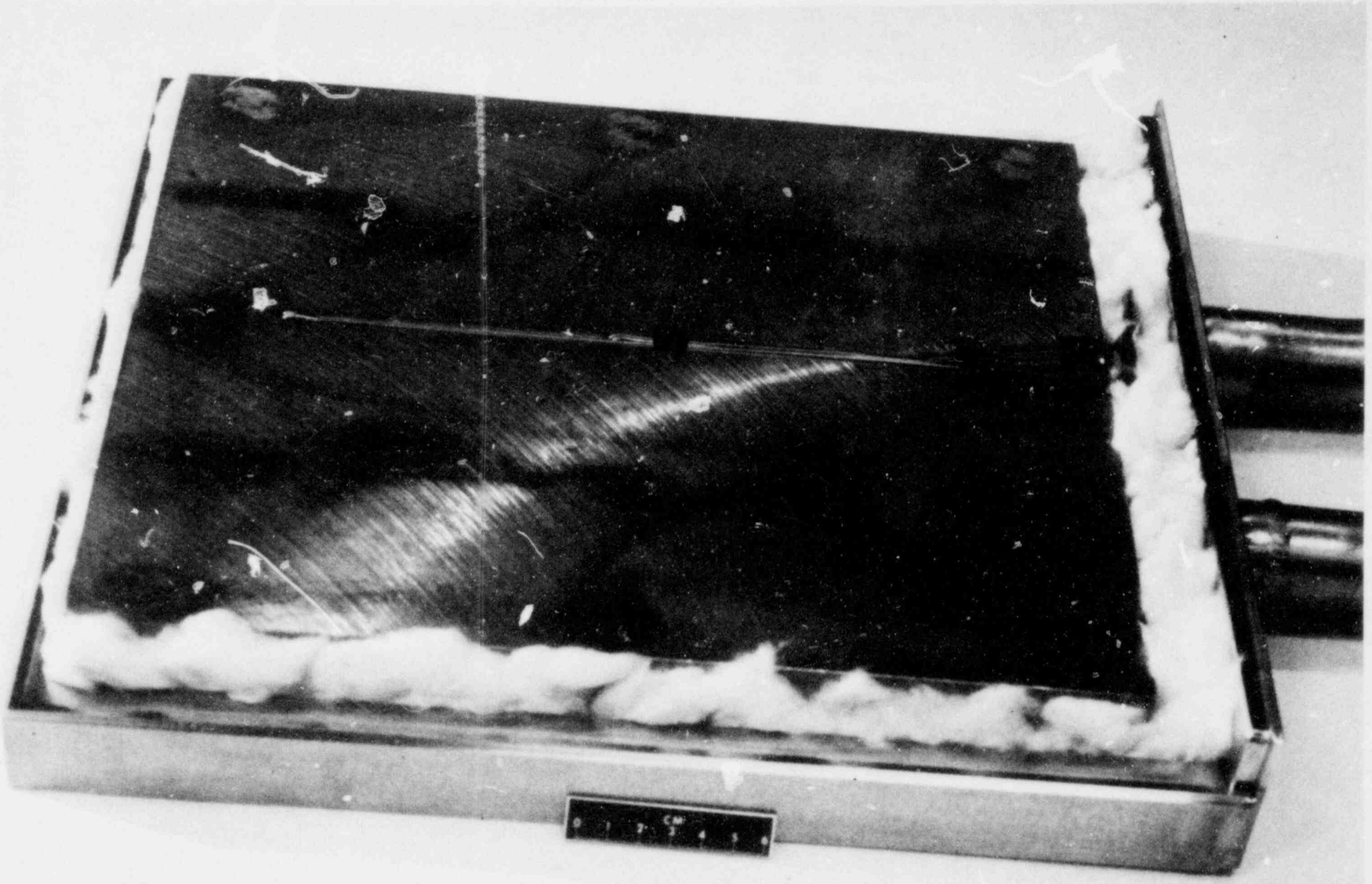

Figure ORNL-MOL-2. Simulated Surveillance Capsule

Table ORNL-MOL-1. Computed Nuclear Heating Rates in Iron for the PVS-Instrumented Irradiation Capsules.

Thermal Shield		Surveillance Specimen Irradiation Capsule		Pressure Vessel Irradiation Capsule		VEPCO Irradiation Capsule	
cm*	Watts/g	cm*	Watts/g	cm*	Watts/g	cm*	Watts/g
0.0	2.020	6.9	0.254	18.0	0.0739	70.49	0.0013
0.304	1.693	7.304	0.227	18.304	0.0668	70.804	0.0013
0.804	1.373	7.804	0.2	18.804	0.0578	71.304	0.0014
1.304	1.156	8.304	0.176	19.304	0.05	71.804	0.0015
1.804	0.970	8.804	0.157	19.804	0.0428	72.304	0.0017
2.304	0.817	9.304	0.141	20.304	0.0366	72.943	0.0021
2.804	0.691	9.804	0.128	20.804	0.0313		
3.304	0.587	10.304	0.118	21.304	0.0268		
3.804	0.501	10.804	0.110	21.804	0.0229		
4.304	0.431	11.401	0.101	24.554	0.0123		
4.804	0.374			27.554	0.0043		
5.304	0.326			28.554	0.0033		
5.75	0.291			29.554	0.0026		
				30.554	0.0021		
				31.554	0.0017		
				33.054	0.0013		
				34.304	0.0010		
				34.804	0.0010		
				35.304	0.0009		
				35.804	0.0009		
				36.304	0.0008		
				36.804	0.0008		
				37.304	0.0008		
				37.804	0.0008		
				38.304	0.0009		
				38.804	0.0009		
				39.304	0.001		
				39.804	0.001		
				40.240	0.0012		

*Distance from front of thermal shield.

Accurate knowledge of nuclear heating rates in thick iron slabs in the test facility was of crucial importance for a successful design.

Available coupled neutron-gamma libraries proved inadequate for reliable prediction of nuclear heating rates in thick iron slabs where secondary gamma reactions in iron become important.

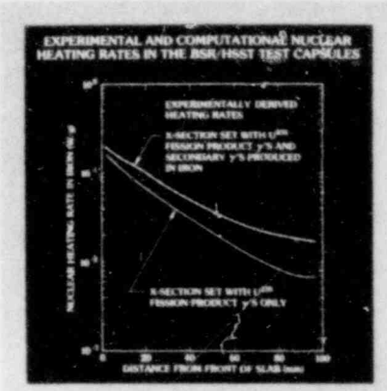

1-D cylindrical model f
heating rates in iron fo

Surveillance Specimen Simulator Capsule (SSC) (I, II):

Contains one matrix of test specimens to be irradiated at 288° C ± 10° C.
Capsule thickness is 50 mm.
Irradiation time is ~ 1 month for capsule I.
Irradiation time is ~ 2 months for capsule II.
A dummy capsule will be inserted for the remaining period.

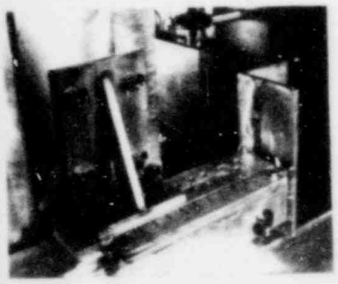

Pressure Vessel Wall Simulator Capsule (PVS):

Contains metallurgical test specimens to be irradiated at 288° C ± 10° C.
Capsule thickness is 225 mm.
Irradiation time is two years.

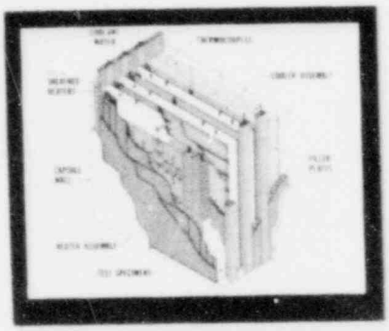

Metallurgical Specimens

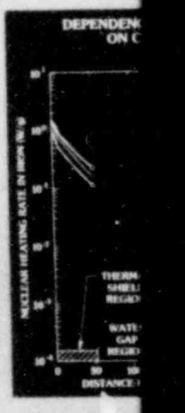

ORNL-MOL-15

Fig. ORNL-MOL-3. Nuclear Heating Rates in

COMPUTATIONAL

EXPERIMENTAL

XSDR[illegible]" calculation of nuclear
the Pr[illegible] Vessel Simulators.

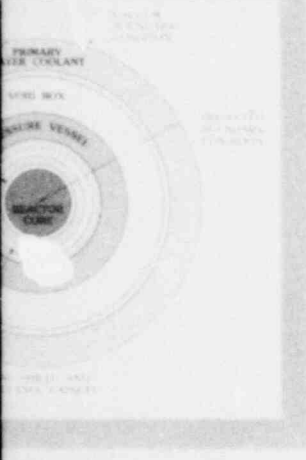

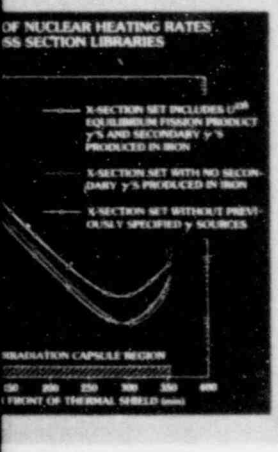

3-D XYZ Heat Transfer model of the SSC simulator using the heat generation rates obtained in the parametric study.

Surveillance Specimen Capsule Simulator.

Computed temperature distribution at 30 MW reactor power with helium as filler gas.

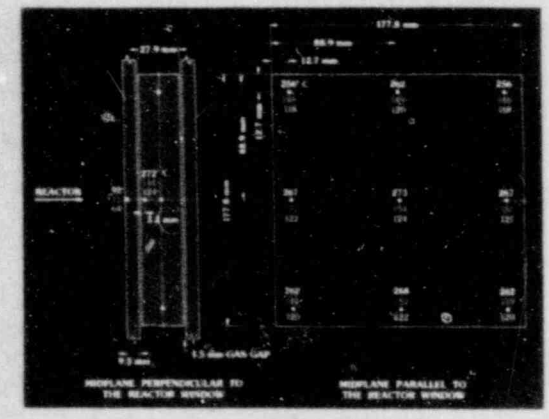

Resulting temperature distribution at 30 MW reactor power with helium as filler gas.

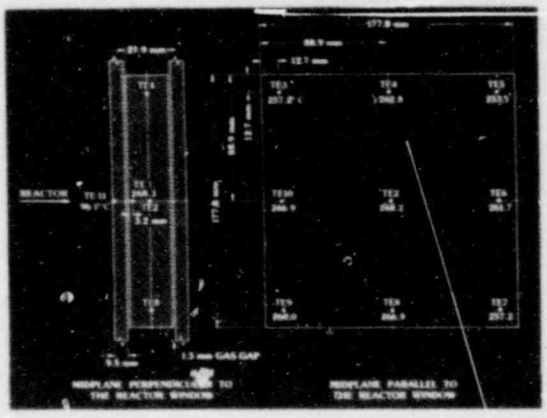

CONCLUSION

Reliable nuclear heating rates in thick iron slabs can be computed when all important gamma sources are taken into account.

LWR Pressure Vessel Irradiation Capsules.

APPENDIX A

APPENDIX A

Evaluation Analysis of the Pressure Vessel Irradiation Capsule

Pertinent calculations have been made in the analysis of the pressure vessel irradiation capsule (PVIC). The purpose of the experiment is to irradiate steel specimens at a specified temperature of 550°F at the neutron flux in the poolside facility of the Oak Ridge Research Reactor (ORR). The objectives of the analysis are (1) to evaluate the capability of each heater to produce a temperature of 550°F in three groups of test samples under the specified conditions and (2) to verify that the specified sample temperature will not be exceeded with the heaters turned off while subjected to the maximum cooling conditions. The irradiation assembly is shown pictorially in Fig. 1. The heat transfer model that was used in this analysis is shown in Fig. 2 using dimensions taken from the construction drawings. The heat sources in the experiment are the six electrical heaters plus the heat generated from the absorption of gamma energy in the assembly. The heat sinks are the 24 coolant tubes located in the three coolers and the pool water in contact with the exterior surfaces of the assembly.

Results of Analysis (Summary)

Calculations indicate that a total of 3433 watts is deposited in the assembly from the absorption of gamma energy from the ORR. Using helium as a cover gas, 13.54 kW of electrical power is required to keep the samples at the required temperature of 550°F. The specified two gpm flow rate of 90°F pool water to each of the three coolers removes 77% of the heat with the remainder being removed by natural convection from the exterior faces of the capsule. If neon is substituted as a cover gas, only 3.98 kW watts of electrical power are required to keep the samples at temperature where 64.8% of the heat is removed by forced convection. The total required electric

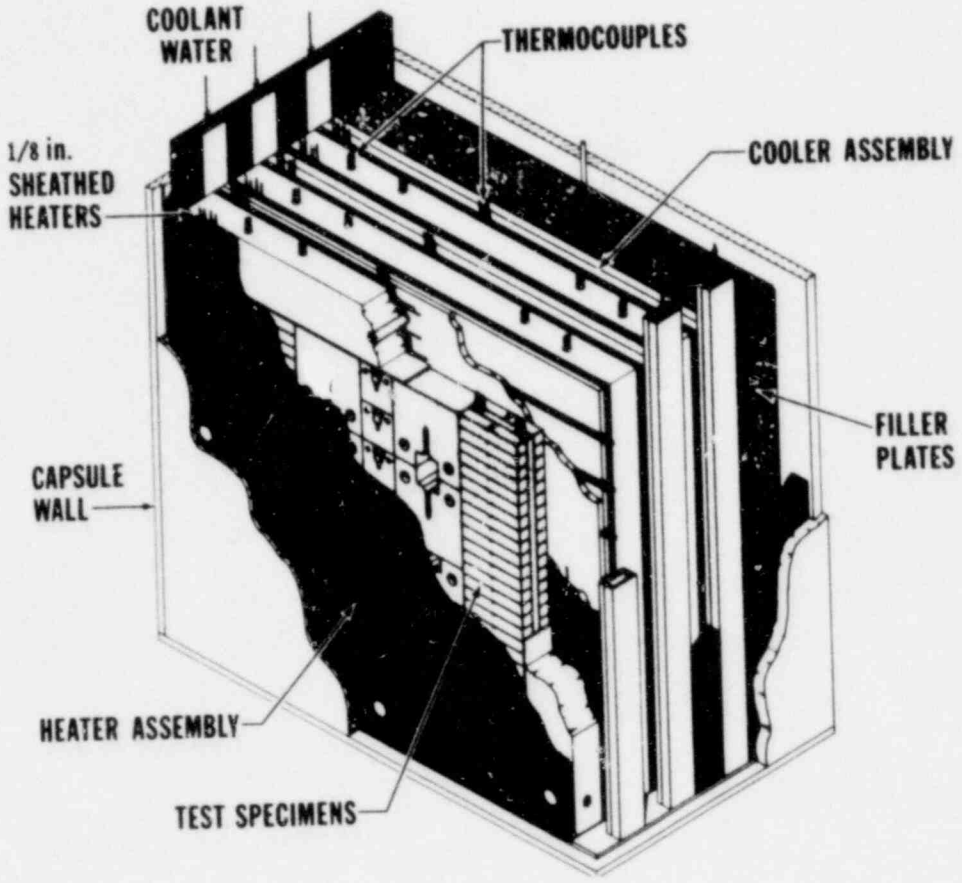

Figure 1. Pictorial View of Irradiation Assembly

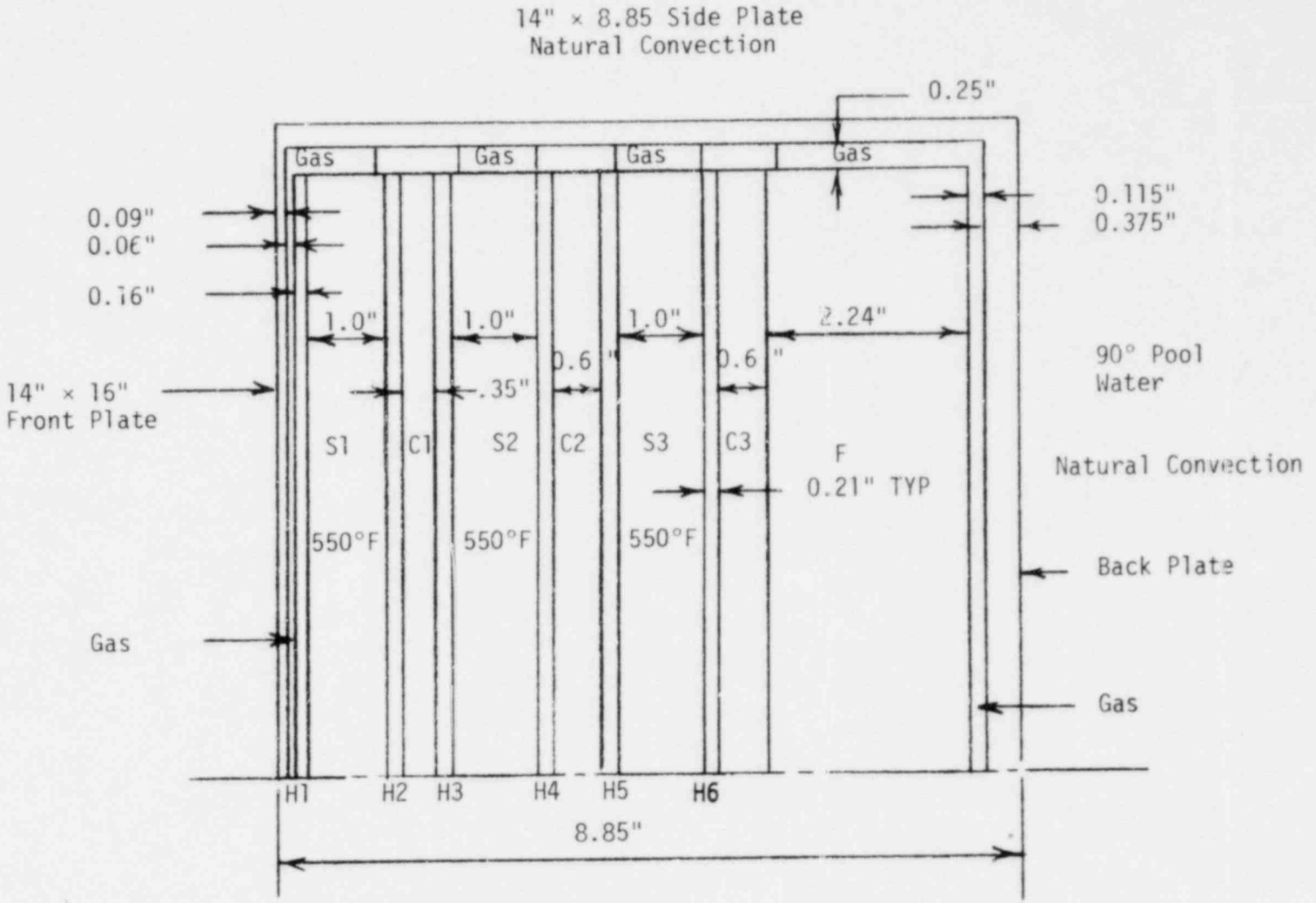

S1, S2, S3 = samples
C = cooler plates
H = heater plates
F = filler plates

Material: Carbon Steel

Figure 2. Heat Transfer Model Used in Analysis

power available for heating is 45 kW. The required and available power distribution to each of the six heaters in the assembly is summarized in Table 1.

TABLE 1. REQUIRED AND AVAILABLE ELECTRIC POWER DISTRIBUTION IN THE ASSEMBLY

Heater	Heater Power, Watts Required Helium	Heater Power, Watts Required Neon	Heater Power, Watts Available
1	2,136	1,125	7,500
2	1,572	144	7,500
3	1,831	402	7,500
4	1,787	358	7,500
5	1,966	537	7,500
6	4,253	1,411	7,500
Total	13,543	3,978	45,000

With the heaters turned off, the maximum expected sample temperatures using helium as a cover gas is 208°F at the front cooler, 161°F at the center cooler, and 0°F at the rear cooler. Using neon as a cover gas, sample temperature of 492°F is expected at the first cooler, 350°F at the middle cooler, and 127°F at the rear cooler.

Design Parameters

Specimen box dimensions:

Height = 16 in.

Length = 14 in.

Depth = 8.85 in.

Heat transfer area (front or back) = 1.56 ft^2

Heat transfer area (each side) = 0.98 ft^2

Heat transfer area (bottom) = 0.86 ft^2

Coolant = 90°F pool water
Flow rate = 6 gpm (2 gpm per cooler)
Eight coolant channels per cooler
Channel diameter = 0.2285 in.
Channel length = 14.25 in.
Channel tube = 0.1875 in. OD x 0.1315 in. ID
Gas annulus = 0.1875 in. ID x 0.2775 in. OD
Emissivity of steel (100° = 0.4; 600° = 0.6)
Gas = helium or neon
Number of heater = 6
Number of coolers = 3
Maximum allowable increase in bulk water temperature = 15°F
Desired sample temperature 550°F

Heat Generation

The irradiation capsule is placed in the ORR poolside facility behind a thermal shield and a surveillance capsule. The gamma heat was calculated by I. I. Siman-Tov, using the EXCEDRIN-PM computer program. The results of this program are shown in Fig. 3, with the gamma heat rate in steel shown as a function of the distance through the capsule from the edge nearest the reactor. The integrated values from the results of this analysis have been summed up for each component region in the capsule assembly and tabulated in Table 2. The total heat produced in the component region by gamma absorption is 3433 watts.

Heat Transfer by Forced Convection to the Coolant Tubes

The hear loss to both the cooler and to the pool is governed by the choice of using either helium or neon as a cover gas for the assembly. The thermal conductivities of these gases are shown in Fig. 4 as functions of temperature. The conductivity of helium is roughly three times the conductivity of the neon. The pool water temperature is assumed to be 90°F and is supplied to each of the three coolers at a rate of 2 gpm.

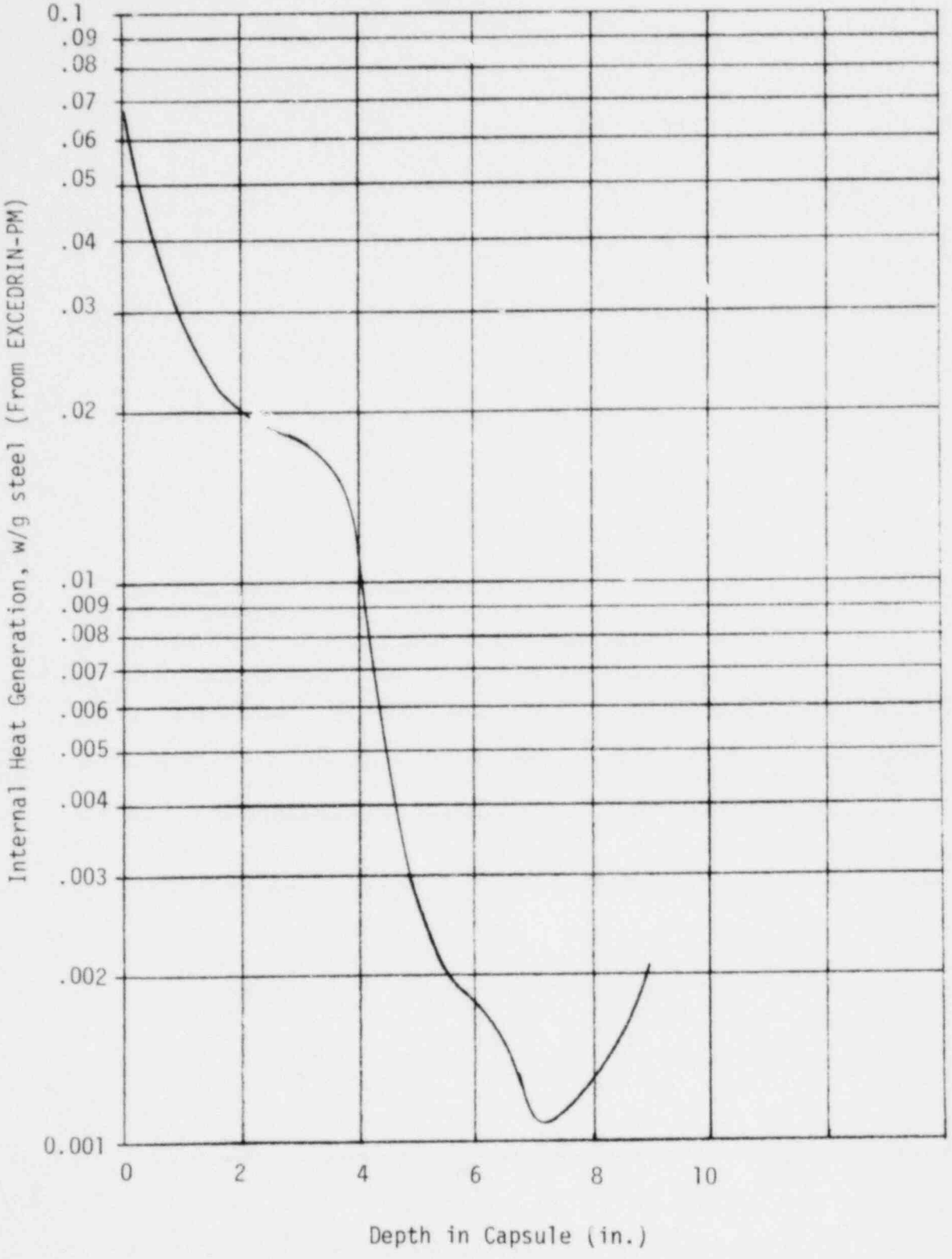

Figure 3. Internal Heat Generation as Function of Depth into Experiment

Table 2. ESTIMATED GAMMA HEAT PRODUCTION FROM EXCEDRIN-PM

Region	Weight (gm)	q''' (w/gm)	Heat (Watts)	Symbol
0.090 wall	2,643	0.0625	165	GI
Heater-HI	4,698	0.0535	251	G2
Specimen-SI	29,361	0.0350	1,028	G3
Heater-H2	6,225	0.0220	137	G4
Cooler-C1	10,276	0.0200	206	G5
Heater-H3	6,225	0.0195	121	G6
Specimen-S2	29,361	0.0185	543	G7
Heater-H4	6,225	0.0183	114	G8
Cooler-C2	17,617	0.0175	308	G9
Heater-H4	6,225	0.0170	106	G10
Specimen-S3	29,351	0.00685	201	G11
Heater-H6	6,225	0.0023	14	G12
Cooler-C3	17,617	0.0020	143	G13
Spacer-1	33,853	0.0011	37	
Spacer-2	32,033	0.00125	40	G4
0.375 wall	11,010	0.00175	19	
Total	248,955	0.0227	3,433	

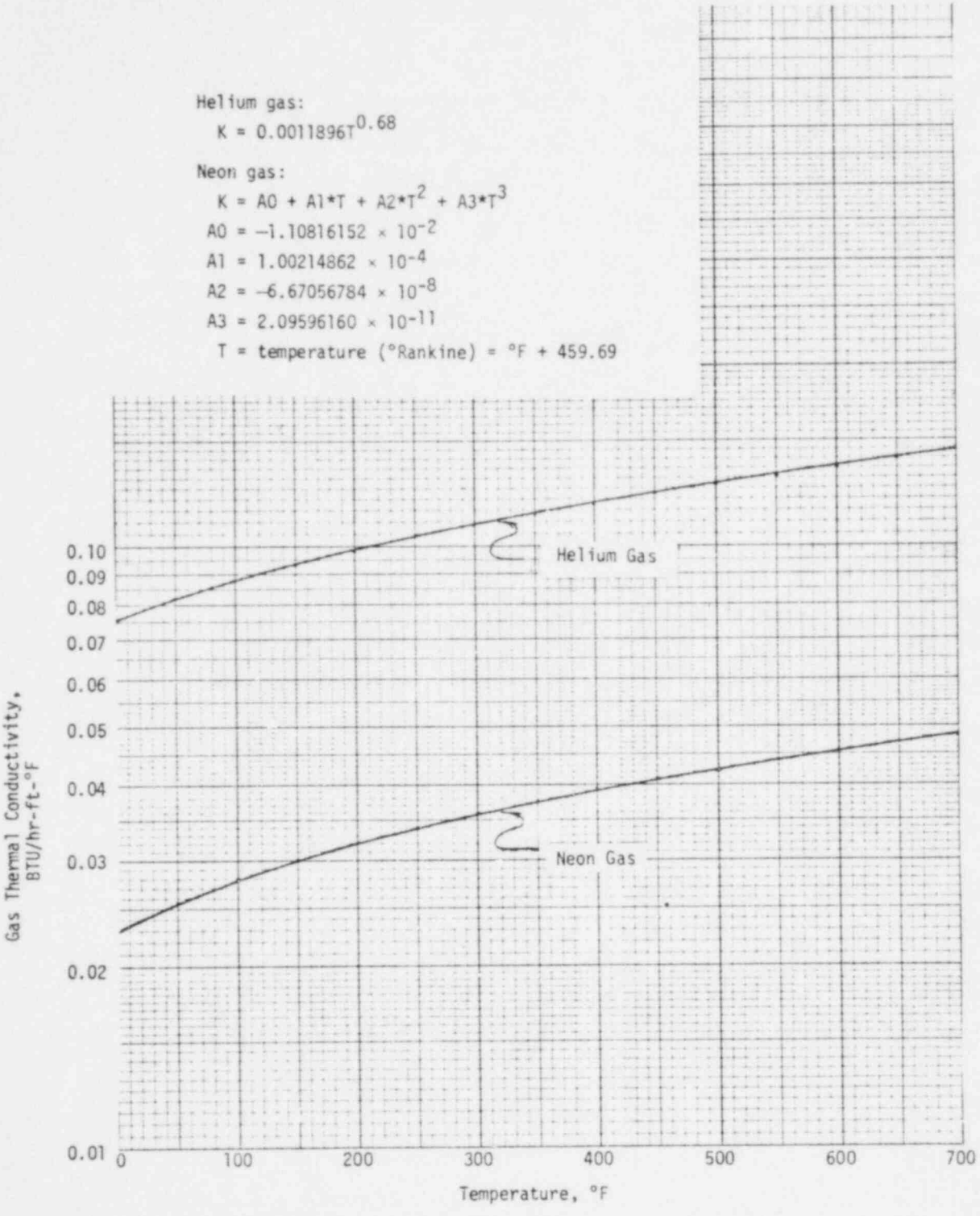

Figure 4. Thermal Conductivity of Helium and Neon as a Function of Temperature

Each cooler has eight coolant channels with a water flow rate of 0.25 gpm per channel. The coolant tubes are concentrically located in the holes drilled in the split cooler block as shown in Fig. 5. A heat balance is formulated on the cooler equating the heat absorbed by the coolant stream to the overall heat transferred to the coolant from the cooler wall which is assumed to be at the desired temperature of 550°F. The pool water enters the tube at a temperature, TC, and leaves at a temperature, TH. The heat transfer coefficient is based on the mean bulk water temperature, TB, and a constant flow rate, W, is used to evaluate the film drop and the temperature, T1, on the inside tube wall. The T across the tube wall is calculated and added to T1 to obtain the outside wall temperature, T2, which is the temperature of the inner gas annulus. Heat is transferred across the gas annulus by mechanisms of both conduction and radiation to produce the cooler wall temperature, TW. Iterative calculations are made to select a coolant outlet temperature, TH, that will produce the specified wall temperature of 550°F. The heat loss from each cooler is the same provided the wall temperature and the resistances are the same; therefore, the total heat loss by forced convenction is calculated by multiplying the heat loss from a single tube by 24. The calculated heat loss to a tube is 545 watts when using helium as a cover gas and 200 watts when neon gas is used. The specified maximum heat rate based on the maximum allowable temperature rise is 547 watts. The Dittus-Boelter correlation was used to calculate the water film coefficent rather than the Sider-Tate or Colburn correlations since this calculation is being used to evaluate a heat loss and is conservative in this case. The calculated rise in the bulk water temperature is 14.98°F when using helium as a cover gas and 5.50°F when using neon gas compared to the maximum allowable rise of 15°F, A 5-mil spacer wire is wrapped around the outside of each of the cooler tubes on a 1 1/2 in. pitch. The effect of this wire has been ignored in these calculations and, though not conservative, contributes only slightly to the heat loss.

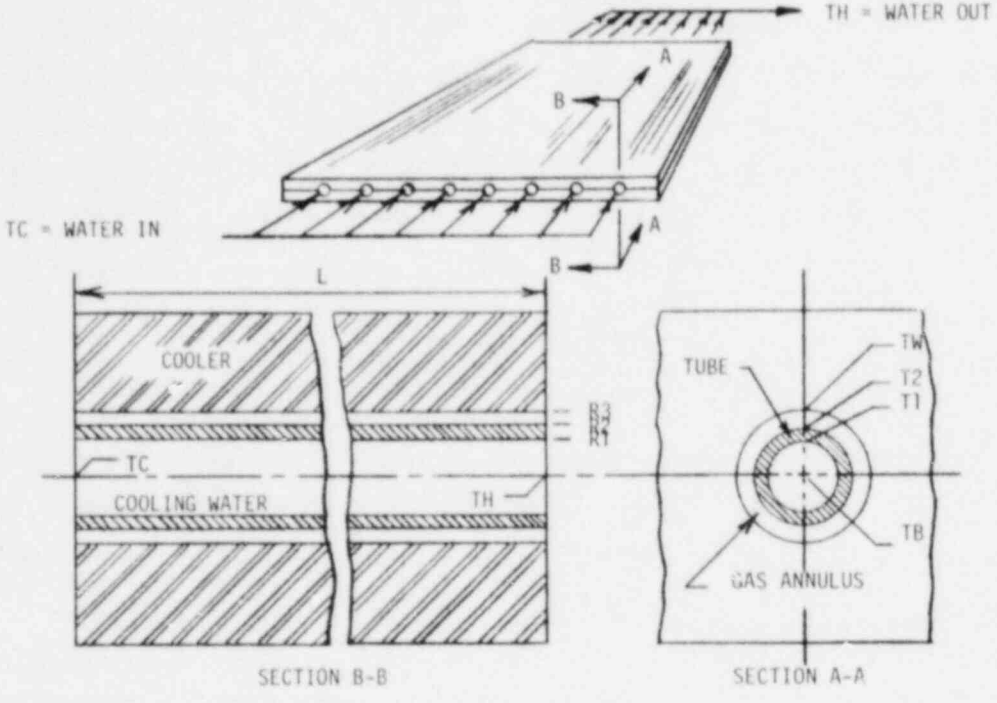

TW = Wall temperature = 550°F

T2 = Outside tube temperature

T1 = Inside tube temperature

TC = Water supply temperature = 90°F

TH = Water discharge temperature

TB = Avg water temperature
= (TH + TC)/2

TM = Avg tube wall temperature
= (T1 + T2)/2

TG = Avg gas temperature
= (TW + T2)/2

H = Water film coef. = f(TB)

$\epsilon 1$ = Emissivity at T2

$\epsilon 2$ = Emissivity at TW

Q = Total heat transferred

W = Mass flow rate of coolant

CP = Specific heat of coolant

KM = Thermal cond. of tube = f(TM)

KG = Thermal cond. of gas = f(TG)

$\sigma = 0.173 \times 10^{-8}$

F = Shape fac = $1/[1/\epsilon 2 - R2/R3(1/\epsilon 1 - 1)]$

TR2 = TW + 459.7

TR1 = T2 + 459.7

$QR = 2\pi \cdot R2 \cdot L(TR2^4 - TR1^4)$

$Q = 2\pi \cdot H \cdot R1 \cdot L(T1 - TB)$

$Q = 2\pi \cdot KM \cdot L(T2 - T1)/\ln(R2/R1)$

$Q = 2\pi \cdot KG \cdot L(TW - T2)/\ln(R3/R2) + QR$

Q = WCP(TH - TC)

FIGURE 5. Heat Transfer in Coolers

Heat Transfer by Natural Convection

Heat transfer to the pool water from the external surfaces of the specimen box by natural convection was calculated and compared with experimental correlations obtained in the ORR pool. The natural convection correlation yielded a slightly higher heat flux for a given temperature differential attributed to the fact that there is a mild forced slow moving downward, inhibiting the natural upward flow on the vertical surfaces. The distribution of the calculated heat loss using helium gas is 23% by natural convection where 75% is lost through the front plate, 22% from the sides and bottom, and only 3% from the back plate. If neon is used as the cover gas, 35% of the heat is removed by natural convection with the same distribution as was calculated when using helium as the cover gas. These solutions were obtained by equating the heat loss by free convection, using either the experimental values or natural convection correlations, to the heat transferred across the gas gaps by iteration on the adjacent gas wall temperature to the 550°F sample temperature using either helium or neon gas in the annulus. These calculations were programmed where any of the parameters could be changed. In the final analysis (shown in Fig. 6), it was decided to use the experimental correlation for the poolside heat loss which was considered more reliable although less conservative. The calculations included radiation heat transfer with the shape factor taken as one over the sum of the reciprocal emissivities. Radiation contributed to less than 2% of the heat transfer from the walls. The poolside wall temperature on the front surface using helium as a cover gas is 134°F and 124°F using neon. The side walls are 108°F with helium an 100°F with neon.

Heat Balance

The heat sources and sinks are shown in Fig. 7 using helium as a cover gas. The heat is transferred from the sources to the pool directly by natural convection off the surface of the box and through the coolers by forced convection. Several simplifying but reasonable asumptions have been made. It is assumed that equal amounts of heat are removed from each of the

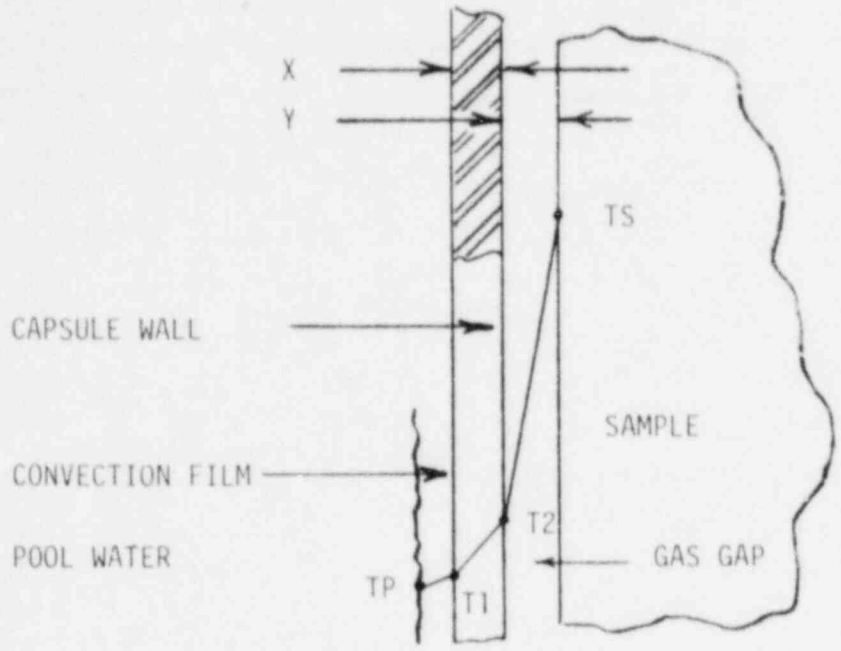

Q = Heat

A = Heat transfer area

Q'' = Flux = Q/A

TP = Pool water temperature = 90°F

T1 = Inside capsule wall temperature

T2 = Outside capsule wall temperature

TS = Sample temperature = 550°F

H = Heat transfer coef. = f(Q'')

TR1 = T2 + 459.7

TR2 = TS + 459.7

$\varepsilon 1$ = Emissivity at T2

$\varepsilon 2$ = Emissivity at TS

$F = (1/\varepsilon 1 - 1/\varepsilon 2 - 1)$

σ = Steffan Boltzman constant $= 0.173 \times 10^{-8}$

TM = (T1 + T2)/2

TG = (T2 + TS)/2

KM = Thermal condition of wall = f(TM)

KG = Thermal condition of gas = f(TG)

$QR'' = \sigma F[TR2^4 - TR1^4)$

Q'' = [KG(TS - T2)/X] + QR''

Q'' = KM(T2 - T1)/Y

Q'' = H(T1 - TP)

FIGURE 6. Natural Convection Poolside Heat Transfer

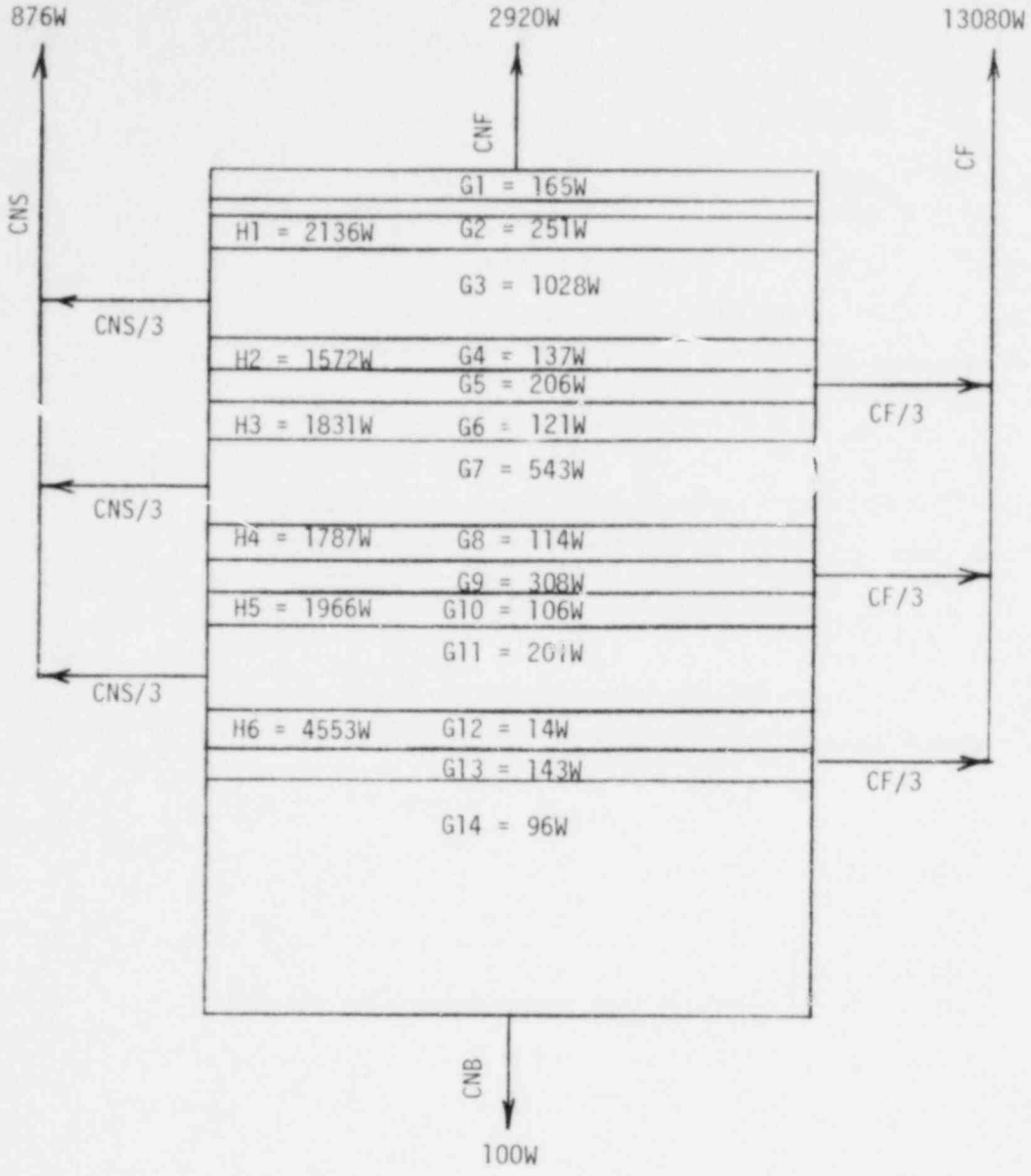

CF = forced cooling

CNF = nat. convection, front face

CNS = nat. convection, bottom and sides

CNB = nat. convection, back face

G = gamma heat

H = heater

Summary

Total heat loss by forced cooling = 13080W

Total heat loss by natural convection = 3896W

Total internal heat generation = 3433W

Total electric power required = 13543W

FIGURE 7. Helium Cover Gas

cooler tubes. Since the resistance is practically the same and there is less than 2% difference in the thermal gradient, the assumptions made seem adequate. It is also assumed that the heat losses from the bottom and sides can be split equally between each of the six heaters. This really is not so bad since natural convection involves only a small amount of the total heat and the fortunate situation is that, even though each of the heaters are supplied with power at different rates, most of the material is at one temperature. A similar analysis was made on the assembly using neon as a cover gas as illustrated in Fig. 8. Both of these systems were programmed for the calculation of the power requirements to each of the heaters by performing energy balances on the system. The heat balance that was used for both models is as follows using the symbols shown in the illustrations.

$$H1 = CNS/6 + CNF - G1 - G2 - G3/2$$
$$H2 = CF/6 + CNS/6 - G3/2 - G4 - G5/2$$
$$H3 = CF/6 + CNS/6 - G6 - G7/2 - G5/2$$
$$H4 = CF/6 + CNS/6 - G7/2 - G8 - G9/2$$
$$H5 = CF/6 + CNS/6 - G9/2 - G10 - G11/2$$
$$H6 = CF/3 + CNS/6 + CNB - G12- G13 - G14 - G11/2$$

Heaters

The heaters are fabricated from 62.5 mil nichrome wire. Each heater is composed of six curcuits containing 49 in. of heater wire and four circuits containing 39 in. of heater wire. The circuits are connected in parallel with a rated resistance of 1.01 ohms/lineal foot at 68°F. The power to the heaters is regulated by variation of the voltage using a constant amperage. The design power rate to the heaters is 400 W/ft providing a maximum power to each heater of 7500 watts and a total maximum electric power input to the assembly of 45 kW.

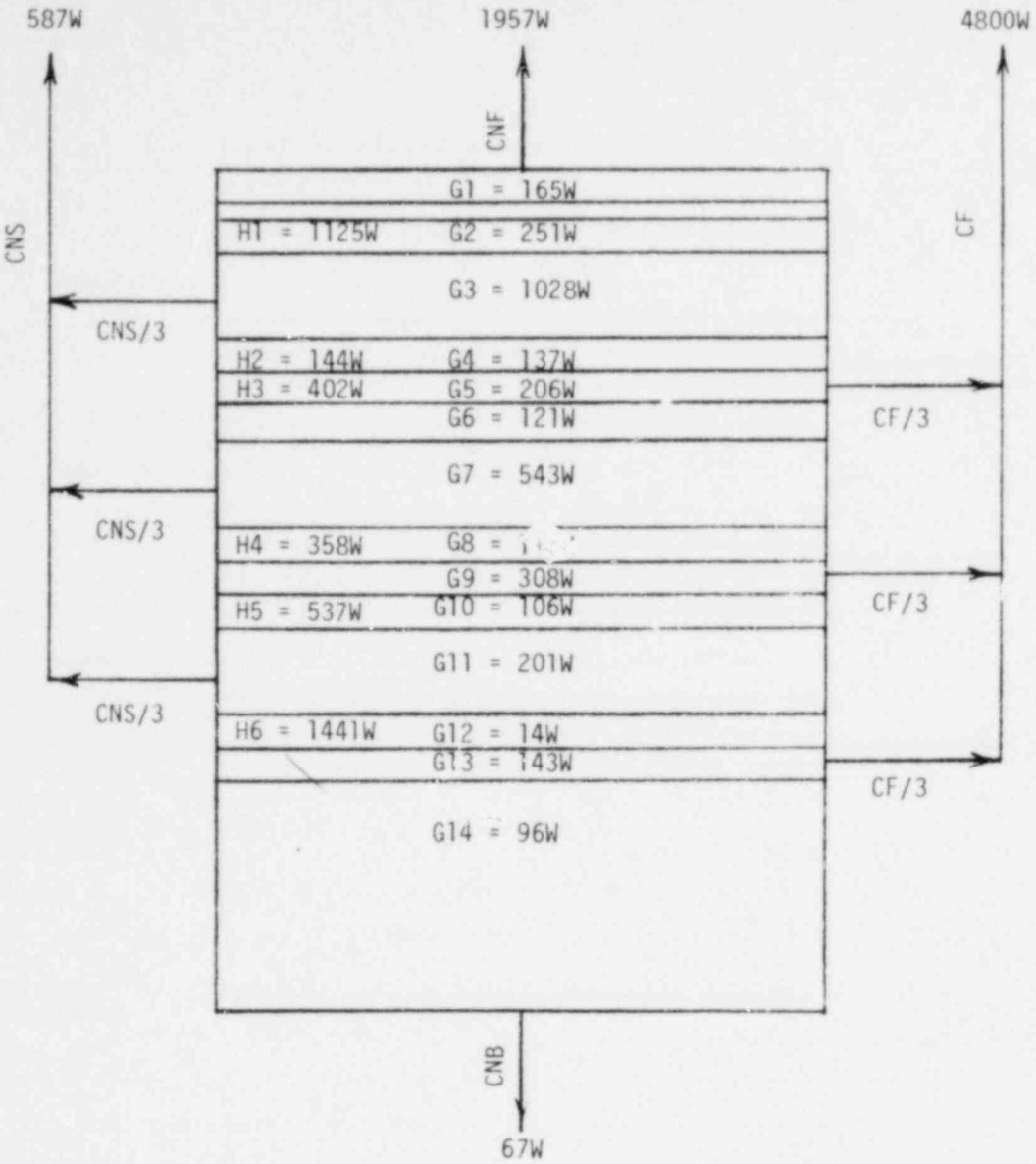

CF = forced cooling

CNF = nat convection, front face

CNS = nat. convection, bottom and sides

CNB = nat. convection, back face

G = gamma heat

H = heater

Summary

Total heat loss by forced cooling = 4800W

Total heat loss by natural convection = 2611W

Total power from internal heat generation = 3433

Total electric power required = 3978W

FIGURE 8. Neon Cover gas.

Conclusions and Comments

The electric power distribution designed for the assembly should be sufficient to provide temperatures in the range of 550°F using either helium or neon gas to fill all of the voids in the assembly. With 10 seperate circuits in each heater suffient control should be available to control slight deviations in the resistances or coolant temperature in the cooling circuit which might otherwise cause anomolies in the sample temperature. The power requirements using neon gas are considerably less, and with the heaters off the calculated sample temperature adjacent to the first heater is within 20°F of normal operating temperature. For this reason it might be desirable to use helium or a mixture of helium and neon as a cover gas rather then pure neon. The temperature difference in the internal heat generation in the steel is quite negligile, being less than 0.001°F. The event of the coolant flow being stopped was not considered since the reactor will be programmed to scram when this happens. Within limits partial loss of flow could be compensated by power reduction to the heaters. As mentioned previously, the spacer-wires will probably require a slight increase in the electrical power input to maintain the temperature but cause less of a temperature increase with the power off. Thermal radiation amounted to less than 3% of the total heat loss and, therefore, is not considered a major source of error in the estimation of the power requirements. The gas conductivities are deemed to be accurate within ±5% and the gap width accurate to within ±5%. A maximum anticipated error in the power estimation is about 10% or from 15 to 425 watts in the power supply to the individual heaters. No allowances were made for contact resistances. This is conservative in the calculation of power losses but adds to the calculated sample temperature with the heaters off.

No attempt was made in this analysis to predict the temperature distribution in these samples or evaluate the capability of the control devices to regulate the temperatures. It is estimated that the assembly should take about 35 minutes to come to steady state by dividing the heat capacity by the heating rate.

APPENDIX B

The following comments intend to simplify and clarify the uncertainty analysis in the quoted document. While there is, with few exceptions, no disagreement with the results obtained, these comments may provide a better understanding of the mechanics which determine the uncertainties. In particular the inclusion of covariances and their possible consequences on the final uncertainties is considered.

To simplify matters, all parameters will be excluded from consideration which are not relevant to the final goal, the determination of the fluence above 1 MeV. Quantities like "spectrum coverage factor" or E_{95}, etc. can be very useful for the characterization of spectrum and sensors but complicate and confuse the calculations (see the long formula NBS-5 on p. 13). We shall assume that the following data are available with appropriate uncertainties (variances and covariances) assigned to them:

- $[R/NG]_{Ark}$ = reaction probability measured at the cavity
- $[R/NG]_{BT}$ = reference reaction probability measured at BIGTEN

  Only the ratio of the two will be used with resulting reduction in the uncertainties
- Calculated group fluxes in the cavity suitably normalized (e.g. unit core power)

$$\zeta_i = \int_{E_i}^{E_{i+1}} \phi(E)\, dE$$

  in a given energy group structure (E_i, E_{i+1})
- The group fluxes at BIGTEN in the same energy group structure determined through a mixture of calculation and benchmark referencing.

$$\chi_i = \int_{E_i}^{E_{i+1}} \chi(E)\, dE$$

- Group averaged reaction cross sections σ_i^{ϕ} and σ_i^{χ} defined as

$$\sigma_i^{\phi} = \int_{E_i}^{E_{i+1}} \phi(E)\ \sigma(E)\ dE/\Phi_i$$

for ϕ and correspondingly for χ.

Thus the measured reaction probabilities are related to the theoretical values via the formulas

$$[R/NG]_{Ark} \tilde{=} (nvt)_{Ark} \sum_i \Phi_i\ \sigma_i^{\phi} \tag{1a}$$

$$[R/NG]_{BT} \tilde{=} (nvt)_{BT} \sum_i \chi_i\ \sigma_i^{\chi} \tag{1b}$$

The $\tilde{=}$ indicates that this is not a mathematical equality since there are uncertainties on both sides. The two terms $(nvt)_{Ark}$ and $(nvt)_{BT}$ convert the normalized fluxes ϕ and χ to the actual fluences received by the sensors. Needed for the determination of the fluence >1 MeV is the value for the reference sensor of BIGTEN

- $(nvt)_{BT}$ = total fluence received by the reference sensor.

Finally we need to define the total fluence above 1 MeV at the cavity. To be applicable to more general integral parameters like dpa, we define

- $I_r^{\phi} = \sum_i \Phi_i\ r_i$

were $r_i = 1$ for $E_i \geq 1$ MeV and $r_i = 0$ otherwise is completely determined. In other applications r_i may be the group average dpa cross section with appropriate uncertainties assigned to it.

Thus the total fluence above 1 MeV F(>1 MeV) at the cavity is

$$F(>1\ \text{MeV}) = (\text{nvt})_{\text{Ark}}\ I_r^{\phi}$$

This can be determined combining measured and calculated data as listed above. For simplicity we define

$$S^{\phi} = \sum_i \phi_i\ \sigma_i^{\phi}$$

and the corresponding term S^{χ} for BIGTEN. We have

$$F(>1\ \text{MeV}) \cong \frac{I_r^{\phi}}{S^{\phi}/S^{\chi}} \cdot \frac{[R/NG]_{\text{Ark}}}{[R/NG]_{\text{BT}}/(\text{nvt})_{\text{BT}}} \tag{2}$$

The right hand side of (2) consists of 2 factors. The second,

$$BR = \frac{[R/NG]_{\text{Ark}}}{[R/NG]_{\text{BT}}/(\text{nvt})_{\text{BT}}} \tag{3}$$

the benchmark referenced reaction rate, is essentially experimental. Its uncertainty analysis is straightforward and discussed in detail in the NBS document. Using table NBS-9 the relative, 2σ, confidence level of BR is $\cong$ 7%.

The first factor may be called CQ for calculated quotient,

$$CQ = \frac{I_r^{\phi}}{S^{\phi}/S^{\chi}} \tag{4}$$

For an uncertainty analysis of CQ we first linearize its variation

$$\frac{\delta(CQ)}{CQ} = \sum_i \left[\frac{\phi_i\ r_i}{I_r^{\phi}} \frac{\delta\phi_i}{\phi_i} - \frac{\phi_i\ \sigma_i^{\phi}}{S^{\phi}} \left(\frac{\delta\phi_i}{\phi_i} + \frac{\delta\sigma_i^{\phi}}{\sigma_i^{\phi}} \right) + \frac{\chi_i\ \sigma_i^{\chi}}{S^{\chi}} \left(\frac{\delta\chi_i}{\chi_i} + \frac{\delta\sigma_i^{\chi}}{\sigma_i^{\chi}} \right) \right] \tag{5}$$

Thus the reactive change in CQ can be expressed in terms of relative changes of group fluxes and group cross sections. Assuming that spectral and cross section uncertainties are essentially independent from each other, we may consider the different contributions to the overall uncertainty separately. Combining first the contributions from the spectral errors in the cavity we have:

$$\sum_i \left(\frac{\phi_i r_i}{I_r^\phi} - \frac{\phi_i \sigma_i^\phi}{S^\phi} \right) \frac{\delta\phi_i}{\phi_i} \qquad (6)$$

The first factors in this sum can be interpreted as residuals of an approximation of the response function r_i by the reaction cross section σ_i^ϕ. The closer response function and cross section resemble each other in shape, the smaller these factors become and the less dependent the final result will be on the calculated spectrum. The values for these factors taken from Tables NBS-6 and NBS-7 are listed in Table 1. For flux above 1 MeV and $^{238}U(n,f)$ reaction, the dominating term, 0.41, occurs in the 1-1.5 MeV group. Thus the contribution from this group to the overall uncertainty is slightly less than one-half of the uncertainty of the spectral shape in this group. This will be the dominating term provided the other spectral and cross section uncertainties are in the range cited in the document and are independent from each other.

However, the assumption that the spectral errors are uncorrelated, needs further discussion. In the document the spectrum was normalized to 1 for the flux above 1 MeV. This introduces automatically a strong correlation between the group fluxes, since, if one group flux increases some others must decrease. Other normalizations may be considered, since the final result is independent of any specific normalization factor. Different normalizations lead to different variances and covariances, however. It is conceivable that for one specific normalization the covariances are indeed zero, but this is highly unlikely. Lets instead look for the effect of covariances in a kind of "worst case" study.

In the given example the first factor has a positive sign in the 1-1.5 MeV group and negative in all other groups. The largest error would thus be encountered if all spectral errors are strictly correlated in such a way that if the first group changes in one direction the others would change the opposite way. The resulting sum (6) would then be about $0.82 \cdot \delta\phi_i/\phi_i$ or about twice as high as for the uncorrelated case.

There is, however, nothing to suggest that such a strong correlation exists. And, considering the fact that both magnitude and correlations of the spectral uncertainties are in themselves very much uncertain, it is probably safe to use formula (6) disregarding correlations, using perhaps slightly conservative estimates for the magnitude of the errors.

The same considerations apply to the spectral uncertainties in BIGTEN. Their contributions are

$$\sum_i \frac{\chi_i \sigma_i^{\chi}}{S^{\chi}} \frac{\delta\chi_i}{\chi_i} \qquad (7)$$

Using the data from the document the total contribution would be 4.78% disregarding correlations.

The cross section error consists of three components. The group averaged cross section σ_i^{ϕ} may be written as

$$\sigma_i^{\phi} = \bar{\sigma} \cdot \bar{\sigma}_i \cdot c_i^{\phi}$$

where $\bar{\sigma}$ is the total average and $\bar{\sigma}_i$ the group average cross section in some reference spectrum (e.g. BIGTEN, compare Table NBS-7). The correction factor c_i^{ϕ} converts the group average cross section in the reference field to that in the measured field ϕ. The $\bar{\sigma}$ is common to all group cross section and cancels out in formula (5); $\bar{\sigma}_i$ is common to BIGTEN and Arkansas, whereas c_i^{ϕ} appears only in the Arkansas field provided the reference field is BIGTEN. Thus the contribution of cross section

errors to (5) are

$$\sum_i \left(\frac{\chi_i \sigma_i^{\chi}}{S^{\chi}} - \frac{\Phi_i \sigma_i^{\phi}}{S^{\phi}} \right) \frac{\delta\bar{\sigma}_i}{\bar{\sigma}_i} - \sum_i \frac{\Phi_i \sigma_i^{\phi}}{S^{\phi}} \frac{\delta c_i^{\phi}}{c_i^{\phi}} \qquad (8)$$

Benchmark referencing reduces the first factors in the first sum to less than 0.1 and thus, if correlations are disregarded, the contributions from the first sum for $^{238}U(n,f)$ and uncertainties from Table NBS-6 are less than 1%. Even the worst correlation would not increase this contribution to more than 0.17 of the single group cross section error.

Contributions from the second sum were not considered in the document. To estimate the errors in c_i^{ϕ} the deviation from the ideal value of 1.0 was taken as a 3σ bound as advocated for similar situations in the document (see Table 2). The resulting contribution is 1.2% (see Table 3) which is small, but larger than the first sum.

Thus the total uncertainty estimate of CQ for the $^{238}U(n,f)$ detector is 16% (2σ), with about 14% coming from spectrum uncertainties in the 1.0-1.5 MeV energy group. Adding to it (in the square sum sense) the approximately 7% uncertainty of BR the total ±18% uncertainty estimate results in agreement with the document. The corresponding uncertainties for the other detectors are listed in Table 3. The total uncertainties for $^{54}Fe(n,p)$ and $^{46}Ti(n,p)$ are slightly lower than those quoted in the document, possibly because of the simplified derivation.

However it is not permissible to combine the results from the four different detectors to a weighted average to reduce the uncertainties, as done in the document on page 25. The quoted uncertainties are heavily correlated since 90% come from the common source of spectral uncertainties. There are straightforward procedures to determine optimal weighted averages and the resulting variances from correlated random variables, but they are tedious and do not, in our case, yield much improvement. Inspection of the data shows that $^{238}U(n,f)$ has the lowest contribution of spectral errors in all energy groups totaling about 16%, the rest coming from uncorrelated data. Thus the combined uncertainty could not be lower than about 17% (2σ) with the weights heavily favoring the $^{238}U(n,f)$ reaction (see Appendix).

The question remains whether benchmark referencing as practiced here gives the optimal results from the given information or whether better results may be obtained from a straight adjustment procedure like STAYSL. The answer is probably no, since STAYSL is strictly linear and becomes invalid for large nonlir adjustments. More studies are however needed, especially better estimates for spectral uncertainties. Improvements can also be obtained by making the differences in formula (6) small, for instance by using linear combinations of cross sections instead of just one single cross section. Second order effects have to be considered, however, since the terms Φ_i, r_i, σ_i^{ϕ} are in themselves uncertain. Thus there is likely no single recipe for optimal uncertainty analysis. To obtain uncertainty bounds which are both reliable and realistic, a careful study of all pertinent information is needed.

Appendix

Combining Correlated Data

Let $x_1, x_2, \ldots x_n$ be unbiased determinations of the same quantity, say X. The variables x_i may be correlated; the variance-covariance matrix assigned to these variables may be

$$V = (v_{ij}) \tag{A1}$$

$$v_{ij} = \mathrm{cov}(x_i, x_j) \tag{A2}$$

The variance of any linear combination z of the x_i with coefficients c_i, i.e.

$$z = \sum_{i=1}^{n} c_i x_i = (c)^T(x), \tag{A3}$$

is therefore

$$\mathrm{var}(z) = (c)^T V(c) \tag{A4}$$

with (x) and (c) representing the column vectors with elements x_i and c_i respectively. z represents an unbiased estimate of x if

$$\sum_{i=1}^{n} c_i = 1 \tag{A5}$$

For a minimum variance unbiased estimate (A4) has to be minimized subject to condition (A5). This leads to the set of equations

$$\sum_{j=1}^{n} v_{ij} c_j - \lambda = 0, \quad i=1, \ldots n \tag{A6}$$

where the Lagrange multiplier λ is determined from (A5). In vector form with (e) being a vector with 1 in every row, the solution of (A7) is

$$(c) = \lambda\, V^{-1}(e) \tag{A8}$$

Formula (A5) can be written as

$$(e)^T(c) = \lambda(e)^T\, V^{-1}(e) = 1 \tag{A9}$$

or

$$\lambda = \left[(e)^T\, V^{-1}(e)\right]^{-1} \tag{A10}$$

The variance of z becomes

$$\begin{aligned} \mathrm{var}(z) &= (c)^T\, V\, (c) = \lambda^2\, (e)^T\, V^{-1}\, V\, V^{-1}(e) \\ &= \lambda^2\, (e)^T\, V^{-1}(e) = \lambda \end{aligned} \tag{A11}$$

Applying this formula to the four determinations of F(>1 MeV) through ^{238}U, ^{58}Ni, ^{54}Fe and ^{46}Ti detectors we obtain for the coefficients c_i

$c_1 = 1.178$

$c_2 = 0.016$

$c_3 = -0.180$

$c_4 = -0.014$

It is interesting to note that the combination from ^{238}U is greater than one and there are negative contributions from ^{54}Fe and ^{46}Ti. This combination actually decreases slightly the total spectral error and leads to a minimum variance estimate of F(>1 MeV) = $3.53 \cdot 10^8 \pm 17.1\%$ which is higher than any of the original values. The relative covariance matrix with standard deviations is listed in Table 4.

Table 1. Coefficients for Calculating Uncertainties

	Energy Groups (MeV)				
	1-1.5	1.5-2.3	2.3-3.7	3.7-8	8-12
Ark. P & L					
ϕ_i (normalized to >1 MeV)	.526	.237	.130	.098	.0083
error	35%	5%	30%	27%	15%
$\phi_i\sigma_i$ / S^{ϕ} - $^{238}U(n,f)$	.1148	.3816	.2499	.2250	.0287
$^{58}Ni(n,p)$	.0262	.0885	.2394	.5812	.0647
$^{54}Fe(n,p)$	0	.0410	.2263	.6572	.0755
$^{46}Ti(n,p)$	0	0	.1258	.7144	.1599
$^{63}Cu(n,\alpha)$	0	0	0	.5145	.4855
$\phi_i r_i$ / I_r^{ϕ} - $\phi_i \sigma_i$ /S^{ϕ} -					
$^{238}U(n,f)$	.4112	-.1446	-.1199	-.1270	-.0204
$^{58}Ni(n,p)$	.4996	.1485	-.1094	-.4832	-.0564
$^{54}Fe(n,p)$	.526	.1960	-.0963	-.5592	-.0672
$^{46}Ti(n,p)$	.526	.237	.0042	-.6164	-.1516
$^{63}Cu(n,\alpha)$	.526	.237	.130	-.4165	-.4772
BIGTEN:					
χ_i (normalized to >1 MeV)	.371	.270	.218	.133	.0074
error	10%	5%	8%	14%	15%
$\chi_i \sigma_i$ /S^{χ} - $^{238}U(n,f)$	.0702	.3511	.3317	.2267	.0203
$^{58}Ni(n,p)$	.0151	0.799	.3246	.5375	.0429
$^{54}Fe(n,p)$	0	.0311	.3175	.6010	.0505
$^{46}Ti(n,p)$	0	0	.0332	.8102	.1566
$^{63}Cu(n,\alpha)$	0	0	0	.4712	.5288
$\chi_i\sigma_i^{\chi}$ /S^{χ} - $\phi_i\sigma_i^{\phi}$ /S^{ϕ} -					
$^{238}U(n,f)$	-.0446	-.0305	.0818	.0017	-.0088
$^{58}Ni(n,p)$	-.0111	-.0086	.0856	-.0437	-.0218
$^{54}Fe(n,p)$	0	-.0097	.0924	-.0528	-.0246
$^{46}Ti(n,p)$	0	0	-.0926	.0958	-.0033
$^{63}Cu(n,\alpha)$	0	0	0	-.0433	.0433

Table 2. Cross Section Uncertainties

		Energy Groups (MeV)				
		1-1.5	1.5-2.3	2.3-3.7	3.7-8	8-12
$\delta\bar{\sigma}_i/\bar{\sigma}_i$ -	$^{238}U(n,f)$	20%	4%	3%	5%	6%
	$^{58}Ni(n,p)$	20%	10%	10%	15%	20%
	$^{54}Fe(n,p)$	40%	20%	15%	15%	30%
	$^{46}Ti(n,p)$	-	-	40%	20%	30%
	$^{63}Cu(n,\alpha)$	-	-	-	30%	20%
$\delta c_i^{\phi}/c_i^{\phi}$ -	$^{238}U(n,f)$	6%	1%	-	4%	-
	$^{58}Ni(n,p)$	7%	4%	6%	6%	-
	$^{54}Fe(n,p)$	-	8%	7%	7%	-
	$^{46}Ti(n,p)$	-	-	57%	15%	1%
	$^{63}Cu(n,\alpha)$		-	-	29%	1%

Table 3. Summary of Uncertainties (2σ) %

	Detector				
	$^{238}U(n,f)$	$^{58}Ni(n,p)$	$^{54}Fe(n,p)$	$^{46}Ti(n,p)$	$^{63}Cu(u,\alpha)$
Spectral error ϕ_i	15.3	22.1	24.0	25.0	23.1
Spectral error χ_i	4.7	8.0	8.8	11.6	10.3
Cross section error					
from $\overline{\sigma}_i$	0.8	1.2	1.8	4.2	1.6
from c_i^{ϕ}	1.2	3.8	4.9	12.9	14.9
Total error of CQ	16.0	23.8	26.1	30.7	29.4
Reactive rate error BR	7.0	7.0	7.0	7.0	7.0
Total error for F(>1 MeV)	18	25	27	32	30

Table 4. Standard Deviation and Relative Covariances of F(>MeV) Determinations with Different Detectors.

Detector	F(>1 MeV) Estimate	% std	Relative Covariances			
$^{238}U(n,f)$	$3.49 \cdot 10^8$	17.4	1	0.79	0.77	0.65
$^{58}Ni(n,p)$	$3.44 \cdot 10^8$	24.8		1	0.89	0.80
$^{54}Fe(n,p)$	$3.30 \cdot 10^8$	27.0			1	0.81
$^{46}Ti(n,p)$	$3.40 \cdot 10^8$	31.5				1

Combined minimum variance estimate: $3.53 \cdot 10^8 \pm 17.1\%$

APPENDIX C

Covariances and Other Statistical Atrocities in the Uncertainty Analysis of Reactor Dosimetry. A Memorandum to the ASTM E10.05.01 Task Group on Uncertainty Analysis

F. W. Stallmann

This brief memorandum tries to clarify some of the issues in uncertainty analysis which confuse many members of the dosimetry community. It does not intend to answer all questions but rather to focus on specific problems in the determination, reporting, and application of covariances and possible assistance this Task Group may provide. Problems arising from common and dependent error sources are well recognized and have traditionally been circumvented by special techniques, like creating random and systematic errors as separate entities. Such approaches are no longer feasible if spectrum unfolding or other sophisticated model fitting procedures are applied. To avoid wrong and misleading conclusions, it is absolutely necessary to face the issues squarely. The sensitivity of the output to input variances and covariances must be investigated and better input information should be provided whenever needed. The Task Group could give assistance in a number of ways which are listed below.

Statistical Background

Definitions and procedures to calculate covariances and correlations are given in all texts on probability theory and statistics. Unfortunately, the examples given in these texts have very little relevance to the problems in dosimetry and the necessary generalizations are left as "an easy exercise" to the reader.

Since most derived quantities are nonlinear functions of basic measurements, linear approximations are necessary to obtain variances and covariances in an effective manner. Gaussian distribution must also be assumed to keep the computations manageable. Perhaps the Task Group should provide some brief and concise recipes on how covariances can be calculated and reported in routine dosimetry procedures in addition to the more customary determination and reporting of standard deviations.

Systematic Errors

One of the major sources of covariances and correlations are the systematic errors since they are common to a series of measurements by the same instrument. Procedures must be established to determine, report, and calculate variances and covariances arising from systematic errors. Her again the Task Group may become instrumental to establish guidelines for such procedures.

Covariances in Cross Section and Spectral Data

Covariance information for cross section measurements will be included in the new ENDF/B-V data file. Much more important--and much more difficult to establish--is corresponding information for the neutron spectra which serve as input for the newer unfolding (or adjustment) procedures. The reason is that spectral uncertainties are usually much larger than either the cross section and the reaction rate uncertainties. Thus, the resulting unfolded spectrum and its integral fluxes depend substantially on the variances and covariances which were assigned to the input spectrum. The Task Group could develop guidelines for assigning uncertainties to the input spectra and for proper interpretation of the output spectra and their variances and covariances.

Benchmark Referencing

Benchmark referencing can substantially reduce the uncertainties to reaction rate measurement as well as to those of the input spectra. One of the sets of new standards for RPV will address this issue. Aside from being involved with this particular standard, the Task Group could consider more general applications of this principle and provide appropriate guidance.

REFERENCES

1. J. J. Wagschal, R. E. Maerker, and D. M. Gilliam, "Covariances of Fission-Integral Measurements at the NBS ^{252}Cf and ISNF Facilities and at the ORNL-PCA Facility", Proceedings of the Third ASTM-EURATOM Symposium on Reactor Dosimetry, Ispra, Italy.

2. W. Mannhard and F. G. Perey, "Covariance Matrices of ^{252}Cf Spectrum-Averaged Cross Sections", Proceedings of the Third ASTM-EURATOM Symposium on Reactor Dosimetry, Ispra, Italy.

NATIONAL BUREAU OF STANDARDS

(NBS)

NEUTRON FLUX MEASUREMENTS IN THE PRESSURE VESSEL CAVITY OF AN OPERATING U.S. POWER REACTOR

J. A. Grundl, C. M. Eisenhauer, E. D. McGarry

National Bureau of Standards, Washington, D.C. 20234

OBJECTIVE: Establish elementary methods for determining the neutron flux above 1 MeV from activation dosimetry measurements in the pressure vessel cavity of an operating U.S. power reactor. Include in the methodology benchmark referencing of detector response and appropriate error assessment and propagation.

SUMMARY: Reaction rates of four detectors [$^{238}U(n,f)$, $^{58}Ni(n,p)$, $^{54}Fe(n,p)$, $^{46}Ti(n,p)$] from exploratory dosimetry measurements at the reactor beltline in a power reactor pressure vessel cavity have been used to calculate the neutron flux above 1 MeV based upon benchmark neutron field referencing. The final cavity flux for the reactor at full power, is reported as the weighted average of the flux obtained from each detector:

$$[\psi(> 1\ \text{MeV}) \cdot (nv)_o] = [3.44 \pm 12\%(2\sigma)] \times 10^8\ n/cm^2\ sec$$

A detailed error analysis and propagation is developed in terms of formulations which are appropriate for benchmark referencing of dosimetry and are explicit with regard to individual detector response features. These formulations and associated detector response parameters are described in the NBS Compendium of Benchmark Neutron Fields For Pressure Vessel Irradiation Surveillance [1]. Some conclusions concerning error sources from this still provisional analysis are as follows:

(1) benchmark referencing strongly suppresses the most generous estimate of cross section shape errors (less than 1% of the total error); (2) the

uncertainty in the transport computation of the cavity spectrum largely governs the final error (more than 90% of the total); moreover, nearly all of this spectrum computation uncertainty comes in the energy region 1-1.5 MeV (again, more than 90%); and (3) the contribution of the lowest energy threshold detector, $^{238}U(n,f)$, to final average flux value is equal to that of all other detectors combined when the weighting factor is taken as the inverse square of the propagated error for each detector.

Contents

ACCOMPLISHMENTS

Introduction

Reaction rates of several detectors from exploratory dosimetry measurements in the pressure vessel cavity of Arkansas Power and Light, Unit #1 have become available recently. In a first cut interpretation of these measurements the neutron flux above 1 MeV and its associated error are calculated based upon the technique of neutron flux transfer. The latter is a special case of benchmark neutron field referencing of neutron dosimetry measurement methods. Two important detector response parameters are involved in the development: (1) the truncated cross section defined as the spectrum averaged cross section above the detector threshold; and (2) the spectrum coverage factor which is the fraction of the neutron spectrum above 1 MeV to which each detector responds. A detailed description of the error analysis and propagation for these parameters shows quantitatively the relative importance of uncertainties in cross section shape, in the computed cavity spectrum, and in benchmark field characteristics. The degree of spectrum coverage by individual detectors is also taken into account.

The calculation is carried out in two steps the first of which establishes a weighted average of the flux above 1 MeV from individual detector reaction rates using a computed cavity spectrum exclusively. In the second step spectral indexes are examined in order to evaluate the adequacy of the ad hoc uncertainty assigned to the computed cavity spectrum in step 1. Sections 1 and 2 along with Appendices A and B present the developments of step 1; Section 3 describes the spectrum uncertainty assessment of step 2.

1. Experimental Results

Two experimental dosimetry capsules were placed in the pressure vessel cavity of Arkansas Power and Light, Unit #1 for a full power run that began on December 8, 1977 and ended on February 2, 1978. A summary description of the irradiation is given in Table NBS-1. Foil counting was undertaken by Hanford Engineering Development Laboratory and by the University of Arkansas. Counting results were reported as dps/mg at time of removal (TOR) by L. Kellogg of HEDL in a memo to E. Lippincott dated September 8, 1978.

These data reduced to a single average value for each reaction are given in columns 2 and 3 of Table NBS-2. The last column lists the reaction probabilities derived from the data. This quantity is equal to the product of reaction cross section and neutron fluence. The terminology for this table and for all subsequent analysis is described in reference [1]. Appendix A outlines the calculation of the G-factor (column 4 of Table NBS-2) using the summary of irradiation time history given in Table NBS-1.

2. Neutron Fluence Above 1 MeV From Individual Detectors

In this section the cavity neutron fluence above 1 MeV will be established as the weighted average of the fluence results obtained from individual threshold detectors. The neutron fluence will be calculated from each detector response in two ways: first, in the conventional manner based on absolute reaction rates and effective cross sections, and second, by the method of neutron fluence transfer. The latter method involves detector calibration in a benchmark field of known neutron flux intensity. The fluence obtained will be converted to a full-power cavity neutron flux and then subject to an error analysis which assesses and propagates all uncertainties associated with the measurement. The focus of this section is not on specific error assignments

and their justification, but on the application of information in the NBS benchmark compendium to a dosimetry measurement based on benchmark referencing, and on the development of a linear least-squares error analysis scheme appropriate for such measurements.

The reaction rate equations from the NBS Compendium of Benchmark Neutron Fields (1) for integral detector measurements are as follows:

measured reaction rate: $R = [\varepsilon \cdot \mu] \cdot D$ NBS-1

calculated reaction rate: $R_c = G \cdot N \cdot \bar{\sigma} \cdot (nvt)_o$, NBS-2

where R_c, R = reaction rate in disintegrations per second at time-of-removal, (sec^{-1})

D = gamma-counter response of activation detector, (sec^{-1})

ε = detection efficiency factor

μ = composite factor exclusive of ε that relates counts per sec to disintegration rate, R, (e.g. decay constant, branching ratio, isotopic abundance, fission yield, neutron self-absorption, etc.).

G = activation decay factor (see equation A-2 in Appendix A), (sec^{-1})

N = number of detector atoms

$(nvt)_o$ = total energy-integrated neutron fluence, (n/cm^2)

$\bar{\sigma}$ = total spectrum-average reaction cross section (cm^2)

R_c/NG = reaction probability sometimes referred to as total reactions per target nucleus.

Other quantities which will be used in this report are,

$\psi(> 1\ \text{Mev})$ = fraction of neutron spectrum above 1 MeV

$\psi(> 1\ \text{MeV}) \cdot (nvt)_o$ = neutron fluence greater than 1 MeV (n/cm^2)

p = fraction of detector response above E_p

E_p = truncation energy corresponding to response fraction p. (For this report p = 0.95 and E_p (p = 0.95) will be written as E_{95}.)

$\psi(> E_p)$ = spectrum fraction above E_p

$\psi(>E_p)/\psi(>1\ \text{MeV})$ = spectrum coverage factor

$\bar{\sigma}(>E_p)$ = cross section truncated at E_p

$$\bar{\sigma}(>E_p) = \frac{\int_{E_p}^{\infty} \sigma(E)\ \psi(E)dE}{\int_{E_p}^{\infty} \psi(E)dE} \approx \frac{p\ \bar{\sigma}}{\psi(> E_p)}$$

2.1. Conventional Calculation of $[\Psi(> 1\ \text{MeV}) \cdot (nvt)_o]$

The expression for the fluence is obtained directly by substituting the measured reaction rate into equation NBS-2.

$$\frac{R}{NG} = \bar{\sigma} \cdot (nvt)_o$$

and $$[\psi(> 1\ \text{MeV}) \cdot (nvt)_o] = \frac{R}{NG} \cdot \left[\psi(> 1\ \text{MeV}) \cdot \frac{1}{\bar{\sigma}}\right] . \qquad \text{NBS-3}$$

The experimental results, reduced to reaction probabilities, (R/NG), are given in Table NBS-2.

The spectrum fraction, $\psi(> 1$ MeV), and the cross section must come from some ad hoc assumption concerning the spectrum or from a transport calculation. Both calculation and ad hoc assumption will be used here. Results of transport computations for a typical PWR cavity have been made available by N. Lurie of IRT Corporation [2]. The assumption is made that the spectrum given by this computation for mid-core elevation and opposite the flat portion of the core is applicable to the B&W design of Arkansas Power and Light, Unit #1. The spectrum in 22 energy groups was run through the DETAN code which generates a 620-group spectrum interpolation and then calculates spectrum-averaged cross sections based on the ENDF/B-IV Dosimetry File. These cross sections are presented in Table NBS-3. The spectrum fraction above 1 MeV from the IRT calculation is $\psi(> 1$ MeV) = 0.057.

The calculation using equation NBS-3 is summarized below. Results from the three detectors with thresholds below 3 MeV are seen to differ by 8%. The average of all five detector results is 1.59×10^{15} n/cm^2 with a standard deviation of $\pm$ 9%.

Results of Conventional Calculation of Cavity Fluence Above 1 MeV

Reaction	E_p(p=0.95)	Reaction Probability (R/NG)	Cross Section $\bar{\sigma}(> 0.4$ eV) (10^{-24}cm^2)	Fluence [$\psi(>1$ MeV)$\cdot(nvt)_o$]
^{238}U(n,f)	1.2 MeV	4.55×10^{-10}	0.0167	1.55×10^{15} n/cm^2
^{58}Ni(n,p)	1.7 MeV	1.30×10^{-10}	0.00482	1.54×10^{15}
^{54}Fe(n,p)	2.4 MeV	0.91×10^{-10}	0.00361	1.44×10^{15}
^{46}Ti(n,p)	4.2 MeV	1.72×10^{-11}	6.04×10^{-4}	1.62×10^{-15}
^{63}Cu(n,α)	6.2 MeV	0.92×10^{-12}	2.95×10^{-5}	1.78×10^{15}

This conventional derivation of neutron fluence above 1 MeV from a set of threshold detectors provides no indication of how much the result depends upon the spectrum calculation provided by IRT, nor does it explicitly recognize the relationship of detector response characteristics to the quantity being derived. The ^{238}U fission detector, for example, has a response threshold of E_{95} = 1.2 MeV in the cavity spectrum, close to the fluence boundary of 1 MeV. Such a detector measures the fluence above 1 MeV with much less dependence upon the calculated spectrum than does the ^{54}Fe detector with E_{95} = 2.4 MeV, for example. The latter responds to less than 25% of the spectrum above 1 Mev as compared with 70% for ^{238}U. Likewise, the spectrum average cross sections, $\bar{\sigma}(> 0.4\ eV)$, are dominated by the fraction of the spectrum in the sub-MeV range, a component of the spectrum that is of little relevance for the measurement of a fluence above 1 MeV with threshold detectors.

2.2. Reformulation of the conventional calculation

The calculation above may be reformulated so that detector response features are more explicit. The calculated reaction rate equation (Eq. NBS-2) may be written in terms of a truncated cross, $\sigma(> E_{95})$, which is defined as the spectrum average cross section above the detector threshold and is not influenced by the spectrum of neutrons below threshold. The threshold or truncation energy, defined as the energy above which 95% of the detector response occurs, does not, in general, depend strongly upon spectrum for RPV related neutron fields (e.g., for a $^{238}U(n,f)$ detector E_{95} = 1.5 MeV for the fission spectrum vs. 1.2 MeV for the Ark. P. & L. cavity spectrum).

Substituting the definition of a truncated cross section into equation NBS-2 and rearranging gives the desired expression for the fast fluence:

$$R = G \cdot N \cdot \left[\frac{\bar{\sigma}(> E_{95}) \cdot \psi(> E_{95})}{0.95}\right] \cdot (nvt)_o$$

and

$$\left[\psi(> 1\ \text{MeV}) \cdot (nvt)_o\right] = \left[\frac{R}{NG}\right] \cdot \left[\bar{\sigma}(> E_{95}) \cdot \frac{1}{0.95} \cdot \frac{\psi(> E_{95})}{\psi(> 1\ \text{MeV})}\right]^{-1} \quad . \quad \text{NBS-4}$$

The spectrum quantity which arises in this formulation, $[\psi(>E_{95})/\psi(> 1\ \text{MeV})]$ called the spectrum coverage factor, gives the fraction of the spectrum above 1 MeV to which the detector is sensitive. As such it is a possible weighting parameter for averaging individual detector results. Table NBS-3 lists truncated cross sections and spectrum fractions for the cavity spectrum and for the benchmark fields involved in this analysis.

The fast fluence calculation for the $^{238}U(n,f)$ detector using Equation NBS-4 is as follows:

$$\left[\psi(> 1\ \text{MeV}) \cdot (nvt)_o\right] = 4.55 \times 10^{10} \left[(0.40 \times 10^{24}) \cdot \frac{1}{0.95} \cdot \frac{0.040}{0.057}\right]^{-1}$$

$$= 1.55 \times 10^{15}\ n/cm^2$$

The result agrees, as it must, with the result of the conventional calculational given in the previous section.

For an ideal threshold detector with a step-function response and E_{95} = 1 MeV, the coverage factor would be unity for any spectrum shape. The derived fluence in such a case would not depend upon the result of transport calculation. For ^{238}U in the cavity spectrum the coverage factor is 0.040/0.057 or 70%. This

may be compared to a ^{238}U coverage factor of 76% for fission neutrons, the source spectrum for the cavity neutron flux. The contribution of the calculation to this part of the measurement, then, is to show that due to neutron transport the 76% coverage factor for the $^{238}U(n,f)$ reaction in the fission source spectrum drops to 70% in the cavity spectrum. Since the fission spectrum coverage factor of 76% is known to a few percent, this part of the uncertainty estimate, can focus on the accuracy with which the transport calculation establishes the 10% shift in coverage factor.

Analogously, the truncated $^{238}U(n,f)$ cross section of 0.40 barns in Table NBS-3 may be compared with corresponding values in the source spectrum and with other benchmark neutron fields that serve neutron dosimetry. Results for the fission spectrum and two other benchmarks are given below.

	$^{238}U(n,f)$ Detector		
	E_{95}	$\sigma(>E_{95})$	Deviation
Arkansas P. & L. cavity (Lurie PWR calc.):	1.2 MeV	0.40 b	1.000
^{235}U fission neutron source:	1.5	0.54	1.35
BIGTEN Critical Assembly:	1.4	0.51	1.28
PCA(1/4 T):	1.4	0.50	1.25

Again, the transport calculation is needed only to establish the shift in the truncated cross section from 0.54 b in the source spectrum to 0.40 b in the cavity.

The most frequently used detector for RPV related neutron dosimetry is the $^{54}Fe(n,p)$ reaction. The response threshold in the cavity for this detector, E_{95} = 2.4 MeV, is substantially higher than for $^{238}U(n,f)$. Consequently, the

reformulated fast fluence calculation shows quite different spectrum coverage and truncated cross section:

$$\left[\psi(> 1 \text{ MeV}) \cdot (nvt)_o\right] = 0.908 \times 10^{-10} \quad (0.275 \times 10^{-24}) \quad \left[\frac{1}{0.95} \quad \frac{0.0124}{0.057}\right]^{-1}$$

$$= 1.44 \times 10^{15} \text{ n/cm}^2$$

The spectrum coverage factor, 0.0124/0.057 = 0.22, indicates that the $^{54}Fe(n,p)$ reaction covers less than 1/3 as much of the spectrum as does the $^{238}U(n,f)$ reaction. The factor 0.22 is to be compared with an $^{54}Fe(n,p)$ coverage factor of 0.43 for the ^{235}U fission spectrum, a difference of nearly a factor of two between the cavity and its source spectrum. Thus, the transport calculation is more important for calculating the flux above 1 MeV with this detector than it is for $^{238}U(n,f)$.

On the other hand, the truncated cross section for ^{54}Fe is much closer to its source spectrum value: 0.275 b for the cavity vs. 0.252 b for the ^{235}U fission spectrum. The cross section is not sensitive to the calculation, therefore, and this detector is particularly well suited for calibration in a fission neutron standard field.

A tabulation of these internal parameters for the reformulated fluence calculation is given in Table NBS-4 for all of the threshold detectors used in this experiment.

2.3 Fluence transfer from benchmark neutron fields

The experimental parameters and nuclear data associated with Eqs. NBS-2 and -3 limit the accuracy of the fluence derivation just outlined -- see Section 2.5 on errors.

This limit can be largely circumvented and a more accurate fluence obtained when benchmark neutron fields are available for detector calibration. The HEDL counting laboratory in its involvement with the DOE supported Interlaboratory Reaction Rate Program (ILRR) has participated in a number of such benchmark calibration irradiations. Most relevant for the Ark. P. & L. cavity measurements are the experiments carried out in the BIGTEN Critical Assembly at Los Alamos. The results of the ILRR benchmark experiments in BIGTEN make it possible to establish a cavity fluence that is traceable to the National Standard Ra-Be Neutron Source at NBS. Such a technique for establishing a neutron fluence in a neutron field under study is called "fluence transfer."

The flux calibration path is as follows:

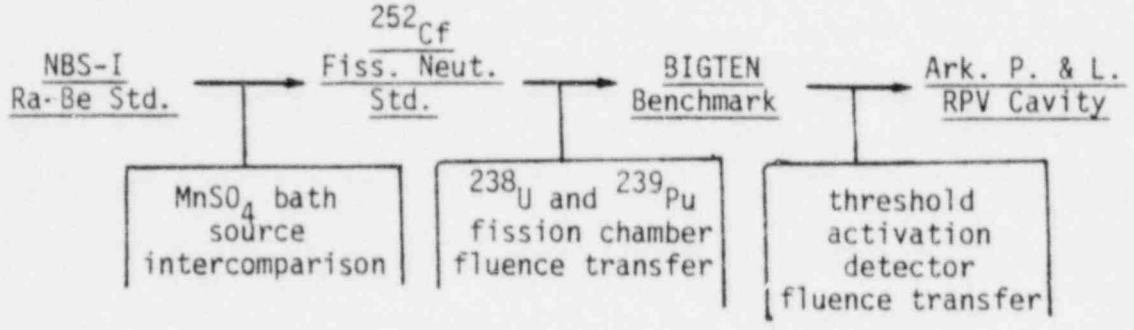

The first two calibration steps have been carried out by NBS and are reported in reference [3]. The last step is based on Laboratory Test No. HEDL 74-20 reported in the ILRR Tenth Progress Report (Oct., 1975).

The expression for neutron fluence transfer from BIGTEN to Ark. P. & L. cavity is obtained by writing Eq. NBS-4 for both neutron fields and dividing:

$$\frac{[\psi(>1\ \text{MeV}) \cdot (nvt)_o]_{Ark}}{[\psi(>1\ \text{MeV}) \cdot (nvt)_o]_{BT}} = \frac{[R/NG]_{Ark}}{[R/NG]_{BT}} \cdot \frac{[\sigma(>E_{95}) \cdot \psi(>E_{95})/(0.95)\psi(>1\ \text{Mev})]_{BT}}{[\sigma(>E_{95}) \cdot \psi(>E_{95})/(0.95)\psi(>1\ \text{MeV})]_{Ark}}$$

Rearranging, the cavity fluence is given by a product of ratios times the BIGTEN fluence,

$$[\psi(>1\text{MeV}) \cdot (nvt)_o]_{Ark} = \qquad \text{NBS-5}$$

$$\underbrace{\frac{[R/NG]_{Ark}}{[R/NG]_{BT}}}_{\text{reaction probability ratio}} \cdot \underbrace{\frac{[\sigma(>E_{95})]_{BT}}{[\sigma(>E_{95})]_{Ark}}}_{\text{truncated cross section ratio}} \cdot \underbrace{\frac{[\psi(>E_{95})]_{BT}}{[\psi(>1\text{MeV})]_{BT}} \Big/ \frac{[\psi(>E_{95})]_{Ark}}{[\psi(>1\text{MeV})]_{Ark}}}_{\text{ratio of spectrum coverage factors}} \cdot \underbrace{[\psi(>1\text{MeV}) \cdot (nvt)_o]_{BT}}_{\text{Benchmark fluence above 1 MeV}}$$

The BIGTEN fluence for Test 74-20 is based on a fluence transfer measurement from the Cf standard field with an NBS U-238 fission chamber (calibration step 2). Using an expression similar to Eq. NBS-5 the result is,

$$[\psi(>1\text{MeV}) \cdot (nvt)_o]_{BT} = 1.48 \times 10^{14} \text{ n/cm}^2$$

The fluence transfer calculation may now proceed. The calculation for $^{238}U(n,f)^{140}Ba$ and $^{54}Fe(n,p)$ will be given explicitly:

(1) $^{238}U(n,f)^{140}Ba$ fluence transfer

$[R/NG]_{Ark} = 4.55 \times 10^{-10}$ (Table NBS-2; irradiation time = 55 days)

$[R/NG]_{BT} = 5.68 \times 10^{-11}$ (ILRR-X, Table HEDL-15; consistent fiss. yield = 0.0595; irradiation time = 13214 sec.)

} reaction probability ratio = 8.01

$$\frac{[\sigma(>E_{95})]_{BT}}{[\sigma(>E_{95})]_{Ark}} = \frac{0.512b}{0.40b}$$ (Table NBS-3)

} truncated cross section ratio = 1.28

$$\frac{[\psi(>E_{95})]_{BT}}{[\psi(>1MeV)]_{BT}} = \frac{0.097}{0.143} = 0.678, \quad \text{(Table NBS-3)}$$

$$\frac{[\psi(>E_{95})]_{Ark}}{[\psi(>1MeV)]_{Ark}} = \frac{0.0398}{0.057} = 0.698 \quad \text{(Table NBS-3)}$$

} ratio of spectrum coverage factors = 0.97

- -

Hence, $[\psi(>1MeV) \cdot (nvt)_o]_{BT} = (8.01)(1.28)(0.97)(1.48X10^{14})$

$$= \underline{1.47 \times 10^{15} \text{ n/cm}^2 \text{ sec}} \quad (^{238}U(n,f) \text{ detector})$$

(2) $^{54}Fe(n,p)$ fluence transfer

ratio

$[R/NG]_{Ark} = 0.908 \times 10^{-10}$ (Table NBS-2)

$[R/NG]_{BT} = 1.29 \times 10^{-11}$ (ILRR-X, Table HEDL-15; irr. time - 13214 sec.)

} 7.04

$$\frac{[\sigma(>E_{95})]_{BT}}{[\sigma(>E_{95})]_{Ark}} = \frac{0.242}{0.275} = 0.88$$

} 0.880

$$\frac{[\psi(>E_{95})]_{BT}}{[\psi(>1MeV)]_{BT}} = \frac{0.0474}{0.143} = 0.331$$

$$\frac{[\psi(>E_{95})]_{Ark}}{[\psi(>1MeV)]_{Ark}} = \frac{0.0124}{0.057} = 0.218$$

} 1.52

- -

Hence, $[\psi(>1MeV) \cdot (nvt)_o] = (7.04)(0.88)(1.52)(1.48 \times 10^{14})$

$$= \underline{1.39 \times 10^{15} \text{ n/cm}^2 \text{ sec}} \quad (^{54}Fe \text{ detector})$$

The fluence transfer calculation is summarized in Table NBS-5 for $^{238}U(n,f)$, $^{58}Ni(n,p)$ and the other detectors that were part of the BIGTEN calibration Test 74-20. The fluence results given in the last column are all within 5% in contrast to the results of the conventional calculat ction 2.1 where for the same four detectors the fluence values depart by more than 15%. The mean fluence by the two methods differ by 7%, and the standard deviation of the mean for the fluence transfer method is one third of that for the convential calculation:

	conventional calculation (Section 2.1 Cu excluded)	fluence transfer method (Table NBS-5)
mean value:	1.55×10^{15} n/cm^2	1.44×10^{15} n/cm^2
standard deviation of the mean:	+ 6.4%	± 2.4%

A combination of activation measurement errors and cross section uncertainties cancel out when benchmark referencing is applied to the fluence measurement and, as this example shows, more consistent results can be expected. An improvement in measurement confidence, however, would exist even if the reduction in the standard deviations were less striking -- see error source list in Section 2.5.

Two factors in Table NBS-5, truncated cross sections and spectrum fractions, are the natural focus of examination in the assessment of errors. (See Section 2.5.3.) They explicitly identify the role of the transport computation in the fluence derivation. Some complications remain, especially for the unusual two-step benchmark referencing used here. For example, the neutron transport problem for the benchmark is very unlike the one for the study spectrum (i.e. criticality in uranium metal for BIGTEN vs water-steel penetration for the PWR cavity). In spite of this difference, the two spectra above 1 MeV are rather similar as will become evident when spectral indexes are examined in Section 3. An important issue of error estimation is how to credit this spectrum similarity.

2.4 Full-Power Neutron Flux in the Vessel Cavity

For this investigation the significant neutron field quantity is the cavity flux corresponding to the reactor operating at full power. The effective full power days for this irradiation was 48.7 days (see Appendix A). A derived fluence, therefore, may be changed to full-power flux by dividing by 4.21×10^6 sec.

The final flux for this first capsule irradiation will be obtained from a weighted average of the fluence transfer values in Table NBS-5. The weighting factor for the average is chosen as the spectrum coverage factor for each detector in the cavity spectrum (Table NBS-4, last column; or Table NBS-5, the denominator in column 5). This choice recognizes that though the spectra above 1 MeV are similar, the neutron transport problem for BIGTEN is very different than it is for the LWR-PV cavity as was noted above. (For a benchmark with neutron transport more closely related to the cavity, a more equal weighting might be justified.) The result for such a weighted average is,

full-power vessel cavity flux above 1 MeV for Ark. PWR. & Light, Unit 1

$$[\psi(>1\ \text{MeV}) \cdot (nv)_o] = 3.45 \times 10^8\ \text{n/cm}^2\ \text{sec},$$

with a standard deviation of $\pm$ 1.1%.

Other averages which may be calculated for comparison are $(3.41 \pm 2.4\%) \times 10^8$ for equal detector weight, and $(3.43 \pm 1.2\%) \times 10^8$ for detectors weighted by dpa coverage. (The dpa, or displaced atom fraction due to neutron exposure, is a neutron-exposure unit often considered appropriate for radiation damge work.)

2.5 Errors

Activation detectors do not measure neutron fluence directly and sources of error are numerous. The expressions for measured and calculated reaction rates (Eqs. NBS-1 and -2) have been set up so that individual errors can be grouped conveniently under appropriate factors. Arranged in this way important activation measurement and interpretation error sources are listed below.

Measured Reaction Rate.

1. gammacounter response, (D)
   - counting statistics
   - backgrounds including competing and impurity activations
   - electronic pulse coincidence corrections
   - gamma attenuation
   - photopeak integration and counting data reduction
   - gamma self shielding of foils
2. gamma detection efficiency, (ε)
   - gamma counting standards
   - effective detector distance
   - energy dependence of detection efficiency
   - long-term reproducibility
3. composite factor, (μ)
   - activation decay constant (for extrapolation to TOR)
   - isotopic abundance
   - branching ratio
   - fission yield
   - neutron self-shielding
   - field perturbation, gradients
   - encapsulation including thermal neutron shields

Calculated Reaction Rate

4. activation decay factor, (G)
   - activation decay constant
   - irradiation time history
5. number of detector atoms, (N)
   - mass of detector material
   - elemental composition
6. reaction cross section, (F)
   - absolute cross section scale
   - energy dependence of cross section
   - spectrum averaging

All of these error sources are involved in a conventional fluence derivation such as the one summarized in Section 2.1. It is well beyond the compass of this report to estimate and propagate such an error list for the Ark. P. & L. experiments. Some of the errors in fact, are very difficult to assess and are treated only in the most carefully done research-oriented measurements. For others, a range of error values could be stated based on evaluations and interlaboratory consensus investigations. In large-scale or routine activation measurements, the problem of keeping all error sources under control is an important one.

Benchmark referencing procedures employed for activation dosimetry circumvent most of the errors listed. Those which are almost entirely eliminated are indicated by closed circles and those partially eliminated (or not amenable to benchmark referencing in all circumstances) are indicated by unclosed circles.

The fluence transfer procedure described in this report involves only uncircled error sources associated with the calculated reaction rates. (The uncircled errors associated with measured reaction rates are not important because the statistical errors of counting are small and the analysis does not include correction to the free-field condition.)

A complete error for the fluence transfer procedure must also include the uncertainty in the National Standard Neutron Source, NBS-1, the $MnSO_4$ bath calibration of the ^{252}Cf fission source, and the fluence transfer measurement in BIGTEN, all part of the calibration path shown in Section 2.3. Each of these errors will be estimated and then propagated in what follows. We begin with the error estimate for the activation decay factor, G.

2.5.1 Activation decay factor.

In Appendix A an activation decay factor, G' , which corresponds to an irradiation time history re-arranged within a $\pm$ 5% uncertainty bound, is defined and compared with the decay factor G" corresponding to a constant level 55 day cavity irradiation at constant power level. The re-arrangement is chosen such that the ratio G"/G' is a maximum. The departure from unity of G"/G' is taken as an upper limit or three standard deviation time history error for this analysis. The time history error for each detector at the 1σ level are as follows:

	$^{238}U(n,f)$				$^{45}Sc(n,\gamma)$		$^{59}Co(n,\gamma)$
	^{140}Ba	^{95}Zr	$^{58}Ni(n,p)$	$^{54}Fe(n,p)$	$^{46}Ti(n,p)$	$^{58}Fe(n,\gamma)$	$^{63}Cu(n,\alpha)$
half-life:	12.8d	64.1d	70.9d	312d	83.9d	44.6d	5.27Y
$\frac{1}{3}$[1- G"/G']:	$\pm$2%	$\pm$0.5%	$\pm$0.6%	$\pm$0.1%	$\pm$0.4%	$\pm$0.7%	$\pm$0.0%

2.5.2 Counter response, D, and Number of detector atoms, N.

The detector foils are large enough to be accurately weighed by conventional gravimetric techniques without obvious complications (scandium and cobalt foils might be an exception). The HEDL laboratory agrees that such routine weight determinations are better than ±1% (1σ) in the worst possible case, e.g., wrapped uranium metal foils of 5 mil thickness. The relative errors in the counter response, e.g. counting statistics, reproducibility, shelf factors etc., are estimated by HEDL in the memo of Sept. 8 from Lippincott. They are less than ±2% (1σ) for all of the detectors considered in this report.

2.5.3 Reaction cross section and spectrum errors.

The truncated cross section ratio and spectrum coverage factors in Eq. NBS-5 are the relevant cross section and spectrum related quantities for fast-neutron fluence transfer. In order to propagate errors for these quantities, uncertainties must be assigned to the energy dependence of the detector cross sections and to the BIGTEN and Ark. P & L. cavity spectra. The spectrum errors will be estimated in a multigroup energy structure similar to that employed for the NBS fission spectrum evaluation. (1) Two assumptions guide the spectrum error assignments:

1. The cavity spectrum above 2 MeV resembles a ^{235}U fission spectrum slope over much of the energy range; departures are provided by neutron transport calculations. The spectrum error bound is taken as the larger of ±5% or 1/3 of the departure of each group flux from its fission spectrum value. The spectrum normalization is $\Sigma_i \psi_i \Delta\Sigma_i = 1$ above 1 MeV.

2. Since a well-preserved ^{235}U fission spectrum exists in BIGTEN above ~1.5 MeV, this benchmark is an adequate substitute for a true fission spectrum standard.[a] The error bound is set between ±(5-15)% in five energy groups. (This bound is also about equal to 1/3 of the departure from the fission spectrum shape with the exception of the first group. In that group, there is good agreement between calculation and experiment for double calculated-to-experimental ratios of spectral indexes involving Np(n,f) and $^{238}U(n,p)$. This agreement allows a reduced error assignment.)

[a] Truncated cross sections in BIGTEN for the threshold detectors in Table NBS-4 are well within ±10% of their fission spectrum values.

The adequacy of the first assumption above can be investigated by examining double calculated-to-experimental (C/E) ratios of spectral indices for the cavity measurements. This will be carried out in Section 4 of this report.

Evaluated cross section shape errors are not readily available from the literature. In lieu of them, a conservative bound for each cross section shape has been estimated on an ad hoc basis from the tabulation in reference [4] and from plots of independent measurements [5]. This bound is taken as an upper limit for those cross section shapes which have been measured often and/or agree well with integral benchmark checks. Hopefully, proper cross section error evaluations from CSEWG and elsewhere are on the way. Since this report is mainly a dosimetry demonstration study this issue will not be discussed further.

The BIGTEN and Ark. P. & L. Cavity spectrum, and corresponding cross section error bounds are given in Table NBS-6. The error bound is taken to be at the 95% confidence level or about 2σ. The spectra are normalized to unity above 1 MeV. Group cross sections, normalized to $\sigma(> E_p)$ for each spectrum, are given for BIGTEN, Ark. P. & L. and the ^{235}U fission spectrum in Table NBS-7. It is the departure of this cross section parameter from unity that governs the overall fluence transfer error as will become apparent.

2.5.4 Propagation of cross section and spectrum parameter errors

The expressions for error propagation of cross section and spectrum quantities in Eq. NBS-5 are set out in Appendix B. The fractional error for the spectrum coverage factors (Eq. B-8) involves two sum terms and a group flux parameter, $\mu_i = \psi_i \Delta E_i / \psi(> E_o)$. The latter parameter is given in Table NBS-6 along with the spectrum error, $\delta\mu_i/\mu_i$, for BIGTEN and Ark. P. & L.

The error propagation calculation for the $^{238}U(n,f)$ detector in outline is as follows:

a. spectrum coverage factors, ($^{238}U(n,f)$, E_o = 1 MeV), (Eq. B-8; μ and $\delta\mu/\mu$ from Table NBS-6)

Ark. P. & L., (E_{95}=1.2 MeV, F=0.0398/0.057=0.70)

$$\left(\frac{\delta F}{F}\right)^2 = \underset{0}{0.0054} + \underset{1.2}{0.0026}\ \underset{12\ MeV}{|} \qquad \text{and} \quad \frac{\delta F}{F} = \pm 8.9\%, \text{Ark}$$

BIGTEN, (E_{95}=1.4 MeV, F=0.097/0.143=0.68)

$$\left(\frac{\delta F}{F}\right)^2 = \underset{0}{0.00088} + \underset{1.2}{0.00020}\ \underset{12\ MeV}{|} \qquad \text{and} \quad \frac{\delta F}{F} = \pm 3.3\%, \text{BT}$$

Results for other detectors are in Table NBS-8.

The fractional error for the truncated cross section ratio (Eq. B4 in Appendix B) involves three sum terms corresponding to the cross section shape error ($\delta si/Si$ given in Table NBS-6) and the two spectrum errors also given in Table NBS-6. Note that the group flux parameter in Eq. NBS-4 is normalized to $\psi(>E_{95})$ rather than to $\psi(>E_o)$ as above: $\mu_i=\psi_i\Delta E_i/\psi(>E_{95})$. Cross sections normalized to $\sigma(>E_{95})$ are listed in Table NBS-7. The error propagation calculation in outline for the $^{238}U(n,f)$ detector is as follows:

b. truncated cross section ratio, (^{238}U(n,f), E_o=1 Mev),

(Eq. B-4; $\mu, \delta\mu/\mu, \delta s_i/s_i$ from Table 6)

	Contribution of lowest energy group (1-1.5 MeV)	Total propagated error
cross section error sum term	± 0.5%	± 0.6%
spectrum error sum terms		
BIGTEN	± 1.0%	± 1.1%
Ark. P. & L.	± 13%	± 14%

final error bound: $\frac{\delta R}{R}$ = ± 14% (2σ)

Results for other detectors are in Table NBS-8.

Clearly, the Ark. P. & L. spectrum uncertainty dominates the final error for the ^{238}U(n,f) detector, and this uncertainty is itself dominated by the ±35% error bound in the lowest energy group between 1.0 and 1.5 MeV. Accuracy improvement efforts therefore would have to focus on the energy range below 2 MeV. Experimentally, this requires an examination of calculated-to-experimental (C/E) spectral index ratios involving ^{238}U and most essentially ^{237}Np fission detectors. Response ranges for these detectors for the Ark. P. & L. cavity spectrum are as follows:

	E_p(p=0.95)	E_p(p=0.90)	E_p(p=0.5)	E_p(p=0.05)
^{237}Np(n,f)	0.052 MeV	0.40 MeV	0.86 MeV	3.4 MeV
^{238}U(n,f)	1.20	1.40	2.3	7.3

Only ^{238}U(n,f) was measured in the first Ark. P. & L. irradiation. The C/E spectral index ratios for this detector, benchmark referenced against BIGTEN, will provide a partial check of the sub-2 MeV spectrum. Analytically, of

course, the cavity spectrum calculation should be examined against calculational benchmarks such as water penetration, steel transmission, or the PCA RPV-mock-up facility. Such an examination may indicate that the first assumption in Section 2.5.3 above is too conservative for the energy range below 2 MeV.

Other detector uncertainties also are dominated by the cavity spectrum calculation although the emphasis shifts to the spectrum coverage factors, i.e., the flux above 1 MeV compared to the flux in the detector response range. For no detector is the cross section shape uncertainty of importance; so much so that these uncertainties could be doubled or tripled with little effect on the overall error. It is the BIGTEN referencing that so strongly suppresses this error contribution (cf. first summation in Eq. B-4 vs. the corresponding summation in Eq. B-2).

2.6 Final Value and Uncertainty for the Cavity Flux Above 1 MeV From Individual Detectors

All of the errors for this experiment are grouped under five headings in Table NBS-9. Errors are estimated at the 2σ or the 95% confidence level. This is considered appropriate for the RPV irradiation surveillance problem which is the primary motivation for the Ark. P. & L. measurements. A final cavity flux above 1 MeV is established as the mean of the four fluence values given in Table NBS-5 translated to flux (see section 2.4) and weighted inversely as the square of the total error for each detector given in Table NBS-9:

Reaction	Flux ($X10^8$)
$^{238}U(n,f)$	3.49 ± 18%
$^{58}Ni(n,p)$	3.44 ± 24%
$^{54}Fe(n,p)$	3.30 ± 29%
$^{46}Ti(n,p)$	3.40 ± 35%

Cavity Flux Above 1 MeV:

$[3.44 + 12\%(2\sigma)]X10^8$ n/cm^2 sec.

This is the concluding result of step 1: a flux value from a weighted average of individual detector results benchmarked in the BIGTEN reference neutron field.

The total error of ± 18% for the ^{238}U fission detector show it to be the most significant for deriving the cavity flux. This total error is as much dominated by cavity spectrum uncertainties as any of the total errors in Table NBS-8.

Since each detector in this experiment has a distinguishable energy response range and because this feature of the measurement has yet to be exploited, it may be expected that the large contribution of the cavity spectrum error can be reduced. This expectation, in fact, is already apparent: The standard deviation of ± (2 - 3%)(2σ) among the detector results given in Section 2.4 suggests that the total error of ± 12% as derived up to this point is too high.

3. Observed and Calculated Spectral Indexes

Spectral indexes among the threshold detectors in the dosimetry capsule may be compared in ratio with those predicted by the transport calculation. These calculated-to-experimental ratios are the basis for evaluating the validity of the cavity spectrum given by the transport computation. This is the second step of the cavity flux calculation. In this report it will be carried out only to the point of evaluating the ad hoc error assigned to the cavity computation (Section 2.5.3 and Table NBS-6) and indicating appropriate changes.

As discussed previously in Section 2.5.3, the spectrum computation may be regarded as a means for transforming the fission spectrum source in the reactor core to its appropriate shape in the cavity. Accordingly, the fission spectrum is the appropriate reference for the calculated-to-experimental spectral index comparisons. The spectrum benchmark for this experiment is BIGTEN, a good substitute for the fission spectrum. Since a number of different detectors responses can be involved in such an analysis, the following subscripted terms from the NBS Benchmark Compendium are defined:

spectral index: $S_{\alpha/\beta} = \bar{\sigma}_\alpha / \bar{\sigma}_\beta$

where α and β refer to the two detectors involved and $\bar{\sigma}$ is the full spectrum averaged cross section.

calculated-to-experimental ratio of spectral indexes:

$$C_{\alpha/\beta} = \left[S_{\alpha/\beta}\right]_{calc} \Big/ \left[S_{\alpha/\beta}\right]_{exp}$$

3.1 Spectrum Response Characteristics

Three independent spectral indexes may be formed from four of the threshold detectors exposed in the cavity. These indexes will be taken relative to the $^{238}U(n,f)$ detector so that the response threshold of each detector compared to that of $^{238}U(n,f)$ points to the energy region where each spectral index is sensitive (see NBS Benchmark Compendium, Table X-16). Called the non-overlap interval, this region is defined as the energy interval between the truncation energy, E_{95}, for each detector and $^{238}U(n,f)$.* For the cavity spectrum non-overlap intervals, $[(E_{95})_\alpha - (E_{95})_\beta]$, are as follows:

	$\frac{^{58}Ni(n,p)}{^{238}U(n,f)}$	$\frac{^{59}Fe(n,p)}{^{238}U(n,f)}$	$\frac{^{46}Ti(n,p)}{^{238}U(n,f)}$
non-overlap interval (MeV):	1.7 - 1.2	2.4 - 1.2	4.2 - 1.2

A more complete display of spectral index response characteristics is shown in the bar chart of Fig. 1. The length of the bars for each detector corresponds to the 90% response range between E_{95} and E_{05}; the indent is the median response energy, E_{50}; and the vertical markers correspond to E_{25} and E_{75}, respectively. Thus, the bar chart presents a four group display of the energy response of each detector in the cavity spectrum. Non-overlap intervals in the Figure for the spectral indexes listed above is the energy interval between 1.2 MeV and the leading edge of the corresponding detector bar. The cavity spectrum above 1 MeV, similarly marked off into four groups, is shown by the top most bar and is followed by the dpa cross section response similarly marked off. The latter is displayed for the full energy range of the cavity spectrum.

*Analysis of spectral indexes in terms of non-overlap intervals is satisfactory for the measurements considered in this report, but may not be applicable for all combinations of detectors and spectra.

The dpa response display shows that nearly 3/4 of the response is below 1 MeV. The consequent limitation of dosimetry measurements which are restricted to $^{238}U(n,f)$ and higher threshold detectors is apparent. In this connection the importance of the Np fission detector in dosimetry is shown by the last bar in the figure (also plotted for the full energy range of the cavity spectrum but with the lower end of the response range set at E_{90}). It is the only detector with a well known cross section that is sensitive to more than 1/2 of the dpa energy response range for the cavity spectrum as shown at the top of the figure.

3.2 Ratio of Spectral Indexes: Calculated-to-experimental

Conventionally, an experimental spectral index is the ratio of detector reaction probabilities. Such absolute spectral index values for this experiment are given in column 2 of Table NBS-10 based on the reaction probabilities listed in Table NBS-2. In this report, however, it is benchmark referenced spectral indexes which are of interest because they are more reliable and are amenable to a complete error analysis. This holds true for any benchmark (i.e., a neutron field whose spectrum is better known than the field under study), but it is even more significant if the benchmark spectrum resembles the study spectrum sufficiently well that cross section shape errors become negligible in the calculated-to-experimental ratios.

The benchmark neutron field for this experiment is BIGTEN and the resemblence of its spectrum to that of the cavity spectrum above 1 MeV is close enough to make cross section shape errors small (see Section 2.5.4). The measured spectral indexes for the cavity calibrated against calculated spectral indexes for BIGTEN are given by

$$\left[S_{\alpha/\beta}\right]_{cvy,\ exp} = \underbrace{\frac{\left[(R/NG)_\alpha/(R/NG)_\beta\right]_{cvy}}{\left[(R/NG)_\alpha/(R/NG)_\beta\right]_{BT}}}_{\text{Table NBS-5}} \cdot \underbrace{\left[\frac{\sigma_\alpha(>0.4\ eV)}{\sigma_\beta(>0.4\ eV)}\right]_{BT}}_{\text{Table NBS-3}}$$

The values of $\left[S_{\alpha/\beta}\right]_{cvy,\ exp}$ are given in Table NBS-10, column 3.

The assigned error is the rms sum of two components: (1) the BIGTEN spectrum error propagated in the calculated spectral index (2nd sum term in eq. B-6, Appendix B); and (2) the counter response and number of detector atoms errors given in Table NBS-9.

The spectral indexes predicted by the IRT calculation may be formed from the cross sections in Table NBS-3,

$$\left[S_{\alpha/\beta}\right]_{cvy,\ calc} = \left[\frac{\sigma_\alpha(>0.4\ eV)}{\sigma_\beta(>0.4\ eV)}\right]_{cvy},$$

and the calculated-to-experimental ratio of spectral indexes is

$$\left[C_{\alpha/\beta}\right]_{cvy} = \frac{\left[S_{\alpha/\beta}\right]_{cvy,\ exp}}{\left[S_{\alpha/\beta}\right]_{cvy,\ calc}} .$$

These double ratios are given in the last column of Table NBS-11. Errors are the same as in Table NBS-10 since cross section uncertainties are not important.

The departures of the three $C_{\alpha/\beta}$ ratios from unity are small, statistically insignificant in view of the assigned errors. Because these errors are not more than $\pm$ 10%, the ad hoc error assumption for the cavity spectrum in Section 2.5.3 can be regarded as too conservative. In order to indicate a

possible revision of that assumption, it is useful to interpret each spectral index in an elementary two-group analysis. The two energy groups are the non-overlap interval and the remainder of the energy range up to ~ 10 MeV -- see Figure 1. Employing simple linear scaling based on the overlap fraction listed in Table NBS-11, it can be shown that the maximum uncertainty in the cavity spectrum as seen by the threshold detectors is the error assigned to $\left[C_{\alpha/\beta}\right]_{cvy}$ in Table NBS-11 scaled by the reciprocal of [1 - (overlap fraction)]. The result is as follows:

	^{58}Ni/U8	^{54}Fe/U8	^{46}Ti/U8
Non-overlap interval (MeV):	1.2 - 1.7	1.2 - 2.4	1.2 - 4.2
error in $\left[C_{\alpha/\beta}\right]_{cvy}$, (2σ):	± 6.2%	± 7.7%	± 10.4%
[1 - (overlap fraction)]$^{-1}$:	4	1.9	1.3
maximum group-flux uncertainty in non-overlap interval (2σ):	± 25%	± 14%	± 13%

It will be assumed that the boundaries of the non-overlap intervals match the five group boundaries of Table NBS-6 well enough for purposes of error analysis; that is, there would be little difference if the analysis were redone with all parameters defined with matching boundaries. Starting then with the ^{58}Ni/U8 index result of ± 25% in the 1.2 - 1.7 MeV interval we conclude that it would be appropriate to reduce the cavity spectrum error in the first group shown in Table NBS-6 (1.0 - 1.5 MeV) from ± 35% to ± 25%. Next, the ^{54}Fe/U8 result of ± 14% for 1.2 - 2.4 MeV does not agree with errors of ± 35% and ± 5% in groups one and two, respectively, since the average of these two errors (weighted by group flux) is ± 26%. An error of ± 20% in the first group would be more appropriate giving an average error over the 1.0 - 2.3 MeV interval of ± 15%. (Reducing the ± 5% error in the second

group, already set at a minimum, would have little effect.) Finally, the $^{46}Ti/U8$ result of $\pm$ 13% does not agree with the average error for groups 1 through 3, the interval 1.0 - 3.7 MeV:

$$\text{average error} \cong [35\ (0.53) + 5\ (0.24) + 30\ (0.13]/0.9$$
$$\cong \pm\ 26\%$$

Reducing the error in the first and third groups (1.0 - 2.3 MeV and 2.3 - 3.7 MeV) by 1/2 would yield a more consistent average error:

$$\text{average error} \cong [18\ (0.53) + 5\ (0.24) + 15\ (0.13)]/0.9$$
$$\cong \pm\ 14\%$$

Alternatively, reducing the error by 1/2 in the fourth of fifth groups (3.7 - 12 MeV) would also yield a nearly consistent average error.

It may be concluded from this semi-quantitative examination that the ad hoc cavity error bound set at about 1/3 of the departure from the fission spectrum (but not less than $\pm$ 5%) in section 2.5.3 could be better set at 1/5. The error bounds for the cavity spectrum then would be,

	1.0	1.5	2.3	3.7	8	12 MeV
2σ error bound:	$\pm$ 19%	$\pm$ 5%	$\pm$ 17%	$\pm$ 16%	$\pm$ 9%	

A repeat calculation of the neutron flux above 1 MeV with these reduced spectrum errors will not be carried out in this report. Other schemes for examining the implications of the three $C_{\alpha/\beta}$ values for the cavity spectrum

uncertainty are possible, of course. For example, a three-group, least-squares adjustment procedure, with error propagation, would be more satisfying analytically.

There is a more important point. The uncertainty assigned to each $C_{\alpha/\beta}$, with all sources of error accounted for by means of the BIGTEN benchmark referencing, leads to an uncertainty estimate for the cavity calculation based on experiment. These new error bounds, although well below the $\pm$ (25 - 35%) of the ad hoc assumption, are still in excess of $\pm$ 15%. In contrast, if absolute measured values of the spectral indexes had been used to construct $C_{\alpha/\beta}$ and examined without regard to errors, as is commonly done, it could be concluded in this particular case that the nominal cavity calculation is rather good. The result is as follows,

	$\left[S_{\alpha/\beta}\right]_{cvy,\ exp}$ (Table NBS-10, col. 2)	$C_{\alpha/\beta}$ based on absolute values
$^{58}Ni/U8$	0.288	1.00
$^{54}Fe/U8$	0.200	1.09
$^{46}Ti/U8$	0.0380	0.95

The departures from unity came out surprisingly small and an adjusted cavity spectrum based on these values would show average departures of perhaps 10% from the transport calculation result. It might not be evident that the uncertainty on such an adjusted spectrum should be set in excess of $\pm$ 15%.

REFERENCES

[1] "Compendium of Benchmark and Test Region Neutron Fields for Pressure Vessel Irradiation Surveillance," LWR Pressure Vessel Irradiation Surveillance Dosimetry Quarterly Report, NUREG/CR-0551 (July-September, 1978). Also available from NBS directly.*

[2] Lurie N., Private Communication (April, 1977).

[3] Grundl, J., Spiegel, V., Eisenhauer, C. M., Heaton III, H., Gilliam, D. M., and Bigelow, J., "A Californium 252 Fission Spectrum Irradiation Facility for Neutron Reaction Rate Measurements," Nuclear Technology, 32, 315 (March, 1977).

[4] McElroy, W. N., and Kellogg, L.S., "Fuels and Materials Fast-Reactor Dosimetry Data Development and Testing," Nuclear Technology, 25 No. 2, 180 (1974).

[5] Schett, A., Okamato, K., Lesca, L., Frohner, F., Liskien, H., and Paulsen, A., "Compilation of Threshold Reaction Neutron Cross Sections for Neutron Dosimetry and Other Applications," EANDC 95 "U".

*Available for purchase from the GPO/NRC Sales Program, U.S. Nuclear Regulatory Commission, Washington, D.C., and the National Technical Information Service, Springfield, VA 22161

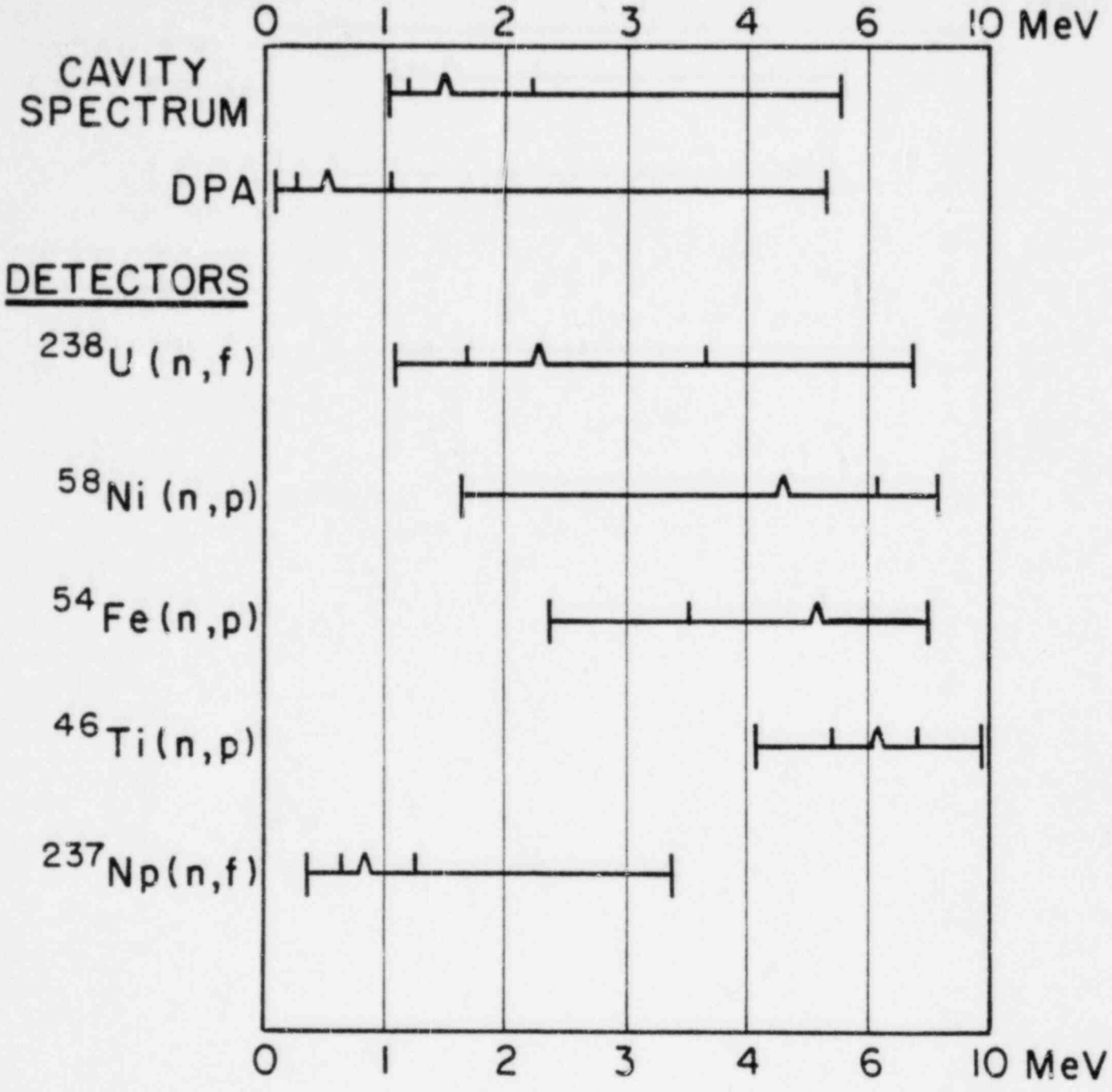

Figure 1. Response range chart for threshold detectors and for the dpa exposure unit. Each bar covers 90% of the energy response range and is marked off into four sub-intervals of equal response by means of an indent at $E_R(p=0.5)$ and two vertical markers at $E_R(p=0.25$ and $0.75)$. The range of the cavity spectrum itself is shown at the top normalized to unity above 1 MeV.

TABLE NBS-1. Description of First Experimental Dosimetry Irradiation in Arkansas Power and Light Unit #1

(1) Detectors in capsules: ^{235}U, ^{238}U, Fe, Ti, Co, Ni, Ta, Cu, Sc, Ag, and S (cadmium covered)

(2) Placement: Midcavity near the reactor beltline

(3) Irradiation Time History:

- startup on 12-9-77; shutdown on 2-2-78; time-of-removal (TOR) at 2400 CST on 2-2-78; capsule exposure time = 55 days; equivalent full power days = 48.7

- condensed time history from reactor power log:

days to TOR:	55	12	11	6	TOR 0
% full power:	0.995	0.69	0.564	0.395	

(4) Ratio of average flux to full-power flux = 0.885.

TABLE NBS-2. Counting Results and Isotopic Reaction Rates

Detector Reaction	Product Reaction Rate: [a] dps/mg @ TOR	Product Reaction Rate: [b] dps/nucl. @ TOR	Activation Decay Factor (G) (sec^{-1}) [c]	Reaction Probability [R/NG] [d]
Threshold Reactions				
$^{238}U(n,f)^{95}Zr$	5.42 ± 3.2%	0.211×10^{-17}	9.1×10^{-8}	4.55×10^{-10}
$^{238}U(n,f)^{140}Ba$	11.35 ± 3.0%	0.449×10^{-17}	1.65×10^{-7}	4.52×10^{-10}
$^{54}Fe(n,p)^{54}Mn$	1.417 ± 2.7%	2.20×10^{-18}	2.42×10^{-8}	0.908×10^{-10}
$^{46}Ti(n,p)^{46}Sc$	1.374 ± 3.0%	1.324×10^{-18}	7.68×10^{-8}	0.172×10^{-10}
$^{58}Ni(n,p)^{58}Co$	77.8 ± 2.9%	1.105×10^{-17}	0.848×10^{-7}	1.303×10^{-10}
$^{63}Cu(n,\alpha)^{60}Co$	0.0248 ± 4.0%	3.77×10^{-21}	4.12×10^{-9}	0.915×10^{-12}
Nonthreshold Reactions				
$^{235}U(n,f)^{95}Zr$	2625 ± 3.1%	1.025×10^{-15}	9.1×10^{-8}	1.746×10^{-7}
$^{58}Fe(n,\gamma)$	0.0311 ± 3.1%	9.08×10^{-19}	1.21×10^{-7}	0.750×10^{-11}
$^{45}Sc(n,\gamma)$	76.5 ± 2.9%	5.72×10^{-18}	7.68×10^{-8}	0.745×10^{-10}
$^{59}Co(n,\gamma)$	18.3 ± 2.7%	1.794×10^{-18}	4.12×10^{-9}	4.35×10^{-10}

[a] Counting results reported by HEDL

[b] dps/nucl. = [dps/mg] x [atomic no.] ÷ [6.02×10^{20} (isotopic abundance)]. This quantity is often referred to as the total reactions per target nucleus.

[c] See Appendix A. For a long half-life, G is equal to the activation decay constant.

[d] R/NG is equal to the product of reaction cross section and neutron fluence. In this data reduction scheme it is the ratio [(column 3 value) ÷ (fission yield)]/[column 4 value]. The fission yields are from ILRR program measurements (see Section 2).

TABLE NBS-3. SPECTRUM-AVERAGED CROSS SECTIONS,

SPECTRUM FRACTIONS, AND ENERGY RESPONSE RANGES.

Cross Sections: ENDF/B-IV Dosimetry File

Detector Reaction	Cross Section[a] $\sigma(> E_p)$		Spectrum[b] Fraction	Median[c] Response Energy	Response Range[c]	
	E_p=0.4 eV	E_p(p=0.95)	$\psi(>E_{95})$	E_p(p=0.5)	E_p(p=0.95)	E_p(p=0.05)
	Spectrum: BIGTEN; Designation: BIG10-7-L1					
$^{237}Np(n,f)$	0.460	1.054	0.414	1.00	0.395	4.3
$^{238}U(n,f)$	0.0523	0.512	0.0970	2.5	1.40	6.7
$^{58}Ni(n,p)$	0.01612	0.2295	0.0667	4.01	1.91	7.8
$^{54}Fe(n,p)$	0.01207	0.2421	0.0474	4.32	2.41	8.1
$^{46}Ti(n,p)$	1.567 E-3	0.0828	0.0180	5.91	3.87	9.9
$^{63}Cu(n,\alpha)$	6.26 E-5	0.01542	3.85 E-3	8.24	6.18	11.8
	Spectrum: PWR, Midcavity; Designation: PWR/CVY-7-I					
$^{237}Np(n,f)$	0.231	0.425	0.518	0.863	0.052	3.4
$^{238}U(n,f)$	0.0167	0.399	0.0398	2.28	1.20	7.3
$^{58}Ni(n,p)$	4.82 E-3	0.209	0.022	4.64	1.70	8.4
$^{54}Fe(n,p)$	3.61 E-03	0.275	0.0124	5.15	2.40	8.6
$^{46}Ti(n,p)$	6.04 E-4	0.1145	0.00502	6.4	4.2	9.9
$^{63}Cu(n,\alpha)$	2.95 E-05	0.0145	0.00194	8.0	6.2	11.4

Footnotes for TABLE NBS-3

(a) The value given first is a full-spectrum averaged cross section above a cadmium cut-off 0.4 eV. The second value is for a truncation energy E_p, above which 95% of the detector response occurs - see column 6. The spectrum average cross section truncated at energy E_p is given by

$$\sigma(> E_p) = \int_{E_p}^{\infty} \sigma(E)\psi(E)dE \int_{E_p}^{\infty} \psi(E)dE \quad .$$

(b) The fraction of the spectrum above $E_p(p = 0.95)$: $\psi(> E_p) = \int_{E_p}^{\infty} \psi(E)dE$. For $p = 0.95$ the full-spectrum-averaged cross section $\sigma(> 0.4\ eV)$ is equal to $[\sigma(> E_p) \cdot \psi(> E_p)/0.95]$.

(c) The fractions $p = 0.95$, 0.5, and 0.05 define energies above which 95%, 50% (median), and 5% of the detector response occurs, respectively. E_p is defined by the relation

$$\int_{E_p}^{\infty} \sigma(E)\psi(E)dE = p \cdot [\sigma(> 0.4\ eV)]$$

where $E_p(p = 1) = 0.4$ eV, and $E_p(p = 0) = 20$ MeV; and $\int_{0.4\ eV}^{\infty} \psi(E)dE = 1$.

Table NBS-4. Spectrum Coverage Factors and Truncated Cross Section Ratios

Reaction	^{235}U Fiss. Spec.			BIG TEN			Ark. P. & L. Cavity		
	E_{95} (MeV)	$\frac{\bar{\sigma}(>E_{95})}{\bar{\sigma}(>E_{95})]_{Ark}}$	$\frac{\psi(>E_{95})}{\psi(>1MeV)}$	E_{95} (MeV)	$\frac{\bar{\sigma}(>E_{95})}{\bar{\sigma}(>E_{95})]_{Ark}}$	$\frac{\psi(>E_{95})}{\psi(>1MeV)}$	E_{95} (MeV)	$\bar{\sigma}(>E_{95})]_{Ark}$ (barns)	$\frac{\psi(>E_{95})}{\psi(>1MeV)}$
^{238}U(n,f)	1.5	1.35	76%	1.4	1.28	68%	1.2	0.400	70%
^{58}Ni(n,p)	2.1	1.26	54%	1.9	1.10	47%	1.7	0.209	39%
^{54}Fe(n,p)	2.5	0.92	43%	2.4	0.880	33%	2.4	0.275	22%
^{46}Ti(n,p)	3.9	0.69	18%	3.9	0.72	13%	4.2	0.1145	8.9%
^{63}Cu(n,α)	6.1	0.96	3.5%	6.2	1.06	2.7%	6.2	0.0145	3.4%

Table NBS-5. Cavity Fluence Above 1 MeV Based on Fluence Transfer from BIGTEN

Reaction	E_{95} (p=0.95)	Reaction Probability Ratio CVY/BIGTEN	Truncated Cross Section Ratio BIGTEN/CVY	Ratio of Spectrum Coverage Factors	Fluence above 1 MeV $[\psi(>1\ MeV)\cdot(nvt)_o]$ (n/cm^2)	
$^{238}U(n,f)$	1.2 MeV	8.1	1.28	0.678/0.698 =0.971	$1.47X10^{15}$	1.000
$^{58}Ni(n,p)$	1.7	7.36	1.10	0.47/0.39 =1.21	1.45	0.99
$^{54}Fe(n,p)$	2.4	7.04	0.880	0.331/0.218 =1.52	1.39	0.95
$^{46}Ti(n,p)$	4.2	9.37	0.72	0.126/0.088 =1.43	1.43	0.97

The fluence in the last column is the product of the three preceding factors and the BIGTEN fluence above 1 MeV of 1.48×10^{14} n/cm^2 -- see Eq. NBS-5.

Table NBS-6. Spectrum and Cross Section Errors Bounds, (2σ)

	E N E R G Y G R O U P S				
	1.0	1.5	2.3	3.7	8 12 MeV
^{252}Cf Fiss. Spect.,(μ):[a]	0.219	0.275	0.284	0.208	0.0127
Ark. P. & L. Cavity					
group flux, (μ):[a]	0.526	0.237	0.130	0.098	0.0083
error:	± 35%	± 5%	± 30%	± 27%	± 20%
BIGTEN					
group flux, (μ):[a]	0.371	0.270	0.218	0.133	0.0074
error:	± 10%[b]	± 5%	± 8%	± 14%	± 15%
Cross Section Shape Errors					
^{238}U(n,f)	20%	4%	3%	5%	6%
^{58}Ni(n,p)	20%	10%	10%	15%	20%
^{54}Fe(n,p)	40%	20%	15%	15%	30%
^{46}Ti(n,p)	--	--	40%	20%	30%
^{63}Cu(n,α)	--	--	--	30%	20%

[a] Normalized to unity above 1 MeV: $\mu = \psi \cdot \Delta E/\psi(> 1\ \text{MeV})$

[b] Reduced error because 37/28 double ratio, BIGTEN/(^{238}U fiss. spec.), agrees with calculation to better than 10%.

Table NBS-7. Normalized Five-Group Cross Sections, $(\sigma_i/\sigma(> E_{95}))$, For BIGTEN and Ark. P. & L. Cavity

	$\sigma(> E_{95})$ (barns)	ENERGY GROUPS				
		1.0	1.5	2.3	3.7	8 12 MeV
$^{238}U(n,f)$						
^{235}U fiss. spect.	0.543	0.1500	0.876	1.013	1.129	1.823
BIGTEN	0.512	0.1336	0.918	1.074	1.203	1.933
Ark. P. & L.	0.399	0.1565	1.155	1.379	1.647	2.481
$^{58}Ni(n,p)$						
^{235}U fiss. spect.	0.262	0.02	0.131	0.647	1.727	2.49
BIGTEN	0.230	0.02	0.145	0.730	1.981	2.84
Ark. P. & L.	0.209	0.02	0.150	0.740	2.383	3.13
$^{54}Fe(n,p)$						
^{235}U fiss. spect.	0.252	0	0.05	0.496	1.506	2.29
BIGTEN	0.242	0	0.04	0.506	1.570	2.37
Ark. P. & L.	0.275	0	0.04	0.402	1.549	2.10
$^{46}Ti(n,p)$						
^{235}U fiss. spect.	0.0794	0	0	0.02	0.826	2.88
BIGTEN	0.0828	0	0	0.02	0.800	2.78
Ark. P. & L.	0.1145	0	0	0.10	0.753	1.99
$^{63}Cu(n,\alpha)$						
^{235}U fiss. spect.	0.01386	0	0	0	0.1014	2.13
BIGTEN	0.01542	0	0	0	0.09667	1.95
Ark. P. & L.	0.0145	0	0	0	0.1822	2.03

Table NBS-8. Propagated Spectrum and Cross Section Error Bounds (2σ) for Spectrum Coverage Factors and Truncated Cross Sections (Eq. NBS-5)

	U238(n,f)	Ni58(n,p)	Fe54(n,p)	Ti46(n,p)	Cu63(n,α)
E_{95}:	1.2 MeV	1.7	2.4	4.2	6.2
Spectrum Coverage Factors					
BIGTEN Spectrum	±3.3%	±4.8%	±6.4%	±12%	±29%
Ark. P. & L. Spectrum	±8.9%	±20%	±24%	±31%	±39%
rms sum:	±9.5%	±20.6%	±24.8%	±34%	±49%
Truncated Cross Section Ratio					
Cross Section Shape	±0.6%	±1.2%	±1.8%	±2.3%	±26.2%
BIGTEN Spectrum	±7.1%	±4.2%	±4.1%	±3.1%	±1.0%
Ark. P. & L. Spectrum	±14%	±9.9%	±12%	±6.8%	±27%
rms sum:	±14%	±10.8%	±12.7%	±7.8%	±38%
Total Spectrum and Cross Section Error (2σ)	[a] ±17%	±23%	±28%	±34%	±62%

[a] More than 95% of this final error is due to the 35% error in the lowest group-flux between 1.0 and 1.5 MeV in the Ark. P. & L. Spectrum (see Table NBS-6).

Table NBS-9. Summary of All Errors in the Determination of Flux Above 1 MeV From Individual Detectors (2σ or 95% confidence level).

	U238(n,f)	Ni58(n,p)	Fe54(n,p)	Ti46(n,p)	Cu63(n,σ)
Neutron source strength of NBS-I:	±2%	±2%	±2%	±2%	±2%
$MnSO_4$ bath intercomparison:	<±1%	<±1%	<±1%	<±1%	<±1%
Neutron fluence at ^{252}Cf fission spectrum irradiation facility:	±2.5%	±2.5%	±2.5%	±2.5%	±2.5%
Neutron fluence transfer to BIGTEN:	±3%	±3%	±3%	±3%	±3%
rms sum:	±4.5%	±4.5%	±4.5%	±4.5%	±4.5%
Activation decay factor: (section 2.5.1)	±1%	±1.2%	±0.2%	±0.8%	±0.0%
Counter response: (section 2.5.2)	<±4%	<±4%	<±4%	±4%	±4%
Number of detector atoms: (section 2.5.2)	<±2%	<±2%	<±2%	<±2%	<±2%
Spectrum parameter errors including cross sections (Table NBS-8)					
Ark. P. & L. spectrum:	±16.3%	±22.3%	±26.8%	±31.8%	±47.6%
Other:	±3.5%	±6.5%	±7.8%	±13.0%	±39.0%
rms sum:	±17.0%	±23.2%	±27.9%	±34.4%	±61.5%
Total Error (2σ):	±17.9%	±24.1%	±28.6%	±34.9%	±61.8%

TABLE NBS-10. EXPERIMENTAL SPECTRAL INDEXES FOR THE CAVITY

Detector Reactions	Absolute[a] value	Referenced to BIGTEN[b] $[S_{\alpha/\beta}]_{cvy}$	ERRORS (2σ) BIGTEN spectrum	R/NG ratio	Total
$^{58}Ni(n,p)/U8$	0.288	0.283	± 4.6%	< ± 4.2%	< ± 6.2%
$^{54}Fe(n,p)/U8$	0.200	0.203	± 5.5%	< ± 4.2%	< ± 7.7%
$^{46}Ti(n,p)/U8$	0.0380	0.0351	± 8.9%	< ± 4.2%	< ±10.4%

[a]Ratio of reaction probability, R/NG, given in last column of Table NBS-2.

[b]Ratio of reaction probability ratios, $[R/NG]_{cvy}/[R/NG]_{BT}$, given in third column of Table NBS-5 multiplied by the calculated spectral index for BIGTEN, $[S_{\alpha/\beta}]_{BT, calc}$, from full spectrum cross sections, σ(< 0.4 eV), listed in Table NBS-3.

TABLE NBS-11. Calculated-to-Experimental Ratio of Spectral Indexes, $\left[C_{\alpha/\beta}\right]_{cvy}$

Detector Reactions	Non-overlap Interval (MeV)	Overlap[a] Fraction	Calculated-to-Experimental[b] $\left[C_{\alpha/\beta}\right]_{cvy}$
$^{58}Ni(n,p)/U8$	1.7 - 1.2	75%	1.02 $\pm$ 6.2% (2σ)
$^{54}Fe(n,p)/U8$	2.4 - 1.2	46%	1.07 $\pm$ 7.7% (2σ)
$^{46}Ti(n,p)/U8$	4.2 - 1.2	21%	1.03 $\pm$10.4% (2σ)

(a) Percent of $^{238}U(n,f)$ response above E_{95} of detector α.

(b) $\left[S_{\alpha/\beta}\right]_{cvy}$ calculated from cross sections, $\sigma(> 0.4$ eV), in Table NBS-3; benchmarked experimental values from Table NBS-10.

APPENDIX A

APPENDIX A: Calculation of Activation Decay Factor, $G(\lambda,T)$

The activation decay factor converts a reaction product decay rate into a reaction probability for that product according to the definition,

$$\frac{R}{N} = G \cdot \left[\begin{matrix}\text{reaction} \\ \text{cross section}\end{matrix}\right] \cdot \left[\begin{matrix}\text{neutron} \\ \text{fluence}\end{matrix}\right] , \qquad \text{A-1}$$

where R/N = specific reaction rate (dps/nucleus),

$$G(\lambda,T) = \lambda \frac{\int_{-T}^{0} e^{\lambda t}\, \phi(t)dt}{\int_{-T}^{0} \phi(t)dt} \qquad \text{A-2}$$

$\phi(t)$ = irradiation time history,
λ = decay constant
T = irradiation time

(See reference [1]).

For an irradiation of length T at constant flux,

$$G = \frac{1}{T}\left(1 - e^{-\lambda T}\right)$$

$$\cong \lambda \quad \text{for} \quad \tau_{\frac{1}{2}} >> T \ .$$

The summary time history given in Table NBS-1 may be used to calculate rather accurate activation decay factors for the Arkansas P. & L. irradiation (T = 55 days):

$$G = \lambda \frac{0.995 \int_{-55}^{-12} e^{\lambda t} dt + 0.69\, e^{-\lambda 12} + 0.564 \int_{-11}^{-6} e^{\lambda t} dt + 0.395 \int_{-6}^{0} e^{\lambda t} dt}{[0.995(43) + 0.69 + 0.564(5) + 0.395(6)]}$$

$$= \frac{1}{48.7}\left[0.995(e^{-\lambda 12} - e^{-\lambda 55}) + 0.69\, \lambda\, e^{-\lambda 12} + 0.564(e^{-\lambda 6} - e^{-\lambda 11}) + 0.395(1 - e^{-\lambda 6})\right] .$$

The arithmetic will be carried out for the $^{58}Ni(n,p)^{58}Co$ and $^{238}U(n,f)^{140}Ba$ reactions.

$\underline{^{58}Ni(n,p)^{58}Co}$: $\tau_{\frac{1}{2}} = 70.9$ d, $\lambda = 0.000978/d$, $\left[\lambda T = 0.537,\ 1 - e^{-\lambda T} = 0.415\right]$

$$G = \frac{1}{48.7}[0.995(0.889 - 0.583) + 0.69\, \lambda\, (0.889) + 0.564(0.94 - 0.90) + 0.395(1 - 0.94)]$$

$$= \frac{1}{48.7}[\underset{\text{-55d}}{0.304} + \underset{\text{-12}}{0.006} + \underset{\text{-11}}{0.023} + \underset{\text{-6}}{0.024}]$$

$$= \frac{0.356}{48.7} = 0.00732/d \text{ or } \underline{0.848 \times 10^{-7}/s}.$$

This result is within 0.1% of the value obtained from a detailed calculation based on the daily reactor power log. Also, a G-factor corresponding to a 55 day irradiation at constant flux (i.e. $G'' = (1 - e^{-\lambda T})/T = 0.874 \times 10^{-7}/s$) differs by only 3% from the above value. For this detector, therefore, credible time history uncertainties would not be important.

$^{238}U(n,f)^{140}Ba$: $\tau_{1/2}$ = 12.8 d, λ = 0.0542/d, $[(1 - e^{-\lambda T})/T = 2.00 \times 10^{-7}/s]$

$$G = \frac{1}{48.7}\left[\underset{\text{-55 d}}{0.469} + \underset{\text{-12}}{0.019} + \underset{\text{-11}}{0.097} + \underset{\text{-6}}{0.110}\right]$$

$$= \frac{0.695}{48.7} = 0.01427/d \text{ or } \underline{1.651 \times 10^{-7}/s}$$

This result is within 1.5% of that given by a detailed calculation. The G-factor for a 55 day constant level irradiation ($G'' = (1-e^{-\lambda T})/T = 2.00 \times 10^{-7}/s$) differs by 21% from the correct value. Thus, for this detector (with a half-life equal to about 1/4 of the irradiation time), an uncertainty bound of $\pm$ 5% on the time history, for example, would introduce a maximum error in G of a few percent. This can be shown by considering a decay factor, G', for an irradiation which is 5% above the average flux for $-T < t < T/2$ and 5% below the average for $-T/2 < t < 0$:

$$G' = \frac{1}{T}(1.05\, e^{-\lambda T/2} - e^{-\lambda T}) + \frac{0.95}{T}(1 - e^{-\lambda T/2}) = \frac{0.92}{T}$$

vs.

$$G'' = \frac{1 - e^{-\lambda T}}{T} = \frac{0.95}{T}$$

The ratio G'/G" is 3% for a departure from constant flux that maximizes the change in G.

For other reactions in Table NBS-2 we have,

	$^{238}U(n,f)^{95}Zr$	$^{54}Fe(n,p)^{54}Mn$	$^{46}Ti(n,p)^{46}Sc$	$^{58}Fe(n,\gamma)^{59}Fe$
$\tau_{1/2}$	64.1 d	312 d	83.9 d	44.6 d
G	9.10×10^{-8}/s	2.42×10^{-8}/s	0.749×10^{-7}	1.15×10^{-7}
$G' = \frac{1-e^{-\lambda T}}{T}$	9.47×10^{-8}	2.42×10^{-8}/s	0.768	1.21×10^{-7}
G'/G"	0.986	0.998	0.988	0.980

Based on this elementary analysis it is suggested that activation decay factors be explicitly given and compared with G' and G" when it is necessary to estimate the contribution of time history uncertainty to reaction probabilities.

APPENDIX B

Appendix B. Error Propagation Formulae for Spectrum Parameters

1. Spectrum-Averaged Cross Section, $\bar{\sigma}$

$$\bar{\sigma} = \sigma_o \frac{\sum_i s_i \psi_i \Delta E_i}{\sum_i \psi_i \Delta E_i} \equiv \sigma_o \frac{U}{V} \quad ; \qquad \text{B-1}$$

where s_i is the cross section shape and σ_o the factor which establishes the absolute cross section scale: $\sigma_i \equiv \sigma_o s_i$.

The fractional standard error, $\delta\bar{\sigma}/\bar{\sigma}$, without covariance is,

$$\left(\frac{\delta\bar{\sigma}}{\bar{\sigma}}\right)^2 = \left[\frac{1}{\bar{\sigma}} \frac{\partial\bar{\sigma}}{\partial\sigma_o}\right]^2 (\delta\sigma_o)^2 + \frac{1}{\bar{\sigma}^2} \sum_k \left[\frac{\partial\bar{\sigma}}{\partial s_k}\right]^2 (\delta s_k)^2 + \frac{1}{\bar{\sigma}^2} \sum \left[\frac{\partial\bar{\sigma}}{\partial\psi_k}\right]^2 (\delta\psi_k)^2$$

$$= \left[\frac{\delta\sigma_o}{\sigma_o}\right]^2 + \sum_k \left[\frac{1}{U} \psi_k \Delta E_k\right]^2 (\delta s_k)^2 + \sum_k \left[\frac{1}{U} s_k \Delta E_k - \frac{\Delta E_k}{V}\right]^2 (\delta\psi_k)^2 .$$

For normalized spectra, $V = 1$ and $U = \bar{\sigma}/\sigma_o$,

$$\left(\frac{\delta\bar{\sigma}}{\bar{\sigma}}\right)^2 = \left[\frac{\delta\sigma_o}{\sigma_o}\right]^2 + \sum_i \left[\frac{\sigma_i}{\bar{\sigma}} \psi_i \Delta E_i\right]^2 \left(\frac{\delta s_i}{s_i}\right)^2 + \sum_i \left[1 - \frac{\sigma_i}{\bar{\sigma}}\right]^2 (\psi_i \Delta E_i)^2 \left(\frac{\delta\psi_i}{\psi_i}\right)^2 . \qquad \text{B-2}$$

The quantities $\delta\psi_i/\psi_i$ and $\delta s_i/s_i$ are the fractional errors in the group flux spectrum and the group cross section shape, respectively.

2. Truncated Cross Section Ratio (same detector, two spectra), $R(>E_p)$

$$R = \frac{\sigma_b(>E_p)}{\sigma_s(>E_p)} = \frac{U_b/V_b}{U_s/V_s} \quad ;$$

where

$$U_x = \sum_{i>i_p} s_i \, \psi_{xi} \, \Delta E_i \;, \quad V_x = \sum_{i>i_p} \psi_{xi} \, \Delta E_i = \psi_x(>E_p) \quad ; \qquad \text{B-3}$$

Following the same steps as in (1) the fractional error without covariance is,

$$\left(\frac{\delta R}{R}\right)^2 = \sum_{i>i_p} \left[\mu_b \frac{\sigma_i}{\sigma_b(>E_p)} - \mu_s \frac{\sigma_i}{\sigma_s(>E_p)}\right]^2 \left(\frac{\delta s_i}{s_i}\right)^2$$

$$+ \sum_{i>i_p} \left[1 - \frac{\sigma_i}{\sigma_b(>E_p)}\right]^2 \mu_b^2 \left(\frac{\delta \mu_b}{\mu_b}\right)^2 \qquad \text{B-4}$$

$$+ \sum_{i>i_p} \left[1 - \frac{\sigma_i}{\sigma_s(>E_p)}\right]^2 \mu_s^2 \left(\frac{\delta \mu_s}{\mu_s}\right)^2 \;,$$

where $\mu_x \equiv \psi_{xi} \, \Delta E_i / \psi_x(>E_p)$.

In practice, when E_p does not correspond to a group energy boundary, the affected term in the sum is scaled linearly by the fraction of the detector response in the affected energy group.

3. Spectral Index (two detectors, same spectrum), $S_{\alpha/\beta}$

$$S_{\alpha/\beta} = \frac{\sigma_\alpha}{\sigma_\beta} = \frac{\sigma_{o\alpha} \sum_{i>o} s_{\alpha i}\ \psi_i\ \Delta E_i}{\sigma_{o\beta} \sum_{i>o} s_{\beta i}\ \psi_i\ \Delta E_i} \qquad \text{B-5}$$

The fractional standard error is,

$$\left(\frac{\delta S}{S}\right)^2 = \sum_{i>o} \left[\left(\frac{\sigma_{\alpha i}}{\sigma_\alpha}\right)^2 \left(\frac{\delta s_{\alpha i}}{s_{\alpha i}}\right)^2 + \left(\frac{\sigma_{\beta i}}{\sigma_\beta}\right)^2 \left(\frac{\delta s_{\beta i}}{s_{\beta i}}\right)^2 \right] (\psi_i\ \Delta E_i)^2$$

$$+ \sum_{i>o} \left(\frac{\sigma_{\alpha i}}{\sigma_\alpha} - \frac{\sigma_{\beta i}}{\sigma_\beta}\right)^2 (\psi_i\ \Delta E_i)^2 \left(\frac{\delta \psi_i}{\psi_i}\right)^2 + \left(\frac{\delta \sigma_{o\alpha}}{\sigma_{o\alpha}}\right)^2 + \left(\frac{\delta \sigma_{o\beta}}{\sigma_{o\beta}}\right)^2 . \qquad \text{B-6}$$

4a. Spectrum Fraction (one detector, one spectrum), $\psi(>E_D)$

$$\psi(>E_D) = \frac{\sum_{i>i_D} \psi_i\ \Delta E_i}{\sum_{i>o} \psi_i\ \Delta E_i}$$

The fractional standard error is

$$\left(\frac{\delta \psi}{\psi}\right)^2 = \sum_{o<k<i_p} (\psi_k\ \Delta E_k)^2 \left(\frac{\delta \psi_k}{\psi_k}\right)^2 + \left(\frac{1}{\psi(>E_D)} - 1\right)^2 \sum_{k>i_D} (\psi_k\ \Delta E_k)^2 \left(\frac{\delta \psi_k}{\psi_k}\right)^2 \qquad \text{B-7}$$

4b. Spectrum Coverage Factor (one detector, one spectrum), $F(E_p, E_o)$

$$F(E_o, E_p) = \frac{\psi(> E_p)}{\psi(> E_o)} = \frac{\sum_{i>i_p} \psi_i \, \Delta E_i}{\sum_{i>i_o} \psi_i \, \Delta E} \quad ;$$

E_p = detector truncation energy

E_o = fast fluence boundary, commonly E_o = 1 MeV

The fractional standard error is,

$$\left(\frac{\delta F}{F}\right)^2 = \sum_{i_o<k<i_p} \left(\mu_k \frac{\delta \mu_k}{\mu_k}\right)^2 + \left(\frac{1 - F}{F}\right)^2 \sum_{k>i_p} \left(\mu_k \frac{\delta \mu_k}{\mu_k}\right)^2 \quad , \qquad \text{B-8}$$

where $$\mu_k \equiv \frac{\psi_k \, \Delta E_k}{\psi(> E_o)} \quad .$$

In practice when E_p does not correspond to a group energy boundary, the affected term in the sum is scaled linearly, by the fraction of detector response in the affected energy group.

DISTRIBUTION

R5 (375)

DOE/FFTFPO (5)
P.O. Box 550
Richland, WA 99352

AR DeGrazia (4)
TL King

DOE/RRT-HQ (2)
Mail Stop B-107
Washington, DC 20545

Chief, Reactor Physics Branch
JW Lewellen

AERE HARWELL (2)
Oxfordshire OX11 ORA
UNITED KINGDOM

LM Davies
AJ Fudge

AERE WINFRITH (4)
Dorchester, Dorset

J. Butler
CG Campbell
AK McCracken
J. Sanders

ARGONNE NATIONAL LABORATORY (1)
9700 South Cass Avenue
Argonne, II 60439

Roland J. Armani
Building 316

BABCOCK & WILCOX (1)
Lynchburg Research Center
P.O. Box 1260
Lynchburg, VA 24505

RH Lewis

DISTRIBUTION (Cont'd)

BATTELLE-COLUMBUS (2)
505 King Avenue
Columbus, OH 43201

D. Farmelo
J. Perrin

BROOKHAVEN NATIONAL LABORATORY (3)
National Neutron Cross Section Center
Upton, NY 11973

JF Carew
BA Magurno
Pearlstein, Building T-197

CENTRE D'ETUDES NUCLEAIRES de SACLAY (3)
B. P. No. 2
91190 Gif sur Yvette
FRANCE

AA Alberman
JM Cerles
JP Genthon

CENTRE D'ETUDE de 1'ENERGIE NUCLEAIRE (4)
Boeretang 200
Mol, Belgium

J. Debrue
G. DeLeeuw
S. DeLeeuw
A. Fabry

COMBUSTION ENGINEERING (1)
1000 Prospect Hill Road
Windsor, CT 06095

J. Varsik

COMMONWEALTH EDISON (1)
P.O. Box 767
Chicago, IL 60690

AD Rossin

EG&G IDAHO, INCORPORATED (3)
P.O. Box #1625
Idaho Falls, ID 83401

R. Greenwood
Y. Harker
JW Rogers

ELECTRIC POWER RESEARCH INSTITUTE (5)
3412 Hillview Avenue
P.O. Box 10412
Palo Alto, CA 94304

T. Marston
O. Ozer
FJ Rahn
K. Stahlkopf
HA Till

EURATOM (3)
JRC Ispra
I 21020 Ispra (VA)
ITALY

R. Dierckx

Comitato Nazionale Per L'Energie Nucleare
Centro Di Studi Nucleari Della Casaccia
Casella Postale 2400
00060 Santa Maria di Galeria
Rome, Italy

U. Farinelli

ECN Netherlands Energy Research Foundation
Weterduinweg 3
Petten, (N.H.)
NETHERLANDS

WL Zijp

FRACTURE CONTROL CORPORATION (1)
330 South Kellogg Avenue
Suite E
Goleta, CA 93017

RA Wullaert

GENERAL ELECTRIC COMPANY (1)
Vallecitos Nuclear Center
P. O. Drawer B
Vallecitos Road
Pleasanton, CA 94566

GC Martin

INTERNATIONAL ATOMIC ENERGY AGENCY (2)
Karntner Ring 11
P. O. Box 590
A-1011 Vienna
AUSTRIA

V. Chernyshev
J. Schmidt

IKE - STUTTGART (1)
Postfach 801140
7000 Stuttgart-80 (Vaihingen)
PFAFFENWALDRING 31
WEST GERMANY

G. Prillinger

IRT CORPORATION (3)
P.O. Box 80817
San Diego, CA 92183

NA Lurie
C. Preskitt
WE Selph

KFA - ZBB
Kernforschungsanlage Julich Gmbh (2)
Postfach 1913
D-5170 Julich 1
WEST GERMANY

D. Pachur
W. Schneider

LOS ALAMOS SCIENTIFIC LABORATORY (2)
University of California
P.O. Box 1663
Los Alamos, NM 87544

G. Hansen, Group N-2
L. Stewart

DISTRIBUTION (Cont'd)

MACALESTER COLLEGE (1)
Dept. of Physics & Astronomy
St. Paul MN 55105

JH Roberts

NATIONAL BUREAU OF STANDARDS (4)
Center of Radiation Research
U.S. Department of Commerce
Washington, DC 20234

RS Caswell
CM Eisenhauer
JA Grundl
ED McGarry

NAVAL RESEARCH LABORATORY (3)
Thermostructural Materials Branch
Code 6392
Engineering Materials Division
Washington, DC 20375

R. Hawthorne
M. Rosen
L. Steele (Code 6653)

NUCLEAR REGULATORY COMMISSION (13)
Metallurgy & Materials Research Branch
Mail Stop SS-1130
Washington, DC 20555

Chief
Public Document Room (3)
M. Bolotski
M. Dunenseld
R. Gamble
W. Hazelton
L. Lois
S. Pawlicki
PN Randall
CZ Serpan
D. Sieno

OAK RIDGE NATIONAL LABORATORY (17)
P.O. Box Y
Oak Ridge, TN 37830

RG Berggren
CD Cagle
DA Canonico
JA Conlin
JA Cox
RM Freestone, Jr.
SS Hurt
FB K. Kam
RE Maerker
RV McCord
LF Miller
FR Mynatt
F. Perey
I. Siman-Tov
FW Stallmann
JH Swanks
CR Weisbon

ORTEC, INC. (1)
100 Midland Road
Oak Ridge, TN 37830

W. Zimmer

PACIFIC NORTHWEST LABORATORY (2)

WC Morgan
Materials Department
PSL Building/Room 1303
Richland, WA 99352

CA Oster
Engineering Physics Department
Math Building/Room 1248
Richland, WA 99352

RADIATION RESEARCH ASSOCIATES (2)
3550 Hulen Street
Ft. Worth, TX 76107

RM Rubin
MB Wells

ROCKWELL INTERNATIONAL ENERGY SYSTEMS GROUP (2)
P.O. Box 309
Canoga Park, CA 91304

HA Farrar IV
B. Oliver

ROLLS-ROYCE & ASSOCIATES LIMITED (2)
P.O. Box No. 31
Derby, England

M. Austin
P. Burch

SCIENTIFIC APPLICATIONS INCORPORATED (3)
1200 Prospect Street
LaJolla, CA 92037

W. Hagan
L. Simmons
VV Verbinski

SOUTHWEST RESEARCH INSTITUTE (1)
8500 Culebra Road
P.O. Box 28510
San Antonio, TX 78284

EB Norris

UNIVERSITY OF CALIFORNIA SANTA BARBARA (1)
Department of Chemical & Nuclear Engineering
Santa Barbara, CA 93106

GR Odette

UNIVERSITY OF TOKYO (2)
Dept. of Nuclear Engineering
7-3-1, Hongo
Bunkyo-ku, Tokyo
JAPAN

M. Nahazawa
J. Sekiguchi

WESTINGHOUSE ELECTRIC CORPORATION (7)
Advanced Nuclear Systems Division
P.O. Box 355
Pittsburgh, PA 15230

S. Anderson
J. Davison
TR Mager
JJ Taylor
SE Yanichko

WESTINGHOUSE ELECTRIC CORPORATION
Research Division
P.O. Box 355
Pittsburgh, PA 15230

R. Holland
JA Spitznagel

HANFORD ENGINEERING DEVELOPMENT LABORATORY (37)
Supervisor, Document Processing
P.O. Box 1970
Richland, WA 99352

HJ Anderson	W/C-39	WY Matsumoto	W/C-33
RA Bennett	W/B-43	WN McElroy	W/C-39
TK Bierlein	W/A-57	PA Ombrellaro	W/B-45
WL Bunch	W/B-47	LM Osland	W/C-115
LL Carter	W/B-47	FH Ruddy	W/C-39
DG Doran	W/A-57	RE Schenter	W/A-4
DS Gelles	W/A-57	FA Schmittroth	W/A-4
R. Gold	W/C-39	WF Sheely	W/A-62
GL Guthrie	W/C-39	EM Sheen	W/A-56
JJ Holmes	W/A-58	FR Shober	W/E-6
LA James	W/A-40	RL Simons	W/A-57
BJ Kaiser	W/A-56	JA Williams	W/A-40
LS Kellogg	W/C-39	HH Yoshikawa	W/A-44
RL Knecht	W/A-40	Central Files (2)	
EP Lippincott	W/C-39	Program Files (5) c/o WN McElroy	W/C-39
		Publ. Services (2)	W/C-115

NRC FORM 335 (7-77)

U.S. NUCLEAR REGULATORY COMMISSION

BIBLIOGRAPHIC DATA SHEET

1. REPORT NUMBER *(Assigned by DDC)*
NUREG/CR-1240 Vol. IV

4. TITLE AND SUBTITLE *(Add Volume No., if appropriate)*
LWR Pressure Vessel Irradiation Surveillance Dosimetry Quarterly Progress Report, October - December, 1979.

2. *(Leave blank)*

3. RECIPIENT'S ACCESSION NO.

7. AUTHOR(S)
G.L. Guthrie and W.N. McElroy

5. DATE REPORT COMPLETED
MONTH: August | YEAR: 1980

9. PERFORMING ORGANIZATION NAME AND MAILING ADDRESS *(Include Zip Code)*
Hanford Engineering Development Laboratory
P.O. Box 1970
Richland, WA 99352

DATE REPORT ISSUED
MONTH: January | YEAR: 1981

6. *(Leave blank)*

8. *(Leave blank)*

12. SPONSORING ORGANIZATION NAME AND MAILING ADDRESS *(Include Zip Code)*
Office of Nuclear Regulatory Research
U.S. Nuclear Regulatory Commission
Washington, DC 20555

10. PROJECT/TASK/WORK UNIT NO.

11. CONTRACT NO.
NRC FIN No. B5988-7

13. TYPE OF REPORT
Quarterly Progress Report

PERIOD COVERED *(Inclusive dates)*
October - December, 1979.

15. SUPPLEMENTARY NOTES

14. *(Leave blank)*

16. ABSTRACT *(200 words or less)*

This report was compiled at the Hanford Engineering Development Laboratory operated by Westinghouse Hanford Company, a subsidiary of Westinghouse Electric Corporation, for the United States Department of Energy and the Nuclear Regulatory Commission. It describes progress made in the Light Water Reactor Pressure Vessel Irradiation Surveillance Dosimetry Program during the reporting period.

17. KEY WORDS AND DOCUMENT ANALYSIS

17a. DESCRIPTORS

17b. IDENTIFIERS/OPEN-ENDED TERMS

18. AVAILABILITY STATEMENT
Unlimited

19. SECURITY CLASS *(This report)*
Unclassified

21. NO. OF PAGES

20. SECURITY CLASS *(This page)*
Unclassified

22. PRICE
$